Thesis for the Master of Science degree in Molecular Biosciences
Main field of study in Biochemistry

Biochemical and Structural Characterization of the *Bacillus cereus* Thioredoxin BC3987 Mutants

By Marta Hammerstad

Department of Molecular Biosciences

Faculty of Mathematics and Natural Sciences

UNIVERSITY OF OSLO

Biochemical and Structural Characterization of the *Bacillus cereus* Thioredoxin BC3987 Mutants

Acknowledgements

The present work was carried out in the laboratory of Professor K. Kristoffer Andersson at the Department of Molecular Biosciences, University of Oslo.

First of all, I would like to express my deepest gratitude to Professor K. Kristoffer Andersson for accepting me into his high quality research group. As my main supervisor, he has shown tremendous interest in my work and given me valuable guidance in this project.

I am immensely grateful to my co-supervisors Åsmund K. Røhr, Hans-Petter Hersleth and Ane Berg Tomter for all the help they have given me. They have been extremely patient, always answered my questions and given me valuable feedback. I would like to thank them for sharing all their inspiring knowledge about biochemistry and protein crystallography.

Further I would also like to thank my fellow students and the rest of the metallo-protein group for creating a great social and working environment.

Thanks to Camilla Oppegård and Helén Haugen for useful pointers at the lab.

A special thanks goes to Jo Annar, my family and friends, for all their encouragement, support and love.

Oslo, May 2010
Marta Hammerstad

Table of Contents

VII

1 Abstract

Thioredoxin (Trx) is a small ubiquitous protein containing two conserved cysteines that can reversibly form a redox-active disulfide bond, belonging to the Trx superfamily. Ribonucleotide reductase (RNR) was the first enzyme discovered to use Trxs and glutaredoxins (Grxs) for the reduction of active site cysteines. Class Ib RNR uses in many cases a protein called NrdH-redoxin for this purpose. Thiol-disulfide oxidoreductases perform the fast and reversible thiol-disulfide exchange between their active site cysteines and cysteines in the substrate protein. Although most Trx-like proteins do not have a high level of sequence similarity, all enzymes share an overall $\alpha/\beta/\alpha$ sandwich fold, in addition to the conserved C-X-X-C motif. The fundamental reaction mechanism for electron transfer from Trx to its substrate was proposed by Kallis and Holmgren in 1980. As a result of the lowered pK_a value observed for the N-terminal cysteine thiol (-SH) in the *Escherichia coli* Trx C-G-P-C motif, it was suggested that this thiolate (-S$^-$) could perform the initial nucleophilic attack on the substrate disulphide bond. In order for the second nucleophilic attack performed by the buried C-terminal cysteine to take place, deprotonation caused by a conserved aspartate residue in the vicinity of the active site has been proposed. Examples of groups of proteins not encompassing this Asp26, but possessing Trx functionality, are the *E. coli* NrdH-redoxins, described as the reductants of NrdE of bacterial class Ib RNR, and *C. pasteurianum* Cp9-redoxins, involved in the reduction of various hydroperoxide substrates. A protein homologous to the NrdH-redoxins and Cp9-redoxins has been located in the *Bacillus cereus* genome, showing significant amino acid sequence similarity with both of the above mentioned redoxins. However, its function is still unknown. A conserved threonine residue, Thr8, adjacent to the active site is believed to influence the protonation state of the C-terminal cysteine in the active site of this small Trx. Other residues might influence the protonation state of this residue as well. The function and structure of this enzyme, BC3987, has been characterized using various biochemical techniques. The crystal structures of two mutant proteins; BC3987 D11W and T53A, in addition to the native protein, have been solved using X-ray crystallography. Also, determinations of active site cysteine pK_a values and redox potentials of active site cysteine thiols/disulfides were performed.

x

2 Introduction

In this thesis, an investigation of the small thioredoxin (Trx) BC3987 from *Bacillus cereus* has been performed. The potential biological function of BC3987 as a specific reductant for ribonucleotide reductase (RNR) is under debate. Therefore, the work done in this thesis will be introduced with a short description of RNR, and thereby followed by a more specific presentation of the Trx diversity.

2.1 Ribonucleotide Reductase – a Substrate for Thioredoxin-like Proteins

Since the first discovery of RNR (*1, 2*), chemistry involving protein free radicals has become an exiting field of research. RNR is responsible for the conversion of ribonucleotides to 2'-deoxyribonucleotides, through enzymatically radical-induced ribonucleotide reduction. Present in all living cells and organisms, these universal enzymes play a crucial role in DNA repair and replication, providing the building blocks required for DNA synthesis (*3, 4*).

Until now, three different classes of RNRs exist in various organisms. Despite little sequence similarity among the three enzyme classes, conservation of crucial residues in the protein sequence, enzymatic mechanisms and allosteric control among the enzymes suggests a common origin during evolution (*5*). In addition to structural differences, the three main classes of RNR enzymes are classified based on their cofactor requirements, which result in different ways to generate active site radicals (*6*). Class I RNRs require a diiron-oxygen cluster, or possibly a different dimetal-oxygen cluster (*7*), usually coupled to a tyrosyl radical (*8*). Class II enzymes contain a vitamin B_{12} cofactor (5'-deoxyadenosylcobalamin), while class III enzymes require a 4Fe-4S iron-sulfur cluster and S-adenosylmethionine (AdoMet) to generate a glycyl radical. Although the three different classes of RNR enzymes depend on different cofactors for their catalytic activity, all three classes contain a conserved cysteine residue at the active site. The cofactors oxidize this cysteine to a thiyl radical, believed to initiate the substrate turnover in all three classes of RNRs (*6, 9*), promoting 3'- hydrogen abstraction from the ribose ring of the bound ribonucleotide substrate (Figure 2.1) (*3, 10*).
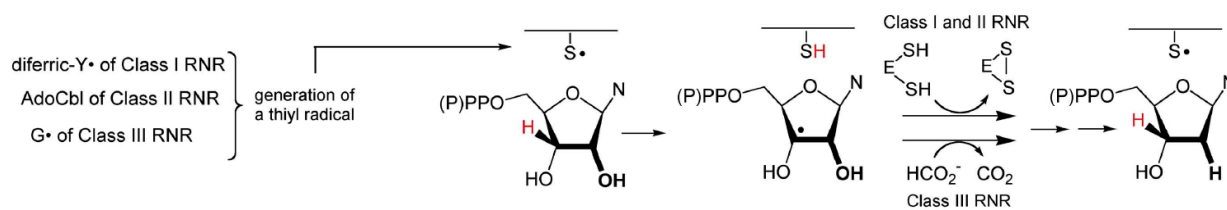
Figure 2.1 General reaction catalyzed by ribonucleotide reductase, leading to the formation of deoxyribonucleotides. Each of the three classes of RNR uses a different cofactor to generate the cysteinyl radical (S·). In class I and II RNR, reducing equivalents for the reaction are provided by the oxidation of two Cys residues of glutaredoxin, Trx or NrdH, to a disulfide. Class III RNR, however, obtains reducing equivalents by the oxidation of formate. The Figure is taken from Sintchak *et al.* (*11*).

Oxygen dependency is another criterion distinguishing the different classes of RNRs. Class I enzymes are oxygen-dependent, and found in aerobic eubacteria as well as nearly all eukaryotes. Some viruses and bacteriophages also express this enzyme class. Class II enzymes show no specific oxygen requirements, and occur in both aerobic and anaerobic eubacteria and archaebacteria. Class III enzymes are only found in facultative anaerobic eubacteria and anaerobic archaebacteria, in addition to some phages (*12*).

Based on allosteric regulation and structural differences, class I RNRs can be subdivided further into three subclasses, Ia, Ib and the newly discovered Ic (*13*), the latter two found exclusively in prokaryotes. All three subclasses consist of two homodimeric proteins; the large, catalytic and allosterically regulated subunit (denoted NrdA in classes Ia and Ic or NrdE in class Ib) and the small, radical-generating subunit (denoted NrdB and NrdB^{Phe} in classes Ia and Ic, respectively, or NrdF in class Ib) (*14*). A significant difference separating class Ic RNR from the remainder two is the presence of a phenylalanine in place of the tyrosine residue in its cofactor subunit, which in classes Ia and Ib harbors the essential tyrosyl radical. Instead, the use of a stable Fe(IV)-Fe(III) or Mn(IV)-Fe(III) cofactor to directly initiate production of the cysteinyl radical in the NrdA subunit has been proposed for the class Ic ribonucleotide reductase (*13, 15, 16*). The operon structures of the genes encoding the RNR subclasses Ia, Ib and Ic are *nrdAB*, *nrdHIEF* and *nrdAB*^{Phe}, respectively, with some variations to the arrangements. Hence, two additional proteins are involved in the regulation of class Ib RNR; NrdH and NrdI. The flavodoxin-like protein NrdI is involved in the generation of the tyrosyl radical in NrdF (*17*), while the NrdH-redoxin reduces a pair of redox active cysteines in the active site of NrdE, acting as a specific hydrogen donor for class Ib RNR (*18, 19*).

2.2 Thiol-Redox Diversity

Redox processes play a significal role in most dominant fields of research, such as chemistry, industry, geology and biology. An important mechanism involving biological systems is the redox chemistry of thiols.

Reduction-oxidation (redox) pathways based on thiols are involved in a variety of cellular processes, such as protein folding (*20*), enzymatic reactions as hydrogen donors (*21*), response to oxidative stress (*22*) and modulation of protein activity (*23*). Reduction and oxidation of disulfide bonds is mediated by thiol-disulfide oxidoreductases, depending on the redox potential and substrate specificity of the catalysts. The reduced form of a redox couple with a large negative redox potential has a low affinity for electrons, and is a strong reducing agent. The opposite is true for reactions with large positive reduction potentials. The thiol-disulfide oxidoreductases perform the fast and reversible thiol-disulfide exchange between their active site cysteines and cysteines in the substrate protein (*24*). Trxs are small ubiquitous proteins that act as thiol-disulfide oxidoreductases in the cell. Many proteins have a Trx-like fold, and among the most studied members are the thiol-disulfide-bond reducing proteins. In addition, proteins involved in the oxidation of disulfide bonds, such as DsbA, as well as eukaryotic protein disulfide isomerases (PDI), both play important and familiar roles in thiol-redox pathways. The latter, which is involved in the processing and maturation of secretory proteins, are enzymes able to catalyse disulfide interchange reactions in proteins and facilitating shuffling of disulfide bonds. Hence, members of the PDI family are involved in the rearrangement of incorrectly disulfide-bonded proteins in the lumen of the endoplasmic reticulum of eukaryotic cells, through the random cleavage and reformation of proteins disulfide bonds (*25, 26*). Members of the Trx structural family are also involved in disulfide bond formation in periplasmic proteins in bacteria, catalyzing the oxidation of peptide and protein cysteines (*27*). The DsbA disulfide oxidorecuctases are such enzymes, encompassing the Trx-like fold, found in the periplasmic space of *Escherichia coli*. The periplasmic space is highly oxidizing, favouring disulfide bond formation. In the cytoplasm of *E. coli*, several pathways play roles in the reduction of disulfide bonds. In this bacterium, two thiol-disulfide bond reducing systems use the reducing potential derived from NADPH in the reduction of multiple cytoplasmic enzymes; the Trx system and the glutaredoxin (Grx) system. The latter consists of three Grxs, glutathione (GSH) and glutathione reductase (Gor), while the former is composed of two Trxs and thioredoxin reductase (TrxR) (*24*). In addition, NrdH-redoxin,

which functions as an electron donor for the bacterial class 1b RNR, also have the Trx-like fold. This small redox protein, found in *E. coli* and several other organisms, is related in amino acid sequence to Grxs, but behave functionally as Trxs (*28*). Other members of the Trx superfamily, are the glutathione S-transferases and the hydroperoxidases (*29*). Regardless of differences in their active sites, all the mentioned proteins are related by their Trx fold, forming distinct, but structurally related families (*30*).

2.3 The Thioredoxin-like fold

Although members of subgroups of the Trx superfamily do not have a high level of sequence similarity, all enzymes share the same overall fold. This fold consists of a four-stranded β-sheet and three flanking α-helices. A subdivision into an N-terminal β/α/β motif and a C-terminal β/β/α motif, connected by a loop that incorporates the third helix, can specify the structure even further (*30*). A common architecture consisting of these secondary structure elements is shared by all Trx-like proteins. The two β-strands from the N-terminal motif, β1 and β2, are lined up in a parallel fashion, while β-strands 3 and 4 from the C-terminal motif are antiparallel. The three α-helices characteristic for the global fold are arranged around the central β-sheet, where helix α2, connecting the two motifs, is located on one side of the β-sheet, opposite and perpendicular to the α1 and α3 helices (*30*). A schematic representation illustrating the architecture of the Trx fold is shown in Figure 2.2.

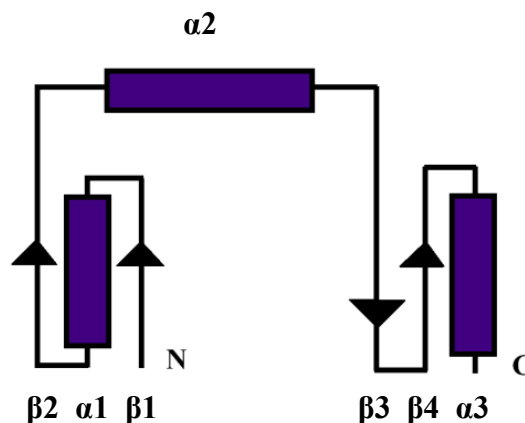**Figure 2.2** A two-dimensional representation of the Trx fold. α-helices are drawn in boxes, while β-sheets are drawn as arrows.

This structural feature, including the C-X-X-C sequence of the active site, is often referred to as the Trx-fold. Some of the proteins identified as having a Trx fold in their structure do not include a C-X-X-C active site, and even though they are involved in sulfur metabolism, their functions are quite different. The glutathione S-transferase and peroxiredoxins are such enzymes, both interacting with glutathione (*31, 32*). Further discussion in this text will not refer to or involve these proteins. The focus will be mainly on thiol-disulfide bond reducing enzymes in the cytoplasm of bacteria.

Trx contains a pair of cysteines which can form a redox-active cysteine dithiol/cysteine disulfide. The structure involving an oxidized active site motif was first solved for the *E. coli* enzyme (*33*), in which the molecule showed to include a central β-sheet core of five parallel and antiparallel strands surrounded by four α-helices. Thus, the characteristic Trx-fold is noticeably smaller than Trx itself, lacking one β-strand and one α-helix. Extra residues and secondary structure elements are present in all other proteins containing the standard fold as well, in addition to the approximately 80 residues making up the Trx fold. The additional N-terminal β/α unit of *E. coli* Trx adds up a 20-fold number of residues to the Trx fold, creating a protein of 108 residues. The parallel β-strands, with the exception of the antiparallel β-strand 4, result in three parallel and two antiparallel strands of pleated sheets, shaping the center of the molecule. Surrounding it, are helices α1 and α3 on one side of the sheet, and α2 and α4 on the opposite side (*33, 34*). Grxs are distantly related to Trxs, also participating in the maintenance of the reductive nature of the cytoplasm through thiol-based electron flow. The four Grx orthologs found in *E. coli* also revealed the classic Trx-like fold with a central pleated sheet surrounded by helices (*35, 36*). All Trx and Grx sequences share an analogous tertiary fold (*34*), and the crystal structure of Grx is quite similar to Trx, apart from some structural differences. In general, the α-helices and β-strands in the Trx fold of Grxs are shorter than those of the Trx proteins. However, a significant feature found in these proteins, not seen in Trxs, is a twist in strand β1. Also, a loop connecting strand β4 and helix α3 in Trxs is not observed in Grxs, where these secondary structure elements are instead more closely associated. This results in a different orientation of the α3 helices in the two proteins, leading to altered substrate specificity (*30*). NrdH seems to be a hybrid of Trx and Grx. Lacking the glutathione-binding site motif found in Grx, NrdH instead binds to TrxR in a protein-protein complex, through interaction at a wide hydrophobic surface pocket (*18, 37*). Despite these differences, functional similarity is found among several important classes of redox proteins,

including Trx, NrdH and Grx, which all share the C-X-X-C motif, and hence, similar reaction mechanisms. Examples of *E. coli* proteins exhibiting different functions, but all having a Trx-like fold, are presented in Figure 2.3.
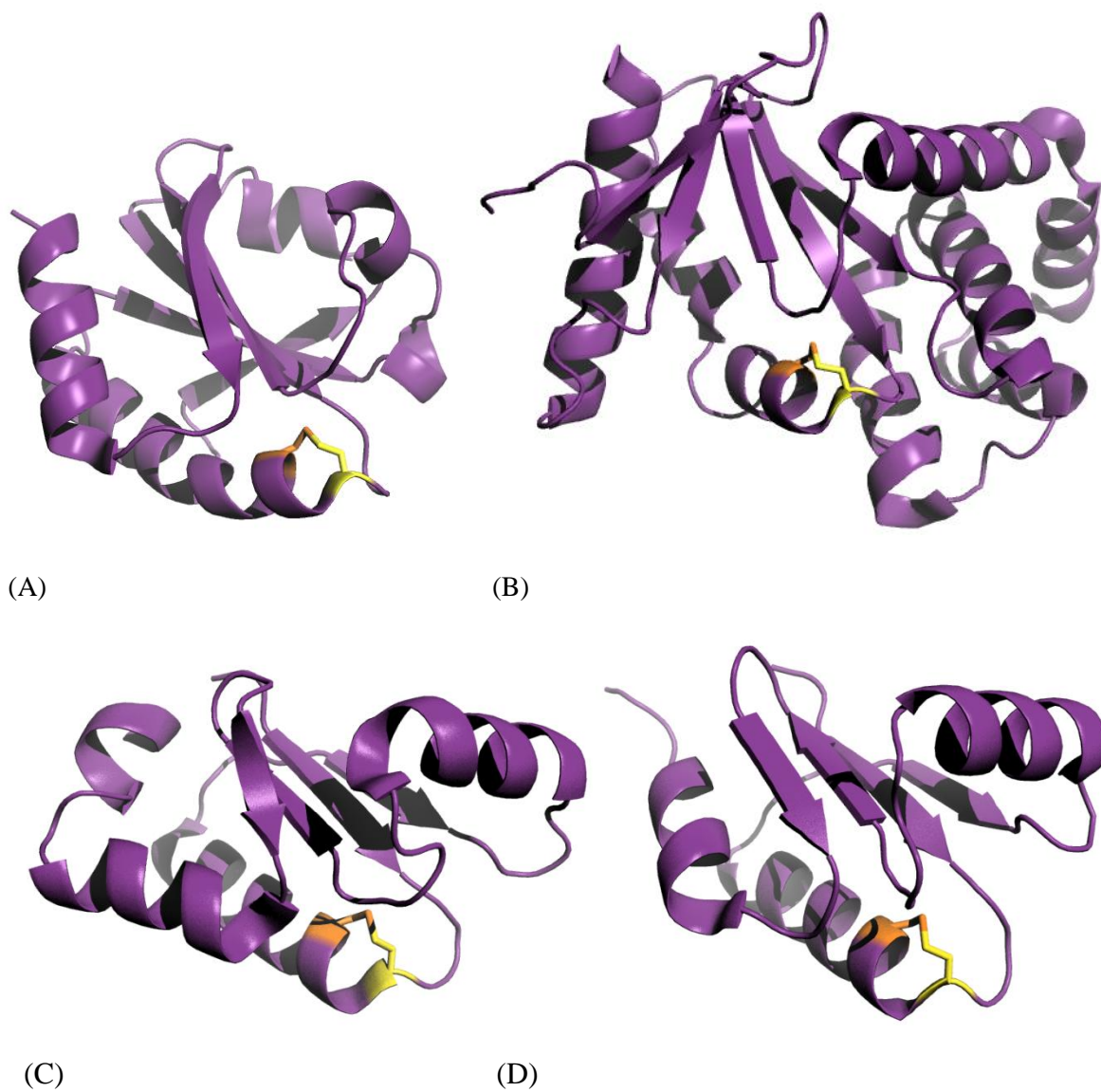

(A)

(B)

(C)

(D)

Figure 2.3 Cartoon-representations of four Trx-like proteins. (A) Trx1 (PDBid:2TRX), with a C-G-P-C motif (*38*). (B) DsbA (PDBid:1FVK), with a C-P-H-C motif (*39*). (C) Grx3 (PDB:1FOV), with a C-P-Y-C motif (*40*). (D) NrdH-redoxin (PDBid:1H75), with a C-V-Q-C motif (*28*). Disulfide bridges are highlighted in yellow.

2.3.1 The C-X-X-C Motif

Common for all thiol-disulfide oxidoreductases is the active site sequence C-X-X-C motif. The two cysteine residues in this motif can reversibly form a disulfide bond, enabling Trx-related proteins to participate in disulfide exchange reactions (*41*). The residues between the two cysteines vary among the different protein classes, including Trxs and Grxs. In *E. coli* Trx, the disulfide bridge is formed from Cys32 and Cys35, spaced by Gly33 and Pro34. Cys32 is the N-terminal nucleophilic cysteine, while Cys35 is the C-terminal, buried cysteines. This conserved four-amino acid motif is located on a protrusion formed by residues 29-37, at the C-terminus of β2 and in the beginning of α-helix 2, located on a surface loop (*29, 33*). Four Grx orthologs found in *E. coli,* Grx1, Grx2, Grx3 and Grx4, generalized into three different isoforms. Grxs 1 and 3, belonging to the first isoform, in addition to the second isoform Grx 2, all share a classical C-P-[F-Y-W]-C active site sequence (*42*). Grx4, a member of the last group of Grxs, is a monothiol enzyme containing an active site C-X-F-X motif, usually Cys-Gly-Phe-Ser. (*43, 44*). NrdH-redoxins typically include a C-[VM]-Q-C motif (*37*). Other variations to the two residues flanking the redox active cysteines are found among additional members belonging to the Trx superfamily. DsbA, a previously mentioned Dsb disulfide oxidoreductase, contains an active site conserved C-P-H-C motif in the Trx domain (*45*), while the eukaryotic PDI contains the active site sequence C-G-H-C (*46*).

2.4 The Thioredoxin system

Both Trxs and Grxs are involved in cellular reduction pathways using NADPH as an electron donor (*47, 48*). The highly reducing NADPH gives two electrons, which is ideally suited to drive reduction of disulfides. The electrons from NADPH are transferred via a class of homodimeric enzymes called pyridine nucleotide disulfide oxidoreductases. These enzymes also contain redox-active thiols, positioned in a conserved Cys-Val-Asn-Val-Gly-Cys redox catalytic site, that channel the received electrons to specific acceptors (*49*). TrxR and Gor are examples of such proteins, that reduce Trx and Grx, respectively (*48*).

E. coli Trx1 was first discovered as the electron donor for RNR (*21*). Based on sequence similarity, a second Trx, Trx2, was also discovered as a reductant for RNR, despite some structural and functional differences compared to Trx1 (*50*). Grx1 was discovered as an alternative electron donor for RNR, coupling the reducing capacities of GSH and Gor to the enzymatic formation of deoxyribonucleotides (*35, 51, 52*). In addition to their involvement in electron transfer in several enzymatic systems, members of the Trx superfamily are involved

in a range of other cellular functions, such as signal transduction pathways, sulfate assimilation and involvement in oxidative stress response (*53-55*). While Grx shuttles electrons from NADPH through Gor via GSH, both Trx and NrdH transfer electrons to their substrate from NADPH via TrxR as illustrated in Figure 2.4.
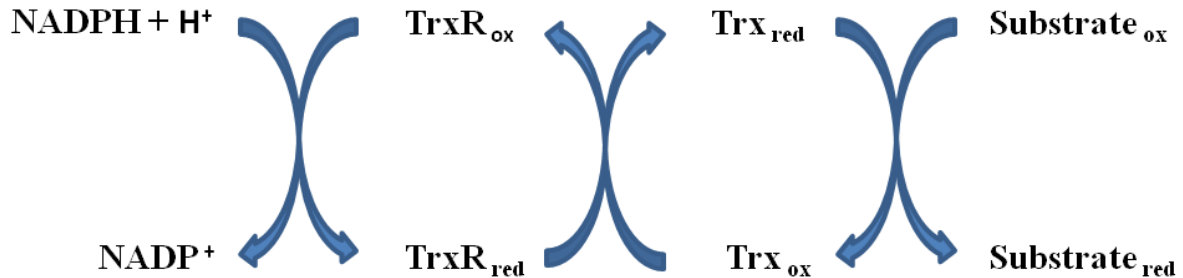
Figure 2.4 The electron flow mediated by TrxR and Trx. Oxidized Trx is reduced by Trx reductase, which receives reducing equivalents from NADPH.

2.4.1 Electron Transfer in Thioredoxin

A simple equation for the reduction of a disulfide is (*48*):

$$S_2 + 2e^- + 2H^+ \leftrightarrow (-SH)_2 \tag{1}$$

Trx is a very efficient disulfide reductant. *E. coli* Trx has a redox potential of -270 mV (*56*). Due to this low reduction potential, Trx can efficiently transfer two electrons when altering between the oxidized disulfide and the reduced dithiol states. The reduction potentials of thiol-disulfide reactions are correlated with the pK_a value of the surface exposed N-terminal reactive cysteines. A low redox potential has been correlated with a relative high pK_a value and vice versa. As already mentioned, proteins having the Trx-like fold play different roles in the cell. In order to span such a functional diversity, the redox potential of the active site cysteine pair has to be tuned to match its substrate. The redox properties, and hence, pK_a values, can depend on the nature of the two residues separating the cysteines of the active site motif, resulting in altered reduction potentials among the various members of the Trx superfamily (*57*) Also, the character of these residues is crucial for enzymatic activity, playing a significant role in enzyme-substrate affinity and the determination of protein function (*58*). Experiments have proven that the -X-X- residues in the active site motif contribute to changes in the pK_a values, and hence the tuning of redox potentials (*56*). Table 2.1 shows the

relationship between the redox potential of the thiol-disulfide reaction and the pK_a value of the nucleophilic cysteines, for different proteins having the Trx-like fold.

Table 2.1 Comparison of nucleophilic cysteine pK_a values and disulfide midpoint-potentials for proteins with Trx-like fold.

Protein	pK_a	E' (mV)	Active site motif
S. aureus Trx	7.1 (*59*)	-268 (*59*)	Cys-Gly-Pro-Cys
E. coli Trx	7.1-7.4 (*60*)	-270 (*61*)	Cys-Gly-Pro-Cys
T. brucei Tryparedoxin	7.2 (*62*)	-249 (*62*)	Cys-Pro-Pro-Cys
B. cereus BC3987	7.3 (*63*)	-271 (*63*)	Cys-Pro-Pro-Cys
E. coli NrdH	n.d.[a]	-248 (*18*)	Cys-Val-Gln-Cys
E. coli DsbA	3.3-3.5 (*57, 64*)	-122 (*57*)	Cys-Pro-His-Cys

a) n.d. is an abbreviation for not determined.

The two cysteine residues in *E. coli* Trx are Cys32 and Cys35. The side chain of Cys32 is exposed to the solvent, and has a lowered pK_a value, close to physiological. The need to lower the thiol pK_a value from approximately 9 to 7 is crucial to drive efficient thiol-disulfide exchange reactions at physiological pH values (*48*). This makes the N-terminal cysteine a good nucleophile. In order to give disulfide reductants low reduction potentials, nature has evolved enzymatic systems with the Cys32 thiol initiating the nucleophilic attack positioned in a special microenvironment. The deprotonation of this nucleophilic cysteine, leading to a lowered pK_a value, has been suggested to involve contributions from several factors, including assistance from a alpha-helix dipole (*65*), charge-charge interactions (*66*) and intra-protein hydrogen bonding (*67*). It has been proposed that the latter is the leading determinant to be considered when predicting pK_a values, resulting in the suggestion that the low pK_a value of the N-terminal Cys32 is due to hydrogen bonding to the Cys35 amide proton (*68, 69*). On the other hand, the pK_a value of Cys35 is estimated to values up to 4 units higher, making this residue virtually unreactive (*41, 70*). As an explanation to the second nucleophilic attack performed by the buried C-terminal cysteine, the participation of a proximal, conserved residue has been proposed. An aspartate residue at position 26 conserved in Trxs from different species, is thought to be able to act as an acid or base in oxidation and reduction reactions, respectively, catalyzed by Trx (*41, 71*). The carboxylate of Asp26 is positioned near the active site. Through the action of a neighboring water molecule, the carboxylate possibly acts as a general acid/base catalyst in the deprotonation of the thiol of Cys35, which can facilitate the attack on Cys32. This hypothesis has later been supported by the analysis of a 1

Å resolution structure of oxidized Trx from *Acetobacter aceti*, where a water molecule is aligned between Asp26 and Cys35, well positioned to participate in proton transfer between the Asp26 and Cys35 side chains (Figure 2.5) (*72*).
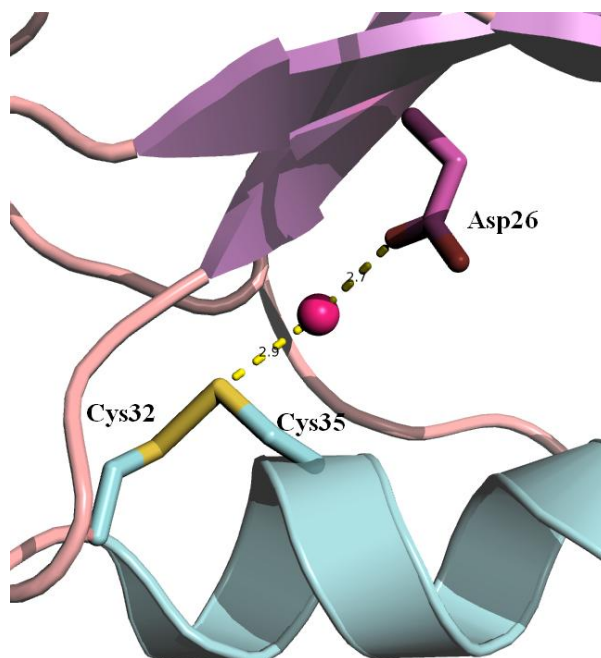
Figure 2.5 The active site of *A. aceti* Trx, displaying a water molecule, possibly involved in general acid/base catalysis, aligned between the buried Cys35 and a neighbouring Asp26 (PDBid:2I4A).

However, reduced crystal structures of Trx showing this feature are yet not solved. Even though the replacement of Asp26 in Trx strongly impairs the catalytic reaction rate in the redox reactions of Trxs (*73*), the deprotonation mechanism of the buried Cys35 is still debated (*41*). The fundamental mechanism of Trx-mediated electron transfer, proposed by Kallis and Holmgren in 1980 (*74*), is explained using *E. coli* amino acid numbering in Figure 2.6. Electrons pass from reduced Trx to the substrate via several steps. The initial nucleophilic attack on the disulfide substrate involves Cys32, with the formation of a mixed disulfide (Figures 4A and 4B). The next step, involving deprotonation of Cys35, makes the second nucleophilic attack caused by this thiolate possible. This resolves the mixed disulfide intermediate, generating a dithiol in the substrate (Figures 4C and 4D). The proton abstraction necessary to induce the nucleophilic attack of the last thiolate, illustrated in step **2**, is possibly assisted by Asp26, but not completely understood. Other features causing variations to the possible catalytic role of Asp26, is the lack of amino acid residues analogous to the *E. coli*

Trx and *A. aceti* AaTrx Asp26 in other subclasses of the Trx superfamily. Examples of such groups of proteins, posessing Trx functionality, are the NrdH-redoxins, previously described as the reductants of NrdE of bacterial class Ib RNR, and *Clostridium pasteurianum* Cp9-redoxins, involved in the reduction of various hydroperoxide substrates (*75*).

Figure 2.6 Stepwise representation of the mechanism for Trx-mediated electron transfer. The Figure is taken from Røhr and Andersson (*63*).

2.5 The BC3987 Thioredoxin

A large number of bacteria encoding class Ib RNR genes, including NrdH-redoxin, have the genes arranged in an *nrdHIEF* operon. One exception is the class Ib RNR operon in members of the *Bacillus cereus* group, which contain an *nrdIEF* operon, lacking the redoxin gene *nrdH*. The *in vivo* reductant of the class Ib R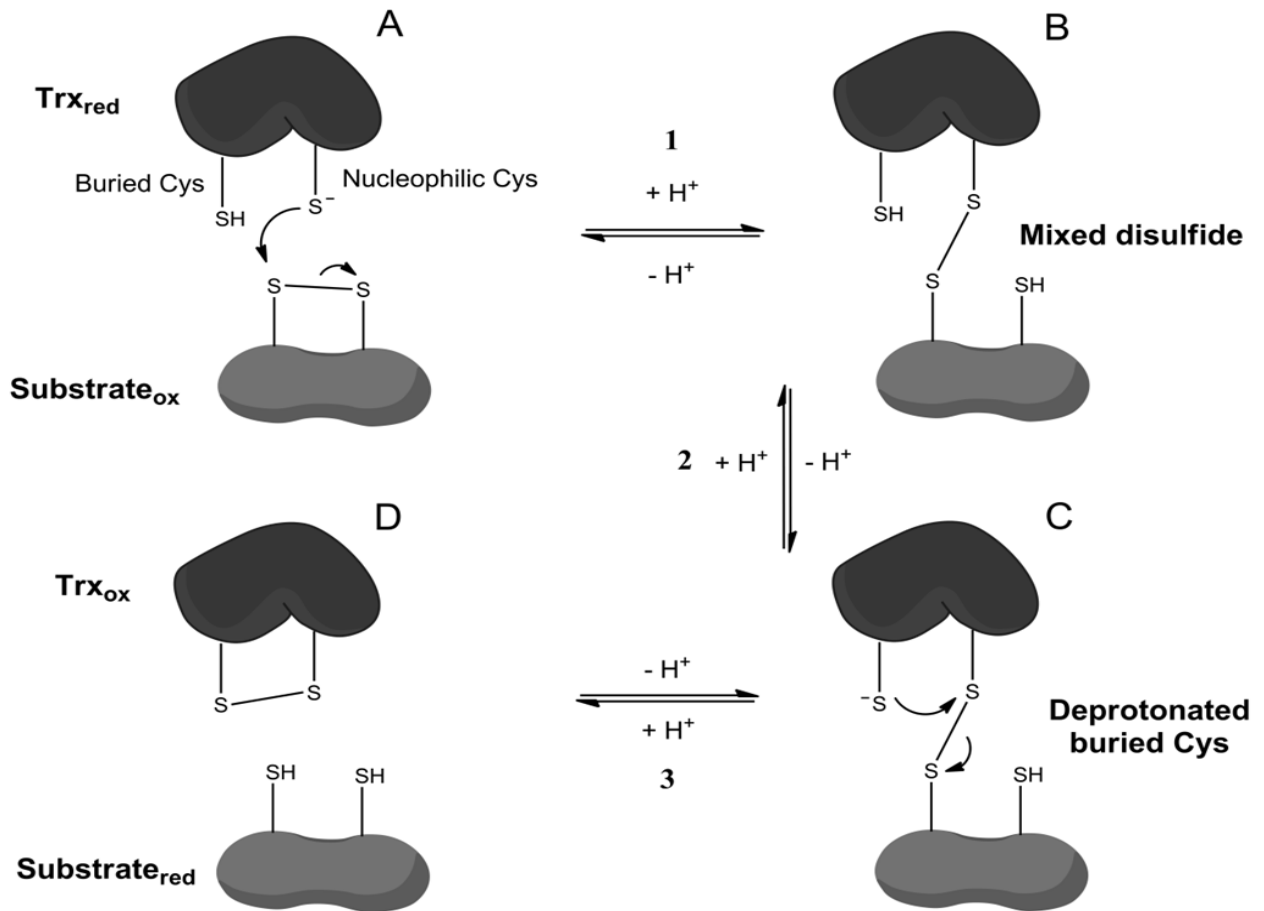NR in these bacteria is not known. However, a protein homologous to the NrdH-redoxins and Cp9-redoxins has been located in the *B. cereus* genome. Based on significant amino acid sequence similarity with NrdH, this protein has been proposed to serve a similar role in the reduction of RNR. This 8.9 kDa Trx, named BC3987, includes several residues that are also highly conserved in NrdH-redoxins, in addition to the cysteines in the C-X-X-C motif. Like NrdH, it also contains the typical α/β/α fold, common for all members of the Trx superfamily. Based on phylogenetic analysis performed by Røhr and Andersson (*63*), BC3987 has shown high amino acid sequence identity to the Cp9-redoxin, which is specialized in reducing peroxiredoxins. This amino acid sequence identity, observed for the *Bacillus* genus BC3987 homolog group and the Cp9 homolog's, is even higher than when BC3987 is compared to the NrdH-redoxin. Another feature involving both the BC3987 and Cp9, is the hydrophobic residue at the suggested TrxR binding site (position 44, BC3987 numbering) in these two proteins, which is deleted in NrdH-redoxins. Contrary to the typical active site motif seen in NrdH, C-[VM]-Q-C, BC3987 contains the more rigid C-P-P-C motif, with the N-terminal and C-terminal cysteines in amino acid positions 12 and 15, respectively. From these findings, one might expect a closer structural and perhaps functional relationship for BC3987 and the Cp9, suggesting that BC3987 may instead serve a role in peroxide degradation in the defence against oxidative stress in *B. cereus* (*63*).

None of the three Trxs mentioned above; BC3987, Cp9 or NrdH, contain an acidic amino acid residue similar to Asp26 in Trx, believed to participate in the deprotonation of the C-terminal cysteine in *E. coli*. Phylogenetic analysis performed by Røhr and Andresson (*63*) has shown that within the 6 amino acids preceding the C-X-X-C motif of Trx-like proteins, there are, in addition to the conserved Asp26 residue found in Trx, additional conserved residues preceding the active site in other Trx-like proteins. Asp, Thr and Ser residues are conserved in various members of the Trx-like proteins, suggested to affect the activity of the enzymes. Table 2.2 displays a categorization of active site motifs in Trx-like proteins.

Table 2.2 Active site motifs in Trx-like proteins. Investigation based on all sequences between 60 and 160 amino acids in the Integrated Microbial Genomes database (http://img.jgi.doe.gov) containing a X(6)-C-X-X-C motif. Table taken from Røhr and Andersson (*63*).

Active site motif	x-x amino acids			
	Thioredoxin	*Glutaredoxin*	*NrdH*	*Other*
	G-P	P-[FYW]	[VIM]-Q	P-P
X(6)-C-X-X-C	1606	661	224	136
X(2)-[ST]-X(3)-C-X-X-C	78	397	223	72 (59 T, 13 S)
[DE]-X(5)-C-X-X-C	1483	0	0	33
[DE]-X-[ST]-X(3)-C-X-X-C	39	0	0	9

Contrary to what is seen in most Trxs, a conserved threonine residue prior to the active site motif has been localized in Cp9, NrdH and BC3987 (See Table 2.2). Using BC3987 numbering, this Thr8 residue is found four residues preceding the C-X-X-C motif. Unlike typical Trxs, BC3987 appears to stabilize both active site cysteines in their deprotonated thiolate forms (*63*). The stabilization of these thiolates, which both appear to have lowered pK$_a$ values, is thought to be assisted by Thr8 through hydrogen bonding. A glutamine residue, Gln9, also found in the vicinity of the active site, is also thought to be a potential hydrogen donor to to BC3987, with its amide hydrogen forming a hydrogen bond to the C-terminal buried Cys15 Sγ-atom. As seen from the crystal structure of NrdH, the hydroxyl group of the Thr side chain points towards the C-terminal buried cysteines. Contrary to this, Thr8 in BC3987 has shown to have a different rotamer, where the hydroxyl group is pointing away from the buried Cys Sγ-atom. A hydrogen bond to a water molecule has proven to stabilize this orientation. Regardless of these structural differences, a reaction mechanism for disulfide reduction carried out by Trxs similar to BC3987, NrdH or Cp9, including the Thr rotamer typically observed in *E. coli* NrdH (*28*) and *Corynebacterium ammoniagenes* NrdH (*76*), has been suggested by Røhr and Andersson (*63*) (Figure 2.7). A feature supporting this mechanism regarding BC3987 is the presence of threonine or serine residues preceding the active site in a tryparedoxin in the parasite *Crithidia fasciculate*, possessing the same active site (*77*). Moreover, the consequences of the rigidity of the C-P-P-C active site motif are still unclear. Considering the similarity of the Thr8 environment with the conditions surrounding Thr7 in *E. coli* NrdH, a low energy barrier between the two seems likely. Also, the conserved Thr/Ser residue found in the position 4 amino acids preceding the N-terminal Cys in NrdH and Trx-like proteins encompassing a C-P-P-C active site motif (See Table 2.2), reinforces the idea of a common catalytic mechanism. The effects of a second threonine residue close to the active site of BC3987, Thr53, might also affect the active site Cys pK$_a$ of BC3987 (*63*).
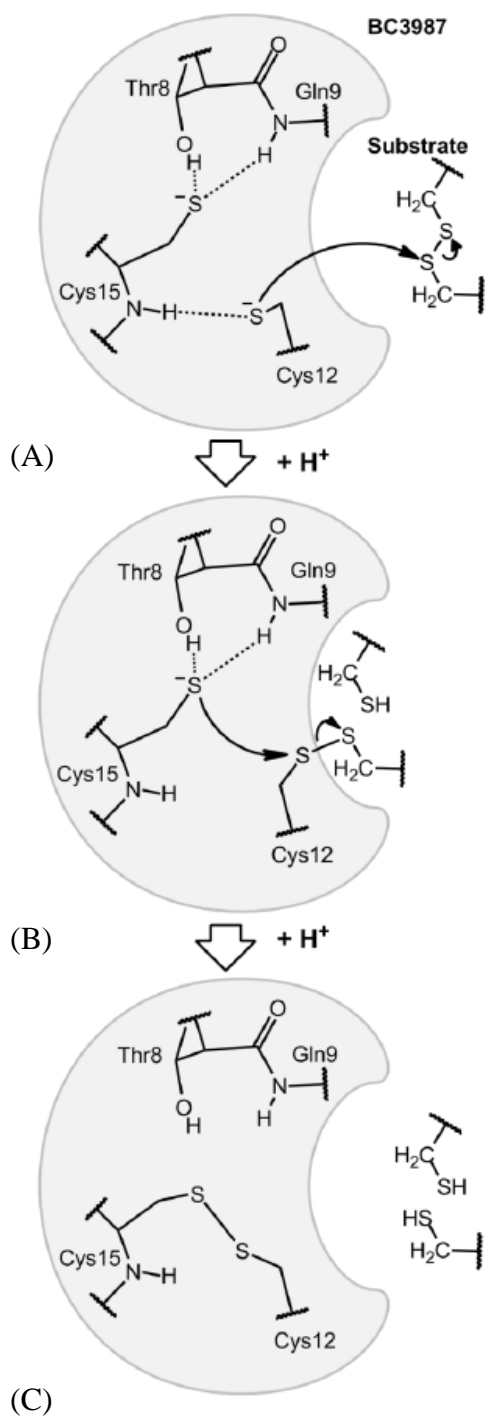
Figure 2.7 A possible substrate reduction reaction mechanism for BC3987 involving two active site thiolates. (A) The reaction is initiated by a nucleophilic attack on the substrate disulfide bridge by the Cys12 thiolate and a mixed disulfide intermediate is formed. (B) The buried Cys15 Sγ-atom that is stabilized in its thiolate form by hydrogen bonding toThr8 and Gln9 perform a second nucleophilic attack on the Cys12 Sγ-atom. (C) The reduced substrate is released and the two active site cysteines in BC3987 form a disulfide bridge. Figure taken from Røhr and Andersson (*63*)

2.6 Aim of the Study

The protein BC3987 from *B. Cereus* is a small Trx-like protein. Based on our present knowledge, this protein is believed to be a potential electron donor to RNR and peroxiredoxin in *B. cereus*, and hence, play a crucial role in this bacterium's survival and reproduction. Previous experiments have shown that both cysteines in the active site of BC3987 are stabilized in their thiolate form. This type of active site, differing from what is observed in *E. coli* Trx, has triggered our curiosity. Since the active site environment found in this protein is also observed in other homologous proteins, such as *E. coli* NrdH-redoxin, a better understanding of its chemistry will possibly contribute to a general reaction mechanism regarding these proteins. Studies have suggested that the thiolates are stabilized through hydrogen bonding to one or two threonines and an amide hydrogen in the vicinity of the active site. The purpose with the work performed in this thesis has been to investigate the effect of this hydrogen bonding on the pK_a values of the active site cysteines. This was performed by making mutant proteins, with point mutations made at residues near the active site. Redox potential determination, as well as pK_a measurements of the native and mutant BC3987 proteins was done. Also, structural studies of the proteins were performed, for even better understanding of the catalytic mechanism and conformation of the BC3987 Trx.

3 A Brief Description of Protein Crystallography

Protein crystallography is a widely used method to determine the three-dimensional structure of molecules.

3.1 Introduction

X-ray diffraction by crystals represents the scattering of electromagnetic radiation from different atoms within the crystal (*78*). The diffraction of X-rays can provide a precise method of analysing a regularly repeating distribution of scattering material, as in the case of a protein crystal. Using crystallography, one can achieve detailed information about macromolecular structure. The technique provides an efficient way of visualizing three-dimensional images of molecules, which can give us important knowledge about the activity, mechanism for binding of substrates, conformational changes and evolutionary relationships between the molecules (*79*). Figure 3.1 illustrates a simple X-ray diffraction experimental setup.
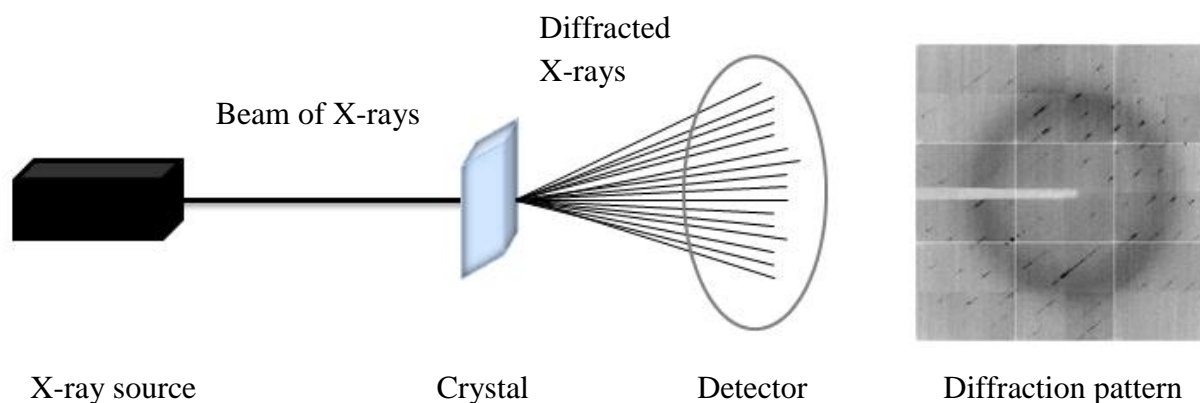
Figure 3.1 Schematic representation of an X-ray diffraction experiment. The electron density map, resulting from the diffraction pattern, leads to the interpretation of the final molecular structure.

3.2 Crystals and Diffraction

Crystals of macromolecules are highly ordered, three-dimensional aggregations of molecules (*80*). The molecules can pack together with a high degree of symmetry. The kinds of symmetry that can be possessed by a local assembly of molecules are called point groups. Due to crystallographic restrictions regarding symmetry operations on protein molecules, 32 crystallographic point groups describing seven crystal systems are allowed. The regular arrangement of crystal assembly results in each equivalent molecule to interact identically with their neighbours, meaning that every repeating unit within the crystal has the same environment. Because of this, crystals form an extended three-dimensional array of molecules; the crystal lattice (*79*). The whole symmetry of the lattice is defined by its space group, which is the complete group of symmetry operations that generate the three-dimensional crystalline lattice. 65 space groups exist for protein crystals, representing a combination of the 32 point groups, translation and screw-axis operations. Based on each equivalent molecule, or point in the crystal, a unit cell, a microscopic repeating unit of six faces, can be defined by specifying three vectors, a, b, c, and three angles α, β and γ, between the axes b-c, a-c and a-b, respectively (*81*) (Figure 3.2). As a result, the lines in the directions a, b and c of the lattice make up the x-axis, y-axis and z-axis. Hence, a crystal can be considered as a stack of unit cells with their edges forming a lattice, and the axes together forming a coordinate system (*82*).
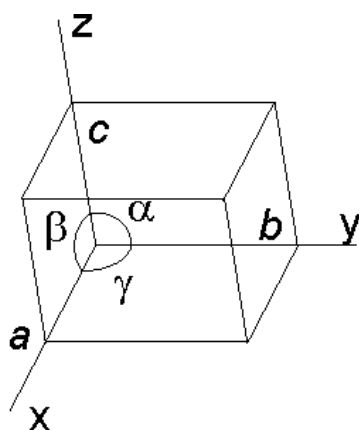
Figure 3.2 Illustration showing a three dimensional unit cell with axial lengths and interaxial angles. Figure from http://xrayweb.chem.ou.edu/notes/crystallography.html

The unit cell is a mathematical construction for describing the arrays of molecules in a crystal, and makes up the smallest unit which can build up the whole crystal by translation of the building blocks in three dimensions (*78*).

When describing diffraction from a crystal, it is useful to consider the crystal as a product of two components, the content of a unit cell and the point lattice. In the simplest cases, placing a point in each corner of the unit cell, the lattice point represents the complete content of the unit cell (Figure 3.3).
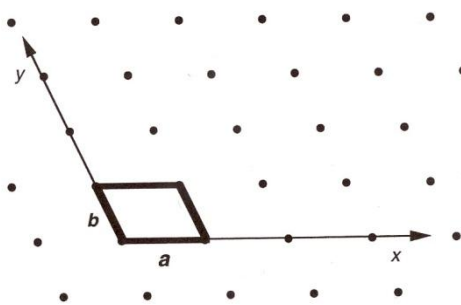
Figure 3.3 A two-dimensional lattice. Figure taken from Blow (*79*).

The lattice points are distributed in a periodic manner through space, and sets of three-dimensional planes can be drawn through the lattice (*80*). When these planes are constructed through the lattice points, diffraction of X-rays by a crystal can be thought of as reflection against the planes. Within a set, the planes are parallel and equidistant with perpendicular distance. The distance along the unit cell edges between pairs of lattice planes can be used to label a particular set of lattice lines. Three integers define a given family of planes. These are called Miller indices, designated h k l, which intersect the unit cell axes at positions $^{a}/_{h}$, $^{b}/_{k}$, and $^{c}/_{l}$ (Figure 3.4). A set of lattice planes is determined by these three indices if the planes cut the x-axis in a/h, y in b/k and z in c/l. If a plane intercepts the axis at infinity (the plane is parallel to the axis), that particular index is 0 (*82*). As the indices become larger, the lattice spacing becomes shorter. X-ray diffraction about the h k l planes can be measured, as a direct consequence of the atomic distribution about them (*80*).

b/1

z

hkl = (110)

y c/∞

x

a/1
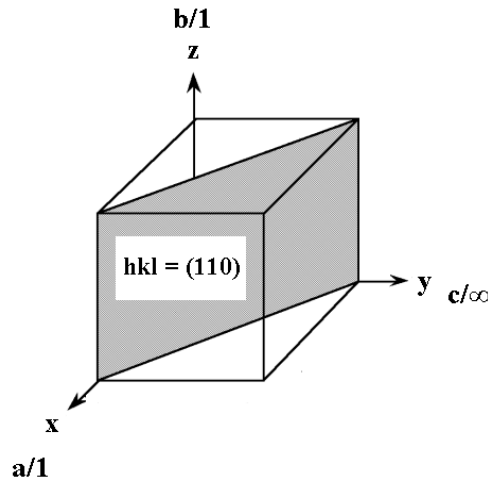
Figure 3.4 A three-dimensional unit cell with intersecting (1,1,0) planes.

The scattered X-ray waves from each set of parallel planes interfere with each other either constructively or destructively, producing a diffraction pattern on a detector. The incident X-ray radiation creates a Bragg peak if the reflection off the lattice planes interfere constructively, meaning that the rays travel the same distance and are in phase (*79*). These diffracted beams reinforce each other by constructive interference with a single reflection arising from each equivalent lattice plane in the crystal. All other diffracted beams undergo some destructive interference, and their resulting weakened intensity does not contribute to the detected Bragg reflections. (*81*) The intensity of the diffraction spots depends on the distribution of atoms in the sample through which X-rays pass, and therefore, the content of the unit cell. The resulting diffraction pattern depends on the nature of the crystal lattice.

Bragg's law shows that the scattered waves remain in phase, contributing to diffraction, only when the path length difference between two waves is equal to an integer value of n, which represents a whole number of wavelengths. The condition for the constructive interference described by Bragg depends on three quantities; the angle of incidence and reflection, θ, the interplanar spacing d for the h k l family of planes, and the wavelength λ of the X-rays.
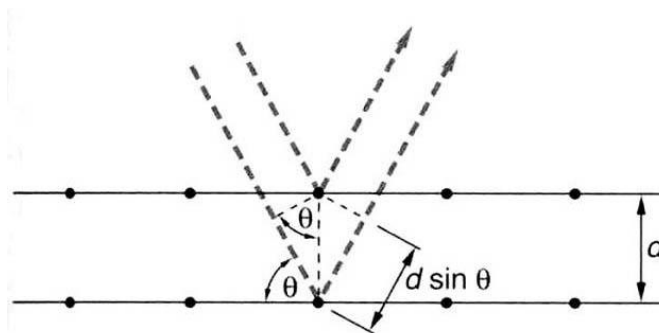
Figure 3.5 Schematic illustration of Bragg's law. d is the distance between two lattice planes, while θ represents the angle of incoming radiation. Figure taken from http://www.farmfak.uu.se/farm/farmfyskem-web/instrumentation/saxs.shtml

The formulation of Bragg's law for a three-dimensional point lattice is described as:

$$\lambda n = 2dsin\theta \tag{2}$$

This indicates that the X-rays incident on lattice planes, at an angle θ, are reflected when obeying Bragg's law of diffraction (*80*).

The reciprocal lattice or reciprocal space illustrates the relationship between the spacing of atoms within the crystal, and the pattern of Bragg reflections obtained during diffraction. This real-space lattice is reciprocally related to points in the crystal lattice, with inverse unit cell dimensions a*, b*, c*, α*, β*, γ*, meaning that the measurements made during a diffraction experiment are directly related to the spacing in the diffracting object (*81*). In practice, this means that small spacing between Bragg reflections represent a large unit cell. The Ewald sphere illustrates this geometrical relationship between the orientation of the crystal and the direction of the X-ray beams diffracted by it (*78*) (Figure 3.6). Inspections of the diffraction pattern allow calculation of the dimensions of the reciprocal lattice, and hence, tell us the orientation and dimensions of the crystal lattice axes.
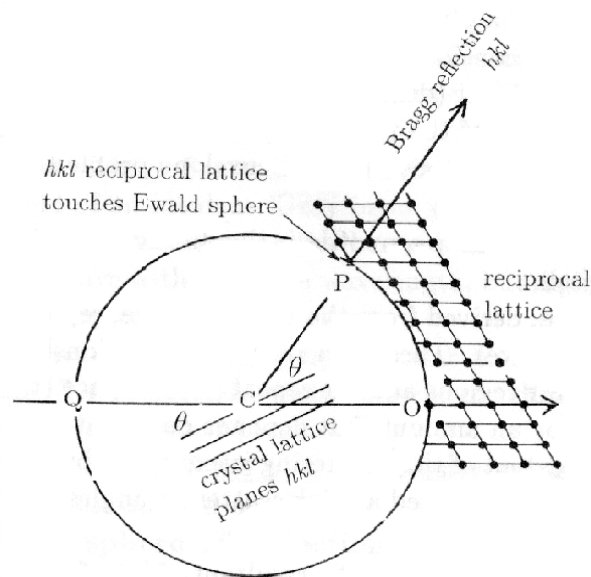
Figure 3.6 The Ewald sphere, used as a tool to construct the direction of the scattered beam. The construction obeys Bragg's law, and indicates observable reflections for a given crystal orientation related to the incident beam. The sphere has radius CO = $1/\lambda$. The origin of the reciprocal lattice is O. Figure taken from Glusker *et al*. (*78*).

3.3 Synchrotron Radiation

Crystallographic structure determination depends upon coherent scattering. This is a result of an electron absorbing an encountered X-ray photon, achieving vibration at X-ray frequency, and finally emitting an X-ray photon of the same wavelength in a random direction. In order to penetrate biological materials sufficiently to be scattered from the whole crystal volume, X-ray used in crystallography typically exhibit wavelengths in the range between 1.6 Å and 0.5 Å (*79*). This range is of the same order of magnitude as chemical bonds, allowing "visualization" of inter-atomic distances. Synchrotrons are the most powerful and intense X-ray sources. Because larger molecules, such as proteins, diffract X-ray beams less than crystals of small molecules, these high intensity sources are preferred in protein crystallography studies (*82*). Synchrotron radiation is created when electrons are accelerated to relativistic velocities in an electron storage ring. Under the influence of a magnetic field, the electrons are forced into a curved track, and the magnetic field causes the charged particles to change their direction. This deacceleration makes the electrons emit excess radiation in the form of a powerful X-ray beam (*81*). The electrons are circulated around the storage ring, and the stream of X-rays is released at a tangent to the orbit and guided through to beamlines, which allows for data collection at various positions (Figure 3.7).

Figure 3.7 Radiation occurring when a relativistic electron travels in a uniform magnetic field, executing a circular motion with acceleration directed toward the centre. Figure taken from Atwood (*83*).

There are three types of magnetic devices commonly used in storage rings: bending magnets, wigglers and undulators, generating various radiation profiles (Figure 3.8). Bending magnets cause a single curved electron path. Particles travel in a circular trajectory, due to the homogenous magnetic field. Insertion devices like undulators and wigglers are more powerful devices inserted into straight sections of the electron beam, and have a repeating structure of dipole magnets with alternating polarity. The alternating magnetic field in an undulator generates sharp bends in the electron trajectory, forcing the electrons to undergo oscillations and radiate. The relatively weak magnetic field contributes to constructive interference of the emitted waves, which results in intense, low-divergence radiation of high brightness. In a similar kind of insertion device, the wiggler, fewer dipoles and a stronger magnetic field produces a continuous, broad radiation spectrum of high flux.

(A)   (B)   (C)
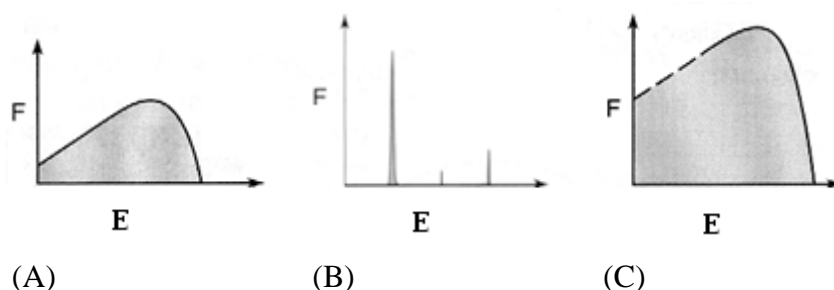
Figure 3.8 The radiation spectrum resulting from different magnetic devices. (A) Bending magnet radiation. (B) Undulator radiation. (C) Wiggler radiation. The frequency spread (energy) of undulator radiation can be very narrow. Figures taken from Attwood (*83*).

Radiation created at synchrotron facilities encompass several advantages over traditional laboratory-scale X-rays. Synchrotron radiation is extremely intense, and highly collimated. The latter refers to a low divergence and convergence of the beam, resulting in sharper diffraction spots. Although the energy spectrum is wide, any suitable wavelength within this range can be sealed with a monochromator. Hence, the radiation is tunable. Furthermore,

synchrotron radiation is emitted in very short pulses, allowing observation of structural changes in the nanosecond time scale. Synchrotron radiation is also highly polarized (*82*).

The European Synchrotron Radiation Facility (ESRF) in Grenoble, France (Figure 3.9), has a Storage Ring with a circumference of 844.39 meters, is operated with an energy of 6 GeV injected from the Booster, and has bending magnets with a magnetic field strength of 0.86 T. The shortest wavelength achieved is $\lambda = 0.6$ Å (*82*).
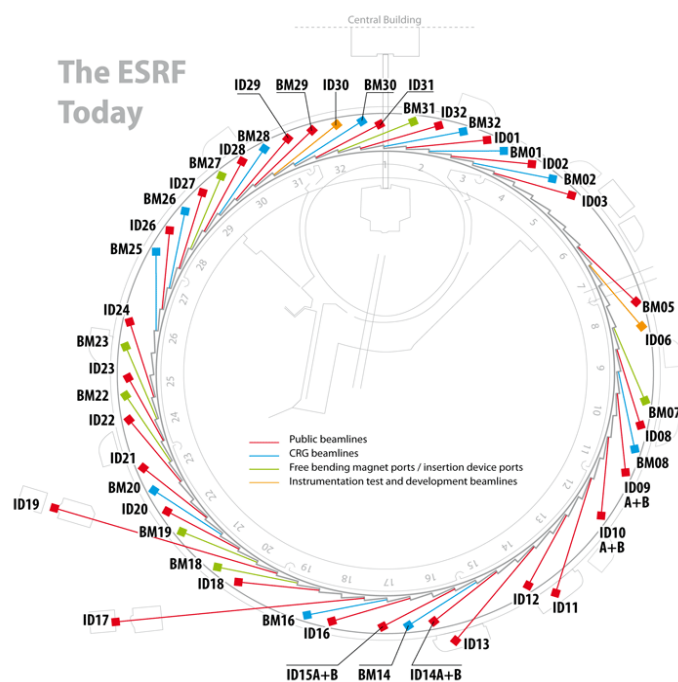
(A)

(B)

Figure 3.9 (A) A plan showing the experimental hall of the ESRF, with links to the 40 beamlines. (B) Photograph of the ESRF**.** Figures taken from http://www.esrf.eu/

3.4 Protein Crystallization

3.4.1 Protein Solubility and Crystallization

The first requirement for protein structure determination is crystallization. There are many parameters as well as the use of different crystallization methods that influence nucleation and crystal growth of biological macromolecules (*84*). Crystallization of protein molecules involves bringing the protein solution to a supersaturation state. This depends on the protein concentration and different parameters affecting the solubility of proteins. Many factors influence crystal growth. Conditions such as pH and temperature can affect solubility drastically, and the inclusion of additives such as detergents and hydrophobic polymers will most often decrease protein solubility, promoting crystallization (*85*). A typical solubility curve of phase diagram for a protein as a function of salt concentration illustrates the various levels of supersaturation (Figure 3.10), with decreasing protein solubility and hence, induced crystal growth, at high and low salt concentrations.
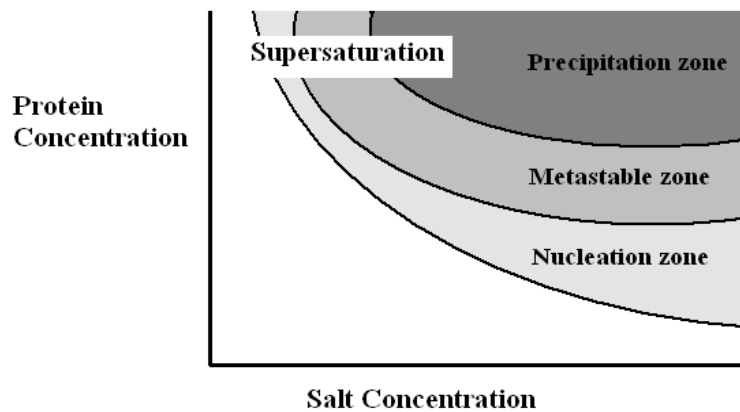
Figure 3.10 A typical solubility curve of phase diagram for a protein.

This is due to the salting-out and salting-in effects, respectively. In an initial accumulation-stage, small protein aggregates are formed, which serve as nuclei for crystal growth. This happens in the nucleation region, which has a level of higher supersaturation than the region required for a slow and stable crystal growth. To avoid the formation of too many small crystals, a reduced level of supersaturation is acquired. In the metastable region, crystals are allowed to grow slowly to reach a maximum degree of order in their structure (*82*). Consequently, the first intention in a successful crystallization experiment is the achievement

of crystal nuclei in the nucleation phase, followed by a transition to lower supersaturation in the metastable phase, where only growth is supported (*85*).

3.4.2 Methods of Crystallization

Vapour diffusion techniques are the most frequently used crystallization methods. A droplet containing the protein mixed with an equal amount of buffer, crystallizing agent and other additives is equilibrated against a reservoir containing a solution of crystallizing agent at a higher concentration than in the droplet. The difference in concentration drives the system towards equilibrium by diffusion through the vapour phase. This leads to a droplet volume change, resulting in an increased protein-and salt concentration. The vapour pressure in the droplet and in the reservoir will approach each other and at some point, if correctly setup, the drop will become supersaturated and crystallization starts. (*84, 86*). Two types of vapour diffusion setups are widely used; hanging drop and sitting drop (See Figure 3.11). A third setup, the sandwich drop, is less frequently used. The same principle applies for all methods, which differ only in the setup procedure.

(A)   (B)
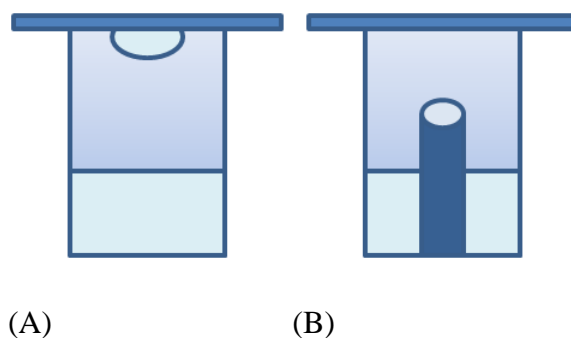
Figure 3.11 The most common vapour diffusion techniques. A droplet containing the protein mixed with the mother liquor is equilibrated against a reservoir containing the mother liquor. (A) Hanging drop. (B) Sitting drop.

In batch crystallization methods, all components are combined into a single solution. A supersaturation level sufficient for nucleation must be achieved directly in the vials containing protein mixed with crystallizing agent. Following nucleation, the protein concentration drops and reasonably large crystals can be obtained in the metastable region (*85*).

In addition to the crystallization methods described above, other methods can be used to obtain adequate crystals, such as dialysis and liquid-liquid diffusion.

3.4.3 Seeding

In order to enhance the crystallization procedure, seeding may provide an effective way to favour the optimization of crystal growth conditions. In favour of producing large, single crystals, it might be essential to decouple crystal growth from nucleation, which can be achieved with the aid of methods like microseeding or macroseeding. The latter consist of the introduction of pre-grown, washed crystals into a pre-equilibrated protein solution. Streak seeding is a popular microseeding technique, which involves the transfer of microscopic crystals from a seed source to a non-nucleated protein solution using an animal whisker (*87*).

3.4.4 Cryo-Crystallography

Protein crystals suffer rigorous radiation damage during room temperature X-ray data collection. Radiation damage is caused initially by primary interactions between the atoms in the crystal and the beam, during which the X-rays lose energy by the photoelectric effect. This might lead to the production of reactive radicals, which due to thermal energy, are allowed to diffuse through the crystal causing secondary radiation damage. Cooling the samples for data collection to cryogenic temperatures (around 100 K) greatly reduces radiation damage and hence, leading to better data, since most of the reactive products are kept immobilized in the crystal (*88*). Cooling with liquid N_2 has proven to be a fast and simple solution (*89*).

Prior to crystal cooling, the crystal needs to be soaked in a cryo-solution, which is usually created by adding cryo-agents (antifreeze) to the original mother liquor stock solution. The antifreeze, in addition to a rapid freezing-rate, enables the crystal to be cooled with no ordered ice formation; instead, a vitreous glass is formed on the crystal surface (*88*). The most generally used technique for mounting single crystals is the loop mounting method, in which the crystal is not in contact with any mechanical support, but rather held by surface tension in a thin film formed in a wire loop. The solution making the film consists of the crystallization buffer mixed with a hydrophilic cryo-protectant like polyethylene glycol (PEG) or glycerol. Crystals are first transferred to the suitable solution and then lifted out with the loop, prior to exposure to N_2 (*90*).

Cryo-cooled crystals tend to exhibit an increased mosaicity compared to crystals at room temperature. Soaking in cryo-solutions added antifreeze prior to cooling is crucial for successful crystal freezing. It may also reduce the mosaicity, and consequently, improve the quality of the crystal data (*88*).

3.5 Crystal Structure Determination

Since no X-ray lens is available, the scattered X-ray beams in a diffraction experiment cannot be converted directly into an image, as when using conventional microscopes. Consequently, there is no way to observe the time of arrival of the peaks of X-rays scattered from different directions. The difficulty in determining the phase of a scattered wave is referred to as the phase problem. This prevents us from calculating what the image looks like, and the use of indirect computational procedures becomes crucial for structure determination (*79*). The intensity of a diffracted beam (h k l) provides information about the molecular content of the unit cell, and is proportional to the square of the amplitude. The amplitude is called the structure factor F(h k l). Hence, the structure factor is considered as the square root of the intensity; $\sqrt{I} = F$ or $F^2 = I$. The structure factor is a function of the atomic distribution in the crystal, and sums up all atoms in the unit cell:

$$F(hkl) = \sum_j f_j\, e^{2\pi i(hx+ky+lz)} \tag{3}$$

The structure factor can also be written in a different form, as a function of the electron density:

$$F(hkl) = V \int_{x=0}^{1} \int_{y=0}^{1} \int_{z=0}^{1} \rho(xyz)\, e^{2\pi i(hx+ky+lz)} \tag{4}$$

With an integration over a continuous range of electrons in a unit cell. The structure factor is the Fourier transform of the electron density, and equally, the electron density is the Fourier transform of the structure. Therefore, the electron density at every position in the unit cell can be calculated, and ρ(x y z) can be written as the function of all F(h k l):

$$\rho(xyz) = \frac{1}{V} \sum_h \sum_k \sum_l |F(hkl)|\, Cos2\pi[hx + ky + lz - \alpha(hkl)] \tag{5}$$

The electron density is a summation of many electron density waves, where all reflexes contain partial information about the whole crystal structure.

Because $I(h\ k\ l) = |F(h\ k\ l)|^2$ the amplitudes can be found, but the phase angles, $\alpha(h\ k\ l)$, cannot be derived directly from the diffracted pattern. Several methods exist for solving the phase problem, and might be used to overcome this complication (*82*).

3.5.1 Solving the Phase Problem

In macromolecular crystallography, the most preferred approaches used for solving the phase problem are multiple isomorpous replacement, anomalous scattering and molecular replacement. Regarding small molecules, direct methods are frequently used. The Patterson function, describing vectors between atoms, is a powerful tool for finding atomic positions, and a crucial part of phasing techniques.

Molecular replacement is a technique used if the general fold of the unknown protein structure is believed to resemble that of a previously determined protein structure, and relies upon the homology between these. A search procedure is used to collect all possible orientations and positions of the reference molecule in the target unit cell, using the calculated Patterson maps for both structures. The operation is done performing a rotational search and a translational search, respectively. The three rotation angles and three translation parameters for which the calculated structure factors agree most closely, provide a good correlation between the structures, and a valuable model for the target crystal (*91*).

In the case of anomalous scattering and isomorphous replacement, the scattering power of a few, defined locations in the unit cell are changed, creating reference waves within the crystal. In isomorphous replacement, this is accomplished by the introduction of a heavy atom ions or compounds to specific locations in the crystal asymmetric unit of the protein. The anomalous scattering method depends on the presence of sufficiently strong anomalously scattering atoms in the protein structure itself, whose scattering power is varied by changing the wavelength of the X-rays. The introduction of selenomethionine into the growth medium of bacteria is a widely used approach (*80*). The comparison of crystals with different scattering qualities is the basis for both these phasing techniques, differing mainly in the choice of references.

3.5.2 Crystal Structure Refinement

All the inputs necessary to produce the electron density map are subject to experimental error, which consequently result in errors in the map. To arrive at a high resolution structure, the model needs to be improved by obtaining atomic parameters that are more precise than those obtained from an initial model. Structure refinement is a process done in a repetitive manner, by cycling through a series of programmes which compare the model to the diffraction data, until any discrepancy between the two has reached a minimum. Two types of information act as input in this procedure; the preliminary model derived from the X-ray diffraction experiment, and empirical knowledge about the chemical components of the sample molecule, which in the case of proteins, include a range of various parameters. An index that gives a crude measure of the correctness of a structure and the quality of the data is the R factor (*78, 81*). This value is a measure of the agreement between the crystallographic model and the experimental X-ray diffraction data, defined as:

$$R = \frac{\sum ||Fobs| - |Fcalc||}{\sum |Fcalc|} \tag{6}$$

4 Methods

4.1 Vector DNA

The expression vector used in the work for this thesis was pET-22b (Novagen), which had a BC3987 gene insertion. The *E. coli* bacterial strain BL21 (DE3) containing the pET-22b plasmid with gene insert as described, in addition to a bacterial strain containing the TrxR gene, was kindly provided by Åsmund K. Røhr (PhD student, IMBV, University of Oslo, Norway).

4.2 Purification of Plasmid DNA from *E. coli* BL21 cells

Principle:

DNA was isolated using the NucleoSpin Plasmid Kit (Machery-Nagel). The kit is designed for rapid, small-scale preparation of pure plasmid DNA. The pelleted bacteria are resuspended and plasmid DNA is liberated from the cells by alkaline lysis. The genomic DNA along with remains of the cells are precipitated and discarded, while the released plasmid DNA remains in solution. Appropriate conditions result in binding of the plasmid DNA to the silica membrane of the NucleoSpin Plasmid column, whereas contaminations are removed by washing with ethanol. The elution procedure is performed using a slightly alkaline 5 mM Tris/HCl buffer, under low ionic strength conditions. A miniprep of the plasmid DNA resulted in approximately 50 ng/µl extracted and purified DNA.

Procedure:

Using a sterile pipette tip, a few cells from the provided -80 ºC stock of *E. coli* BL21 cells were transferred from the tube of frozen cells and spread onto LB agar plates. The agar plates were incubated over night at 37 ºC. The following day, single cell colonies were selected from the dishes with a pipette tip, and transferred to 5 ml LB media. The cell cultures were incubated at 37ºC with constant shaking (225-250 rpm) over night. Cell growth was carried out under antibiotic conditions, in medium containing 100 µg/ml ampicillin.

Methods

1) Pellet cells from 1-5 ml *E. coli* LB culture in a benchtop microcentrifuge for 30 seconds at 11 000 x g. Discard supernatant.

2) Resuspend the cell pellet in 250 µl buffer A1 and vortex the tube thoroughly. Add 250 µl buffer A2 and mix by inverting the tube 6-8 times carefully. Incubate the solution for 5 minutes at room temperature before adding 300 µl buffer A3. Mix gently by inverting the tube 6-8 times.

3) Clarify the lysate by centrifugation for 5-10 minutes at 11 000 x g at room temperature.

4) Load the supernatant from step 3 onto a spin column placed in a collection tube supplied with the kit. Centrifuge at 1 minute at 11 000 x g, and discard flow-through. Place the spin column back into the collection tube.

5) Load 600 ml buffer A4 onto the column. Centrifuge the column at 11 000 x g twice, for 1 and 2 minutes respectively. Discard flow-through both times.

6) Place the spin column in a clean Eppendorf tube and add 50 ml buffer AE. Incubate for 1 minute at room temperature. Elute and collect pure DNA in the Eppendorf tube by centrifuging for 1 minute at 11 000 x g.

General composition of the buffers is as follows:

A1: Resuspension buffer
A2: SDS/alkaline lysis buffer
A3: Neutralizing buffer, creates appropriate conditions for binding DNA to the silica membrane of the NucleoSpin Plasmid column.
A4: Ethanol wash buffer
AE: Elution buffer, 5 mM Tris/HCl, pH 8.5

4.3 Quantification of DNA

DNA and RNA absorb ultraviolet light, with a peak at 260 nm. DNA was quantified using a NanoDrop™ ND-1000 spectrophotometer according to the manufacturer's protocol.

4.4 Site-Directed Mutagenesis

Principle:

The QuickChange® XL Site-Directed Mutagenesis Kit provides a convenient way to make point mutations and delete or insert single amino acid residues. The procedure is efficient and popular in protein structure-function studies, as well as studies involving gene expression and vector modification studies. Compared to the standard QuickChange® Site-Directed Mutagenesis kit (Stratagene), the QuickChange XL Kit features components especially constructed for more efficient DNA replication. The generation of manipulated DNA is carried out with the use of a double-stranded DNA vector with the insert of interest, and two oligonucleotide primers containing the chosen mutation. Both primers are complementary to each other and to opposite strands of the vector, and anneal to their corresponding sequences after denaturation of the vector DNA. The elongation and amplification of the mutagenic primers is performed during temperature cycling by *PfuTurbo* DNA polymerase. This highly successive and heat-stable DNA polymerase ensures a robust, high-fidelity PCR. The enzyme amplifies targets at high yield, has a 3' to 5' exonuclease proofreading activity and constitutes an extensively low error rate. PCR is a widespread method used for amplification of a DNA sequence without the use of living organisms, being able to construct a selective enrichment of a desired DNA sequence by great amounts (*92*). Elongation by *PfuTurbo* DNA polymerase results in a mutated plasmid comprising staggered nicks, which after transformation into competent *E. coli* BL21 cells, are sealed by the cells DNA repair machinery. Prior to transformation of the mutated plasmid, the PCR product is treated with *Dpn*I. *Dpn*I endonuclease has the target sequence 5'-G$_{m6}$ATC-3', and is specifically used to digest hemimethylated and methylated parental DNA. DNA isolated from most *E. coli* strains is subject for this digestion, making *Dpn*I an efficient agent in the selection of a mutation-containing DNA pool.

Procedure:

Mutant strand synthesis reactions were carried out according to the QuikChange® XL Site-Directed Mutagenesis protocol (Stratagene). For the introduction of multiple desired mutations into BC3987, various sample reactions were set up, investigating different concentrations of dsDNA for each reaction. The reaction conditions were set up as follows:

5 µl of 10x reaction buffer

1-5 µl of dsDNA template (5-50 ng)

2 µl of forward primer (125 ng)

2 µl of reverse primer (125 ng)

1 µl of dNTP mix

3 µl of QuickSolution

dH$_2$O to a final volume of 50 µl

1 µl of *Pfu*Turbo DNA polymerase (2.5 U/µl)

The sequences of the mutagenic primers used to introduce the desired amino acid substitutions into BC3987 are listed in section 7.3.

A PTC-200 Peltier Thermal cycler (MJ research) was used to carry out the PCR reactions. Cycling parameters used for the construction of the T53A- and D11W mutants are outlined in Table 3.1. In addition, gradient PCR was used to carry out PCR reactions.

Table 3.1 Cycling parameters used for the mutagenesis.

Segment	Cycles	Temperature	Temperature Step	Time
1	1	95ºC	Hot-Start	2 min
2	16	95ºC	Denaturation	45 sec
		50ºC	Annealing	1 min
		68ºC	Extension	7 min
3	1	68ºC	Final Elongation	10 min

The amplification products were treated with *Dpn*I after temperature cycling. 1 µl of the restriction enzyme (10 U/µl) was added to the reaction mixture, and the sample was incubated at 37 °C for 1 hour to digest the nonmutated dsDNA.

4.5 Agarose Gel Electrophoresis

Principle:

Estimation of the size of DNA molecules following restriction enzyme digestion was done performing an agarose gel electrophoresis. The method is widely used to separate nucleic acids according to their size, by moving the negatively charged molecules through a porous matrix by applying an electric field. Due to less retardation by the agarose gel, smaller DNA fragments migrate faster and further towards the positively charged anode (*93*). Visualization of the DNA bands is done by adding ethidium bromide to the gel; an intercalating agent which makes the DNA bands fluoresce under UV-light.

Procedure:

Agarose was dissolved in 50 ml 1 X TAE buffer to a final agarose gel concentration of 1.0 %. Ethidium bromide was added to the solution before setting. DNA samples were mixed with a bromophenol blue loading buffer before loading, for visualization of the sample. A 1 kb DNA Ladder was used as a standard gene ruler and estimation of the sizes of DNA fragments was done according to the indicated ladder. The electrophoresis was performed using a Hoefer HE33 Mini Horizontal Submarine unit together with an EPS600 as a source of electricity. A voltage of 70 V and an electric current of 80 mA were applied to the gel, which was run for approximately 45 minutes.

4.6 Preparation of Competent *E. coli* cells, CaCl$_2$ Method

Principle:

Genetic competence refers to the ability of some bacteria to undergo transformation. Exposure to calcium ions renders the *E. coli* cells able to take up exogenous DNA plasmids (*94*).

Procedure:

The following procedure has been described by *Seidman et al.*, in *Current Protocols in Molecular Biology* (1997), Unit 1.8, performed with slight alterations:

1) Inoculate a single colony of *E. coli* BL21 cells into 5 ml LB medium. Grow the 5-ml culture over night at 37 °C with shaking, 225-250 rpm.

2) Inoculate 4 ml of the culture into 100 ml LB medium in a sterile 2-liter flask. Incubate at 37 °C with shaking. Grow cells until the optical density at 590 nm (OD_{590}) reaches a value of 0.375.

3) Aliquot the culture into two 50-ml prechilled, sterile polypropylene tubes and leave the tubes on ice for 10 minutes.

4) Centrifuge cells at 3000 rpm (JA-14) and 4 ºC for 7 minutes.

5) Pour off supernatant and resuspend each pellet gently in 10 ml ice-cold $CaCl_2$ solution, while keeping the cells on ice.

6) Centrifuge cells at 2500 rpm (JA-14) and 4ºC for 5 minutes. Discard supernatant and resuspend each pellet in 10 ml ice-cold $CaCl_2$ solution. Keep resuspended cells on ice for 30 min.

7) Centrifuge cells at 2500 rpm (JA-14) and 4ºC for 5 minutes. Discard supernatant and resuspend each pellet well in 2 ml ice-cold $CaCl_2$ solution.

8) Dispense cells into prechilled, sterile eppendorf tubes, in 50-µl aliquots. Freeze immediately at −80 °C.

4.7 Transformation of competent *E. coli* BL21 cells

Principle:

BL21 cells were transformed, with the isolated and mutated vectors (see section 4.2 and 4.3), for over-expression of the BC3987 mutant proteins. Transformation was carried out according to the transformation protocol for BL21 competent cells from Stratagene, with some variations. Both commercially purchased BL21-Gold competent cells (Stratagene) and self-prepared BL21 competent cells (See section 4.6) were used in the transformation reactions.

Procedure:

1) Aliquot 50 µl of the competent cells into the appropriate number of prechilled 14-ml BD Falcon polypropylene round-bottom tubes. Keep cells on ice.

2) Add 1–50 ng of DNA to each transformation reaction and swirl gently.

3) Incubate the reactions on ice for 30 minutes.

4) Heat-pulse each transformation reaction in a 42 °C water bath for exactly 20 seconds.

5) Incubate the reactions on ice for 2 minutes.

6) Add 900 µl of preheated (42 °C) SOC medium to each transformation reaction and incubate the reactions at 37 °C for 1 hour with shaking at 225–250 rpm.

7) Concentrate the cells from the experimental transformation by centrifugation at 200 × *g* for 5 minutes.

8) Plate the transformation reaction using a sterile spreader onto LB agar plates containing 100 µg/ml ampicillin. Divide each transformation reaction in two parts and plate on two petri dishes, in a 3:1 relationship*.

9) Wrap the petri dishes in plastic and incubate at 37 °C over night.

10) The following days, inspect all petri dishes for cell growth. Cover dishes with well defined and isolated cell colonies in plastic and store at 4 °C, for use in over-expression of protein.

---

*Each transformation reaction was divided in smaller amounts to avoid heavy cell layers and to promote easier isolation of single cell colonies.

4.8 DNA sequencing

Following transformation, colonies resulting from successful bacterial growth were selected and plasmid DNA was purified (See section 4.2). All DNA sequencing was performed by the ABI-lab at the University of Oslo. Sample preparation for sequencing of plasmids:

• Mix 8 µl of template (20-100 ng/µl) with 2 µl of a 5 µM T7 primer.

4.9 Over-expression of the recombinant BC3987 and TrxR genes in *E. coli* cells

In addition to the BC3987 proteins, TrxR was over-expressed and purified according to the same procedures, with some variations.

Principle:

The BC3987 and TrxR genes are expressed in a T7 RNA polymerase expression system. T7 RNA polymerase synthesizes RNA at a rate several times that of *E. coli* RNA polymerase and it terminates transcription less frequently. The system is activated by Isopropyl-β-D-Thiogalactopyranoside (IPTG), which binds to the lac-repressor and consequently inactivates it. This leads to an activation of the lac UV5 promoter and transcription of the T7 RNA polymerase gene, which in turn transcribes the target gene (*95, 96*).

Procedure:

The following procedure has been described by Rova *et al*. (*97*).

1) Incubate *E. coli* bacteria stored in LB culture medium containing 20 % glycerol at -80 ºC, at a petri dish containing LB culture agar and 100 µg/ml ampicillin at 37 ºC for about 24 hours.

2) Transfer a colony from the petri dish for an overnight incubation in 200 ml LB culture medium added 100 µg/ml ampicillin at 37 ºC in a shaker at 225-250 rpm.

3) Dilute 2 ml of the overnight culture 100 times in fresh LB culture medium containing 100 µg/ml ampicillin. Incubate the day culture in a shaker at 225-250 rpm for about 8 hours.

4) Add 100 ml buffer A* to 12 x 2 L Erlenmeyer flasks containing 0.9 L TB culture medium added 100 µg/ml ampicillin. Then, add 1 ml of the day culture to each Erlenmeyer flask and incubate at 37 ºC in a shaker at 225-250 rpm.

5) When the bacterial cultures reaches an optical density (OD_{590}) of 1.0, set the temperature in the incubator to 15 ºC and cool down the flasks on ice until they reach a temperature of 15 ºC**. Mount the flasks back in the shaker and add 1 ml 10 % Antifoam*** to each flask.

6) Add IPTG from a freshly prepared stock solution that has been filtered with a Millex-GP 0.22 µm unit to a final concentration of 0.5 mM in each flask.

7) Let the culture grow overnight for about 12 hours.

8) Harvest the bacteria by centrifugation at 5000 rpm (JA-10), at 4 ºC for 15 min.

9) Freeze the bacteria paste in liquid nitrogen and store at -80ºC.

---

*The autoclaved phosphate buffer is added just before use to avoid precipitation of phosphate salts during autoclavation. **The bacteria must be grown at 15 ºC to avoid formation of inclusion bodies. ***Antifoam is added to avoid unnecessary destruction of the cell membrane.

4.10 Purification of the BC3987 and TrxR Proteins

The following procedures were followed to obtain pure proteins. The operations were performed as described Mann *et al*. (*98*), but with slight modifications proven to be efficient by the lab group.

4.10.1 Lysis of Bacteria

Principle:

Due to the fact that most prokaryotic cells are protected by a rigid peptidoglycan wall, a high pressure extrusion is required to rupture the cell walls of bacterial cells. The principal of the X-press® method is to squeeze frozen cells through a small opening under high pressure. This will disrupt the cell membrane (*99*).

Procedure:

1) Cool the X-press® at -20 ºC over night.
2) Transfer 25 g of the frozen bacteria paste directly from the -80 ºC freezer to the the X-press®.
3) Crush the bacteria under high pressure 5 times.
4) Dissolve the lysed cells in 150 ml buffer B.
5) Stir the cell suspension at 4 ºC for approximately 45 minutes, until complete dissolution.
6) Centrifuge the solution at 18 000 rpm (JA-20) and 4 ºC for 1 hour.
7) Measure the volume of the supernatant, and collect for further purification.

4.10.2 Precipitation of DNA

Principle:

Streptomycin sulphate was used as a DNA precipitant in this purification step.

Procedure:

1) Prepare a 10 % (w/v) streptomycin sulphate solution.

2) Adjust the pH to 7.0 by adding ammonia ($NH_3(aq)$).

3) Add to the supernatant from step 4.10.1, the streptomycin sulphate with a volume corresponding to 25 % of the supernatant. This should be done drop by drop over a period of 10 minutes.

4) Stir carefully for 15 minutes.

5) Centrifuge precipitated DNA at 18 000 rpm (JA-20) and 4 ℃ for 30 minutes.

6) Collect the supernatant and measure the volume for further purification.

4.10.3 Precipitation of Protein with Ammonium Sulphate

Principle:

At high ionic strengths, the solubility of proteins decreases. When the salt concentration in a protein solution is increased, the solvent's activity is decreased. The reduced amount of bulk solvent available to solubilise the protein causes the protein to precipitate. The coagulation of proteins caused by the formation of hydrophobic interactions with each other is often executed with the use of ammonium sulphate (*100*).

Procedure:

1) Add 0.43 g $(NH_4)_2SO_4$ per ml supernatant over a period of 15 minutes, while stirring carefully at 4 ℃.

2) Keep stirring gently for 30 minutes.

3) Centrifuge the solution at 18 000 rpm (JA-20) and 4 ℃ for 30 minutes.

4) Dissolve the precipitate in 10-15 ml of buffer B.

4.10.4 Desalting

Prior to anion exchange chromatography, desalting of the protein sample was performed in order to lower the salt concentration. Desalting of protein samples was performed on a 3x5 ml HiTrap Desalting column (GE Healthcare), prepacked with Sephadex G-25, on the Äkta purifier-system. Protein fractions were eluted with 22.5 ml buffer B, and collected for further chromatography.

4.10.5 Anion Exchange Chromatography

Principle:

Ion-exchange chromatography is a method used for separation of ions and polar molecules based on the charge properties of the molecules. The principle is based on the reversible adsorption of charged molecules to an immobilized matrix material with a covalently bound ionic group bound to it. The immobilized ion exchange groups posses a charge opposite to that of the protein molecules. Anion exchange chromatography columns bear a cationic column material with replaceable anionic groups bound to it. Negative charges on the proteins surface will interact with the positively charged matrix. Due to variations in different surface properties, differences in the interactions between the proteins and the matrix material will cause a separation of proteins. At high ionic strength, counter ions in the mobile phase will replace the proteins bound to the column matrix, resulting in an elution of proteins according to their surface charge (*101*).

Procedure:

The strong anion exchange medium used in the HiTrap Q HP column (GE Healthcare) remains charged and has high loading capacities over broad pH ranges.

1) Apply the eluted protein fractions, diluted in buffer B from the previous procedure on a pre-packed 5 ml HiTrap Q HP column on the Äkta purifier-system. Keep the flow at 6 ml/min during the whole procedure.

2) Elute the protein by increasing the salt concentration with a linear gradient using buffer C (See Table 4.1).

3) Collect the eluted fractions with a significant absorption at 280 nm. Analyze the fractions using SDS-PAGE (See section 4.10.7). Concentrate the fractions in an Amicon ultrafiltration cell containing a filter with a cut-off value of 10 000 MW.

Table 4.1 Gradient anion exchange chromatography.

% buffer B, pH = 7.5	% buffer C, pH = 7.5	Volume (ml)
100 % - 95%	0% - 5%	5
95% - 75%	5% - 25%	50
75% - 0%	25% - 100%	2.5

4.10.6 Gel Filtration Chromatography

Principle:

Gel filtration chromatography is a size exclusion chromatography (SEC) technique which separates molecules in an aqueous solution, solely according to their size. The stationary column material is packed with a porous material consisting of polymer beads (*101*). Each size exclusion column contains pores that span a relatively narrow size range of molecular dimensions. The mobile phase, containing an aqueous solution of molecules of different sizes, is passed through the column. Molecules small enough to penetrate the beads are retarded by the stationary phase to a greater extend that large molecules that are unable to pass through the pores. Hence, with an increasing molecule size, the retention of proteins in SEC drops, and the largest proteins are eluted first (*100*). The Superdex 200 column (GE Healthcare) is a composite of dextran and cross-linked agarose, designed for sensitive and high-resolving gel filtration separations of proteins and other biomolecules.

Procedure:

As a final polishing step, all proteins were purified on the Superdex 200 column on the Äkta purifier-system. For each round of purification, 100 µl of proteins sample from the ion exchange chromatography step was applied on the column. Eluting of the protein was done with 20 ml buffer D. Collected fractions were analyzed using SDS-PAGE (See section 4.10.7), and concentrated in an Amicon ultrafiltration cell containing a filter with a cut-off value of 10 000 MW.

4.10.7 Sodium Dodecyl Sulphate Polyacrylamide Gel Electrophoresis (SDS-PAGE)

All fractions from the anion exchange column and the gel filtration column with $A_{280} \geq 0.4$ were analyzed by SDS-PAGE. The GE Healthcare PhastSystem was used for this purpose.

Principle:

Electrophoresis is the motion of particles in a fluid under the influence of an electric field. SDS-PAGE separates denatured macromolecules according to their molecular weight. SDS is an anionic detergent which binds to, and denatures proteins, giving them a negative charge in proportion to their mass. Consequently, proteins can be separated solely according to their size. A reducing agent, mercaptoethanol, is used to disrupt disulphide bonds between polypeptides, ensuring that only monomeric proteins are present during the separation procedure (*102*).

Procedure:

1) Mix 14 µl of the protein solution with 8 µl Phast load mix in an Eppendorf tube.
2) Boil the Eppendorf tubes for 10 minutes. Spin at 12 000 rpm in a micro centrifuge.
3) Prepare the PhastSystem with a PhastGel 10-15 % gradient gel and PhastGel buffer strips. Set the temperature to 16 ℃.
4) Use the application comb to position 1 µl of each sample above the gel in the instrument.
5) Start the PhastSystem using pre-programmed separation.
6) Prepare the Phast staining solution, Phast destaining solution and Phast preservation solution. The automated program for staining, destaining and preservation was not used. Instead, the following procedures was tested and approved effective by the lab group.
7) Place the gel in a 50 ml Falcon tube and cover with staining solution. Leave for staining in a shaker at 50 ℃ for 15 minutes.
8) Discard the staining solution. Add an equal amount of destaining solution, and leave for destaining in a shaker at 50 ℃ for no more than 5 minutes.
9) Discard the destaining solution. Add preservation solution until the gel is completely covered. Leave in room temperature for at least 1 hour, in order to achieve a good result.

4.10.8 Ultra Filtration

Principle:

Further crystallization experiments required higher concentration of the BC3987 protein. Therefore, a higher concentration of the fractions collected from the gel filtration chromatography was necessary. In this procedure, ultrafiltration was performed, using Centricon, MW 10 000.

Procedure:

1) Add maximum 15 ml of protein solution to the centricon tube.
2) Centrifuge for 15 minutes at 3500 x g.
3) Freeze the concentrated protein in liquid nitrogen and store at -80 ℃.

4.11 Protein Quantification

4.11.1 Quantification Using UV/vis Spectrophotometry

The extinction coefficient of BC3987 was determined using the Edelhoch method (*103*), yielding a value of $\varepsilon_{BC3987, 280\ nm} = 8200\ M^{-1}cm^{-1}$. For TrxR, the same method resulted in an extinction coefficient of $\varepsilon TrxR,\ _{450\ nm} = 11300\ M^{-1}cm^{-1}$. As for the D11W mutant protein (described later in this thesis), the extinction coefficient was estimated to a value of $\varepsilon_{D11W,\ 280\ nm} = 13700\ M^{-1}cm^{-1}$. The extinction coefficient indicates how much light a protein absorbs at a certain wavelength.

Principle:

Aromatic side chains, particularly tyrosine and tryptophan, of amino acids absorb UV-radiation at 280 nm. This is due to the excitation of π (bonding) orbital electrons to π^* (anti-bonding) orbital (*104*). The absorption phenomenon may be quantified by the Beer-Lambert law:

$$log\frac{I_0}{I} = \varepsilon cl \tag{7}$$

Where I_0 and I are the intensities of the incident and transmitted light respectively, c is the molar concentration of the protein solution in moles per litre, and l is the length of the light path in centimetres (usually 1 cm). ε is known as the molar extinction coefficient for the protein. The term [log I_0/I] is the absorbance or optical density (*81*). Consequently, with monochromatic radiation, protein concentration can be quantified using the following equation:

$$c = \frac{A}{\varepsilon} \tag{8}$$

Procedure:

A HP 8452A diode array spectrophotometer was used to measure the absorbance of BC3987.

1) Record a baseline of buffer B at the spectrophotometer.
2) Dilute the concentrated protein with buffer A, until absorbance falls below a value of 1.0.
3) Measure $A_{280\ nm}$ and $A_{450\ nm}$ for BC3987 and TrxR, respectively, and calculate the protein concentration in molar (Equation (8)).

4.12 pK$_a$ determination

Principle:

An acidity constant, K_a, is a quantitative measure of the strength of an acid in solution. A logarithmic measure of this acid dissociation constant is commonly used, pK_a, which is equal to $-\log_{10} K_a$. Small values of pK_a correspond to a large extent of dissociation, and hence, strong acids. The pK_a values of ionizable residues of proteins are the basis for understanding the pH-dependent characteristics of proteins and catalytic mechanisms of many enzymes (*68*). Measurement of the thiolate anion on the basis of UV absorption was performed in order to determine the pK_a values of the active site cysteines of the BC3987 proteins. The ionization of the cysteine was monitored at 240 nm during a pH titration (*62*). Measurements of the native BC3987 protein and both mutant proteins were performed.

Dithiothreitol (DTT) is a strong reducing agent, often used to reduce disulphide bonds and dithiols of proteins (*105*). Alternatively, diamide is a reagent which oxidizes sulfhydryl

groups to the disulfide form. In order to prepare the reduced; and oxidized protein samples, incubation with DTT or diamide was carried out prior to absorbance measurements.

Procedure:

1) Prepare reduced and oxidized protein samples by incubating with 100 mM DTT or 100 mM diamide for 1 hour, respectively.
2) Make polybuffer with pH 9.3 (See section 7.2). Purge with argon and degass.
3) Remove excess DTT and diamide using a HiTrap Desalting column (GE Healthcare), equilibrated with polybuffer, on the Äkta purifier-system.
4) Collect fractions of reduced and oxidized protein samples in quartz cuvettes and corrected for the absorbance difference between the two cuvettes and base line drift.
5) Record spectra of 25 µM reduced and oxidized native BC3987 and mutant proteins with a HP 8452 diode array spectrophotometer between 240 and 350 nm.
6) Titrate the solutions between pH 9.5 and 4.0 by adding 2.5-4.5 µl of 25 mM HCl.
7) For each round, measure the pH of both solutions using a PHM240 pH meter (Radiometer Analytical) equipped with a PHC 4000-8 pH electrode.

4.13 Redox Potential Determination

Principle:

Oxidation-reduction systems occur in many enzymatic reactions. The exchange of electrons between molecules of a redox pair characterizes a redox reaction. A general redox reaction can be written as:

$$A_{ox} + B_{red} \leftrightarrow A_{red} + B_{ox} \tag{9}$$

For the Trx system, involving Trx, TrxR and the reducing agent NADPH, reaction (9) will occur:

$$Trx - S_2 + NADPH + H^+ \xleftrightarrow{TrxR} Trx - (SH)_2 + NADP^+ \tag{10}$$
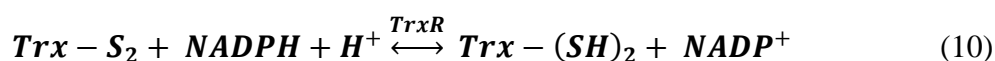
For the reduction of Trx (BC3987) with TrxR, the equilibrium constant K is:

$$\frac{[Trx-(SH)_2][NADP^+]}{[Trx-(S)_2][NADPH][H^+]} \tag{11}$$

At equilibrium, the amount of each component in (9) will be adjusted according to the thermodynamics of the reaction, given as:

$$\Delta G^0 = -nF\Delta E^0 = -RT\ln\left(\frac{[Trx-(SH)_2][NADP^+]}{[Trx-(S)_2][NADPH][H^+]}\right) \qquad (12)$$

Where G^0 is the standard change in free energy of the reaction, E^0 is the standard electrochemical cell potential (voltage) , R is the ideal gas constant, T is temperature, n equals moles of electrons transferred during the redox reaction, F represents the Faraday constant = 96,485 C mol^{-1} . The redox potentials for the reaction (9) will determine the magnitude ΔE^0, and hence, the equilibrium for the reaction.

If the amount of e.g. NADP$^+$ is changed, the system is no longer in equilibrium, and the free energy can be written as:

$$\Delta G = \Delta G^0 + RT\ln\left(\frac{[Trx-(SH)_2][NADP^+]}{[Trx-(S)_2][NADPH][H^+]}\right) \qquad (13)$$

If $\Delta G < 0$, the reaction is spontaneous. If $\Delta G = 0$, however, the reaction has reached equilibrium and no reaction will occur. The redox potential of the Trx-(SH)$_2$/Trx-S$_2$ redox pair can be calculated according to the Nernst equation (*56, 100*):

$$E = E^0 - (RT/nF)\ln\left(\frac{[Trx-(SH)_2][NADP^+]}{[Trx-(S)_2][NADPH][H^+]}\right) \qquad (14)$$

The redox pair can be oxidized or reduced by using an adequate oxidizing or reducing agent, respectively. The redox potential of a protein is determined experimentally with redox titration, by measuring the relative amounts of reduced and oxidized protein species, in redox equilibrium with a compound of known redox potential. NADPH is a cofactor used by TrxR, which shows an intense absorption band at 340 nm. This absorption band is, however, not observed from its oxidized form, NADP$^+$, which shows an absorption band at 260 nm (*106*). These features make the redox pair NADP$^+$/ NADPH a good tool in the determination of Trx redox potentials through optical monitoring by spectrophotometry.

Procedure:

The redox potential of native and mutant BC3987 cysteine pairs was determined by redox equilibration (*18, 56, 107*) with NADP$^+$/ NADPH using *B. cereus* TrxR as a catalyst. All solutions were equilibrated with argon gas and a HP 8452 diode array spectrophotometer was

used to monitor the absorbance spectra at wavelengths in the range between 240 and 450 nm. The following procedure applies for all individual experiments:

1) Prepare a 100 mM phosphate buffer with pH 7 (See section 7.2).

2) Apply 20-80 μM BC3987 to a cuvette containing phosphate buffer, to a total volume of 1 ml. Mix gently, and seal the cuvette. Record spectra.

3) Add 30 μM NADPH to the cuvette, containing BC3987 solved in buffer, and record spectra.

4) Make sure that the solution is kept anaerobic. Add *B. cereus* TrxR to a final concentration of 30-45 nM to start the enzymatic reaction. Record spectra, with 30 second intervals, until the absorption curve stabilizes for 340 nm.

5) Apply $NADP^+$ in three to four successive additions, varying concentrations from 265 to a maximum total concentration of 2000 μM. Record spectra, with 30 second intervals, until the absorption curve stabilizes for 340 nm, succeeding each addition.

6) Calculate the midpoint potential for the cysteine pair from the reversed equilibrium resulting from the following additions of $NADP^+$. During the calculations, make corrections for dilutions and the extinction coefficients $\varepsilon_{NADPH,\ 340\ nm} = 6220\ M^{-1}cm^{-1}$, $\varepsilon_{NADP+,\ 260\ nm} = 18\ 000\ M^{-1}cm^{-1}$, and $\varepsilon_{NADP+,\ 340\ nm} = 54\ M^{-1}cm^{-1}$ used. The midpoint potential for the NADPH/ NADP+ pair used was -315 mV (*108*).

4.14 Protein Crystallization

Principle:

Protein crystallization is in many ways based on trial-and-error. The goal is, as described in section 3.4.1, to bring the crystallization solution into a supersaturated state where crystal seeds are formed for further crystal growing. Many factors play a role in this process, and the purity requirement is particularly high. Altering the protein-protein or protein-solvent contact in order to precipitate the protein as ordered crystals can be achieved using a range of different precipitants. Protein solubility, and hence the crystallization result, can also be affected by the buffer used, the pH of the crystallization solution, the temperature as well as the choice of crystallization method used for setting up the crystallization trials. Furthermore, the choice of crystallization method for setting up crystallization trials might influence the outcome in a great manner.

Procedure:

Crystallization screens sample a series of different crystallization conditions to identify which reagent classes and pH are effective in producing crystals. The Index screen from Hampton Research, CA, USA, utilizes a broad portfolio of crystallization reagent systems. All crystals were obtained based on Index screen conditions 55 and 65 (See section 7.2). Crystals were grown at room temperature, using the hanging drop method. 1 µl protein solution (1.5-50 mg/ml) dissolved in buffer D was mixed with the same volume of crystallizing solution and placed on a glass cover slip. The slip was positioned upside down over a reservoir containing 400 µl crystallization solution and sealed. In each diffraction experiment, prior to crystal cooling, a single crystal was separated from a crystal bundle and transferred into a cryo-solution containing 75% crystallization stock solution added 25 % PEG 400 as antifreeze. A 30 second incubation of all crystals was performed, before subsequent freezing in liquid nitrogen. In addition to the untreated, oxidized crystal forms, all variants of protein crystals were also exposed to reducing conditions. Crystal soaking was done in cryo-solution containing 100 mM DTT for 30 minutes, in order to try to obtain crystals with a reduced active site motif.

4.15 X-ray Data collection

Data was collected at Undulator Beam Lines (ID14 and ID23) at the European Synchrotron Radiation Facility (ESRF), Grenoble, France, both equipped with a Q315r ADSC X-ray detector. Several data sets were collected for each characteristic crystal type; oxidized and reduced mutant proteins, as well as both forms of the native protein. Data collection was performed at a temperature of 100 K. For most crystals, high-resolution and low-resolution datasets were collected and merged during scaling.

4.16 Structure Determination and Refinement

All diffraction data were processed and integrated with MOSFLM (*109*) and scaled and merged using SCALA, in the ccp4 package (*110*). The structure of a monomer of the native BC3987 solved by Røhr and Andersson using a search model generated from the *C.*

ammoniagenes NrdH protein structure (PDBid:1R7H) (*63*), served as a starting model in the structure determination procedure. The program PHASER (*111*) was used to solve the structures by molecular replacement. Free R-values were calculated from 5 % of the data and monitored throughout the refinement procedure. Rigid body refinement was followed by several cycles of restrained refinement using Refmac (*110, 112*). Multiple cycles of model building was performed in Coot (*113*), and addition of water molecules was done using ARP/wARP (*114*). Initially, restrained isotropic refinement was carried out on all crystal structures. Due to the relatively high resolution achieved for all data sets, isotropic refinement was succeeded with round of restrained aniosotropic refinement with Refmac (*115*). At high resolutions, crystal structures can be refined using fewer restraints, allowing more variables per amino acid. Since different atoms in a protein can vibrate differently in different directions, the atoms may be allowed to have anisotropic B factors, permitting the density distribution of atoms to show the particular direction in which they are freer to move. The anisotropy was monitored through the PARVATI program (*116*). To calculate the absorbed X-ray dose (Gy = J kg^{-1}) for the different crystals the program RADDOSE was used (*117, 118*). The figures were prepared with PyMOL (DeLano Scientific; http://www.pymol.org).

5 Results and Discussion

The work carried out in this thesis can be divided into four main parts. A description of the main focus of each part is presented below:

1. **Construction of BC3987 mutants, over-expression and purification of protein**

   The discovery of the BC3987 Trx located in the *B. cereus* genome has triggered our curiosity regarding this small thiol-disulfide oxidoreductase. Even though a conserved Thr8 residue in the vicinity of the active site is believed to participate in the deprotonation of an active site buried Cys, the reaction mechanism involving this Thr8 residue has not been verified. The generation of point mutations in the BC3987 sequence, in the vicinity of the active site, can give insight into structural and biochemical properties of this enzyme. The first parts of the work carried out in this thesis involved making, express and purify mutant BC3987 proteins, for use in later experiments. In addition, over-expression and purification of the native BC3987 protein and TrxR was performed, the latter being necessary as a catalyst for the redox potential measurements.

2. **Determination of pK_a values of the active site cysteines**

   To better understand which amino acids that influence the active site Cys pK_a values of BC3987, determination of pK_a values of the native protein and the various mutants, involving slight amino acid variations surrounding the active site, was performed through pH titration. These measurements can give more knowledge about the catalytic mechanism of this Trx, through the comparison of pK_a values of native and mutant proteins.

3. **Redox potential determination**

   In order to examine the redox potential of the thiol-disulfide bridge of the mutated proteins compared to the native BC3987, redox equilibration with $NADP^+$/ NADPH using *B. cereus* TrxR as a catalyst was performed on all proteins. The substitution of selected amino acid residues near the active site can alter the SS/SH_2-redox potential.

4. Protein crystallization and structure determination using X-ray diffraction

Investigating the native and mutant BC3987 proteins by X-ray crystallography enables us to visualize their protein structures at the atomic level, and thereby enhancing our understanding of their function. X-ray crystallography enables us to specifically study how proteins interact, how they undergo conformational changes, and how they perform catalysis. This method might contribute to improved understanding of the active site chemistry of BC3987.

Findings from the four above mentioned parts are presented in the succeeding sections.

5.1 Construction of BC3987 Mutants, Over-expression and Purification of Protein

5.1.1 Construction of BC3987 Mutants

To study the deprotonation mechanism of the C-terminal cysteine of the conserved C-X-X-C motif in the *B. cereus* BC3987 Trx, a selection of point mutations were introduced in the vicinity of the active site of this protein. Prior to the production of mutants, the native BC3987 sequence was verified by DNA sequencing. An examination of a total of 14 mutant proteins was attempted in the beginning of the experiments. The planned mutant versions of BC3987 were chosen based on their potential effects on the active site chemistry, with the intention to make mutants with active site motifs resembling other Trx-like proteins. The various amino acid residues that can possibly contribute to the deprotonation of the buried C-terminal cysteine, necessary to promote the second nucleophilic attack, have been of specific interest. Figure 5.1 displays the nucleotide and corresponding 78 amino acid sequence of the native BC3987 Trx.

```
5'-ATGAAAAAAATTGAGGTTTATACACAACCCGATTGTCCGCCATGTGTTATTGTAAAA
   M  K  K  I  E  V  Y  T  Q  P  D  C  P  P  C  V  I  V  K
   1                          10

   GAATTTTTGAAGCATAATAACGTTGCATATGAAGAATTTGACGTAAAAAAAGACGCT
   E  F  L  K  H  N  N  V  A  Y  E  E  F  D  V  K  K  D  A
   20                                  30

   GCTGCTCGCAATCGTCTTTTATACGACTATGATTCTTATTCAACTCCAACAGTCGTA
   A  A  R  N  R  L  L  Y  D  Y  D  S  Y  S  T  P  T  V  V
     40                                50

   ATTGATGGCGAAGTAGTTGCAGGTTTTCAAATTGAAAAGTTACAACAACTACTCAAT
   I  D  G  E  V  V  A  G  F  Q  I  E  K  L  Q  Q  L  L  N
       60                                70

   ATAGAATAA - 3'
   I   E  Stop
```

Figure 5.1 Native BC3987 nucleotide and amino acid sequences. The actice site C-P-P-C motif is highlighted in green.

Using *in vitro* Site-Directed Mutagenesis, production of 14 suggested mutant variants was attempted. Table 5.1 gives an overview of the 14 mutations, possibly affecting the interaction with TrxR and the thiol-disulfide exchange reactions carried out by the BC3987 Trx. A ribbon diagram showing the native BC3987 protein, with residues selected for point mutations, is presented in Figure 5.2.

Table 5.1 A brief description of the various mutations attempted in BC3987, describing their potential significance and consequences. Mutants are termed based on the amino acid to be exchanged, followed by the new amino acid replacement, according to the one letter amino acid code.

Mutation	Relevance/Reason for interest
D11W	The replacement of an aspartate residue with the large, aromatic residue, tryptophan may cause the latter to act as a lid over the active site. This might influence i.e. the access of interacting molecules to the active site of BC3987 and hence, the catalysis. The presence of a Trp residue in the position prior to the N-terminal active site Cys is also seen in classic Trx proteins.
P13G	The cyclic structure of the side chain of proline makes this residue conformationally rigid. Replacing it with glycine would make the active site more flexible. The presence of a Gly residue in the position succeeding the N-terminal active site Cys is also seen in classic Trx proteins.
P14H	The cyclic structure of the side chain of proline makes this residue conformationally rigid. Replacing it with histidine would make the active site more flexible. Additionally, the imidazole side chain of His has a pK_a value of 6, meaning that small pH changes close to physiological would affect its charge. The presence of a His residue in the position prior to the C-terminal active site Cys is also seen in DsbA; a Trx-like protein with a high redox potential.
P14W	The cyclic structure of the side chain of proline makes this residue conformationally rigid. Replacing it with tryptophane would make the active site more flexible. The large side chain of Trp could influence the space surrounding the active site. The classical Grx active site includes the amino acid sequence C-P-[FYW]-C, with a Trp observed prior to the C-terminal Cys.
P14Y	The cyclic structure of the side chain of proline makes this residue conformationally rigid. Replacing it with tyrosine would make the active site more flexible. In addition, the phenol side chain could influence activity through hydrogen bonding. The classical Grx active site includes the amino acid sequence C-P-[FYW]-C, with a Tyr observed prior to the C-terminal Cys.
R41G	Arg41, with its positively charged side chain, is believed to participate in TrxR binding. A substitution with glycine could obstruct the TrxR binding site, preventing electron flow from the reductase.

T53A	The replacement of the potential hydrogen-bonding, polar residue threonine in the vicinity of the active site motif with an aliphatic alanine, could eliminate a possible hydrogen bond to Cys15.
T53S	Substituting threonine with serine, both having polar side chains bearing hydroxyl groups, could introduce more flexible hydrogen-bonding to Cys15.
T8A	The replacement of the potential hydrogen-bonding, polar residue threonine in the vicinity of the active site motif with an aliphatic alanine, could eliminate a hydrogen bond to Cys15.
T8S	Substituting threonine with serine, both having polar side chains bearing hydroxyl groups, could introduce more flexible hydrogen-bonding to Cys15.
T8D	An introduction of the acidic residue aspartate in the vicinity of the active site cysteines would potentially influence the deprotonation of Cys15. The negative charge of the carboxylic side chain could influence hydrogen bonding and stabilization.
V6D	An introduction of the acidic residue aspartate close to the active site cysteines would potentially influence the deprotonation of Cys15. Also, it could influence the nature of Thr8. The presence of an Asp residue six positions prior to the active site Cys residues could possibly mimic the potential role of Asp26 in deprotonation of the buried Cys in classical Trxs.
T8A + T53A	A combination of two mutations previously mentioned, eliminating two possible hydrogen bonds close to the C-X-X-C motif.
P13G + P14H	A combination of two mutations previously mentioned, with variations made to the active site motif, as seen in other Trx-like proteins.
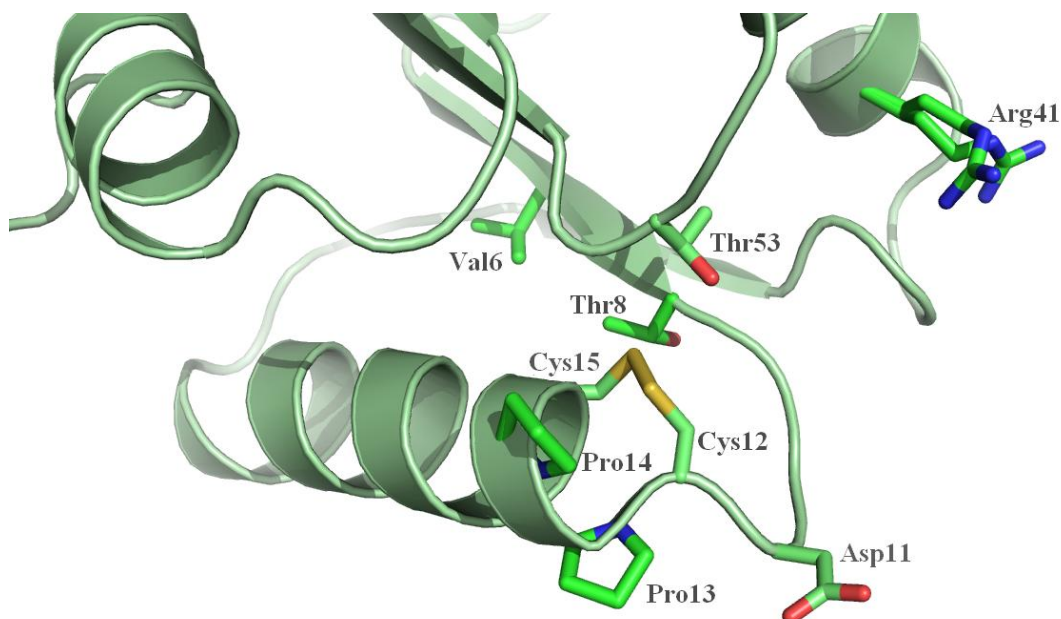
Figure 5.2 Ribbon diagram of BC3987, showing amino acid residues subject to mutations, in addition to the active site cysteines. Arg41 shows two alternative conformations.

Construction of BC3987 mutants was performed according to the QuikChange® XLSite-Directed Mutagenesis protocol (Stratagene). All mutations were introduced by PCR using forward and reverse mutagenic primers. The names and sequences of these primers are listed in section 7.3. Primers were made according to Stratagene's formula from the kit manual. *Dpn*I was used to digest methylated, parental DNA. The *Dpn*I-treated DNA was then used to transform *E. coli* BL21 cells and the successfully transformed cells were selected on LB plates containing ampicillin. Single colonies of the transformed cells were used to inoculate overnight cultures. Plasmid DNA was purified and sequenced for verification of the desired mutations. Mutants were examined by DNA sequencing (results are not shown).

Table 5.2 lists the 14 mutants, indicating which steps of the generation of mutant proteins gave successful results.

Table 5.2 Construction, transformation and approval of mutants, according to the final experiments. Positive and negative results are presented with **+** and **-**, respectively.

Substituted Amino Acid Residues	Mutant versions	Observed PCR Products after Electrophoresis	Transformants giving rise to colonies of *E. coli* BL21 cells	Verification of Mutation by Sequencing
Aspartate	D11W	+	+	+
Proline	P13G	+	+	-
	P14H	+	-	-
	P14W	+	-	-
	P14Y	+	+	-
	P13G + P14H	+	-	-
Arginine	R41G	+	+	-
Threonine	T53A	+	+	+
	T53S	+	-	-
	T8A	+	+	-
	T8S	-	-	-
	T8D	-	-	-
	T8A + T53A	-	-	-
Valine	V6D	+	-	-
Total number of Mutants	14	11	6	2

After multiple attempts and large effort trying to achieve the 14 planned mutant versions of BC3987, a total of only two successfully mutated and expressed BC3987 proteins resulted.

Several PCR reactions were set up for all 14 mutant types, with alterations to the total concentration of plasmid DNA. Unsuccessful results lead to additional attempts to make mutants, altering the amount of different ingredients effecting the total composition of the sample reactions. Several alterations of the PCR reaction mixtures were tried out for all reactions. Also, mutation reactions using *Taq* DNA polymerase were set up, in order to examine various experimental conditions. Some reactions were set up using buffers and enzymes from Fermentas. In addition to the PCR cycling parameters given in Table 3.1, different PCR running parameters, including rounds of gradient PCR ,was tried out on the PCR samples.

PCR reactions were tested on an agarose gel prior to, and after cleavage with DpnI, and bands were observed for most reactions. A total of six mutant transformants gave rise to cell colonies. Only two of these contained the protein sequence with the appropriate mutation. Sequencing results of the remaining four revealed a lack of the two N-terminal amino acids in the BC3987 protein sequence. Regardless of this loss of residues in the amino acid sequence, attempts to over-express these four mutated proteins and growth of bacteria were done. However, none of the four transformants P13G, P14Y, R41G or T8A expressed the corresponding mutated BC3987 protein.

Further attempts of primer design, varying the mutagenic codons, and other mutation kits from different distributors could be tested. A possible reason for the failed mutational experiments may be due to errors in primer annealing. Another reason may be due to errors in the BC3987 template used for mutagenesis. An erroneous DNA sequence would cause failure in protein translation.

**5.1.2 Expression and Purification of TrxR, Native and Mutated BC3987**

Following successful generation of two mutant BC3987 proteins, all proteins were expressed and purified. *B. cereus* native BC3987 and mutant proteins D11W and T53A were over-expressed and purified for later pK_a detemination experiments, redox potential studies and crystal structure analysis. TrxR was expressed and purified for use as a catalyst in redox potential determination. All four proteins were treated approximately equally, using the same expression, purification and quantification procedures (See sections 4.8 – 4.10).

The chromatography was performed starting with a desalting procedure using a HiTrap Desalting column (GE Healthcare). Further rounds of protein purification were performed on a HiTrap Q HP anion exchange column (GE Healthcare). The following, last chromatography step involved size exclusion chromatography, done on a Superdex 200 column (GE Healthcare). Chromatograms from the purification process are presented in Figures 5.3 and 5.4. Figure 5.3 displays chromatograms of the BC3987 protein, with chromatograms for the BC3987 mutant proteins showing similar behaviour. Elution of native and mutant BC3987 proteins on the anion exchange column started when the conductivity had reached values of approximately 20 mS/cm. Figure 5.4 shows chromatograms illustrating purification steps of TrxR. Elution of TrxR started when the conductivity was in the range around 25 mS/cm during anion exchange chromatography. Results from the gel filtration step are also presented in Figures 5.3 and 5.4, for BC3987 and TrxR, respectively. Fractioned peaks are indicated with arrows in all following chromatograms.
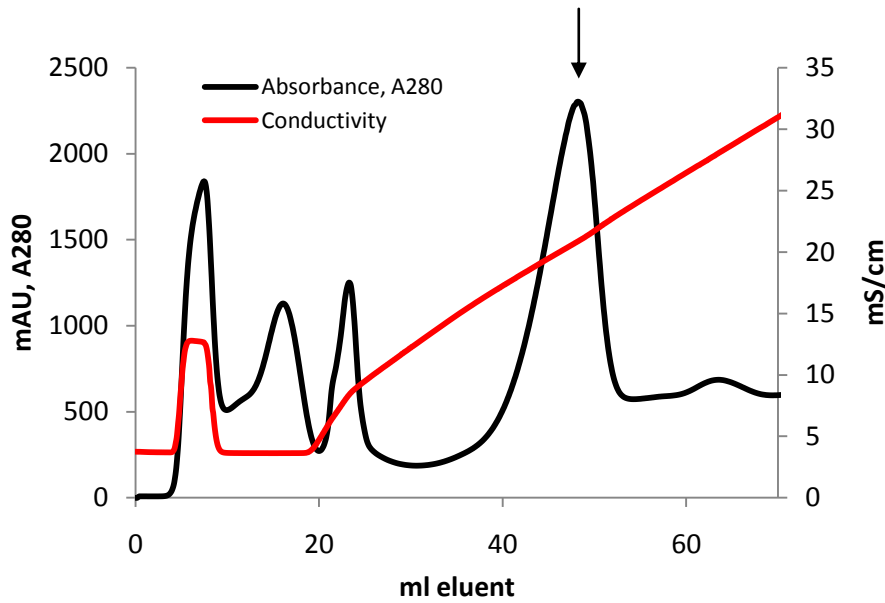
(A) Anion Exchange Column
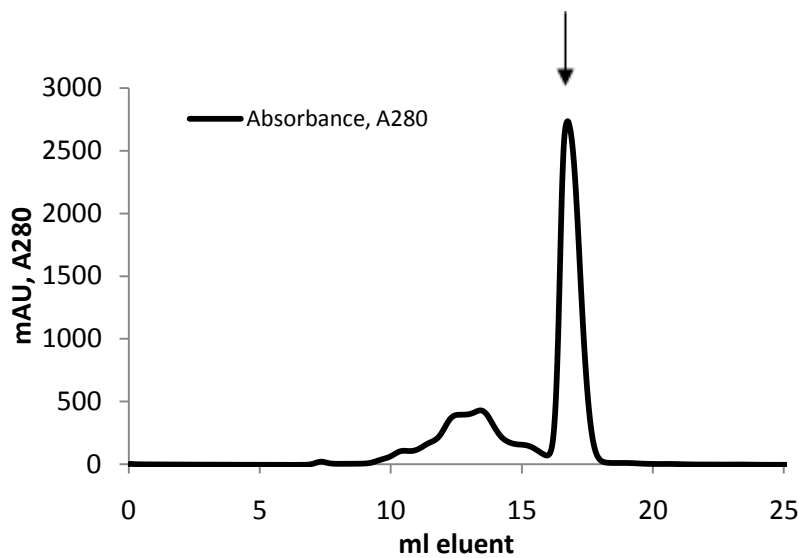
(B) Gel Filtration Column

Figure 5.3 Chromatograms from the purification process of BC3987 (Both from the native BC3987 Trx). (A) Chromatogram resulting from purification of BC3987 on a 2x5 ml HiTrap Q HP column on the Äkta purifier-system. The black line represents the absorbance recorded at 280 nm whereas the red line shows the conductivity. The protein was eluted by increasing the salt concentration with a linear gradient using buffer C. Both absorbance and conductivity was recorded as a function of ml eluent. Fractions corresponding to the large absorption peak in the range of approximately 42-52 ml eluent were collected. (B) Chromatogram resulting from purification of BC3987 on a Superdex 200 column on the Äkta purifier-system. The black line represents the absorbance at 280 nm, recorded as a function of ml eluent. The protein was eluted with buffer D. Fractions corresponding to the small absorption peak in the range of approximately 11-14 ml eluent were collected.
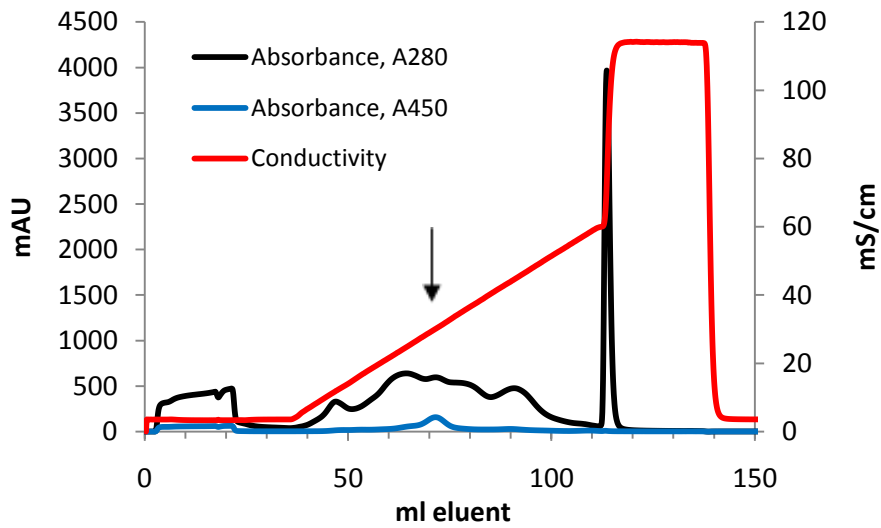
(A) Anion Exchange Column
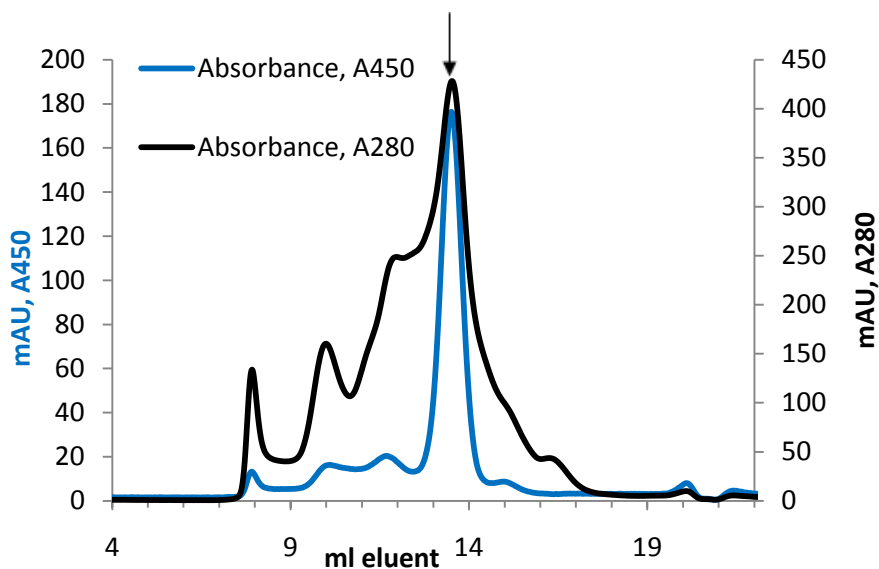
(B) Gel Filtration Column

Figure 5.4 Chromatograms from the purification process of TrxR. Due to the FAD prosthetic group of TrxR, absorbance is shown at both 280 and 450 nm. (A) Chromatogram resulting from purification of TrxR on a 5 ml HiTrap Q HP column on the Äkta purifier-system. The black line represents the absorbance recorded at 280 nm, the blue line represents aborbance at 450 nm, whereas the red line shows the conductivity. The protein was eluted by increasing the salt concentration with a linear gradient using buffer C. Both absorbance and conductivity was recorded as a function of ml eluent, and fractions were collected for eluent corresponding to the small absorption peak between 60-80 ml. (B) Chromatogram resulting from purification of TrxR on a Superdex 200 column on the Äkta purifier-system. The black and blue lines represent the absorbance at 280 and 450 nm, respectively, recorded as a function of ml eluent. The protein was eluted with buffer D. Fractions were collected for eluent corresponding to the large absorption peak between 13 and 14.5 ml.

All protein fractions resulting from gel filtration chromatography were concentrated with ultrafiltration. The yield of the different proteins resulting from approximately 30 g of bacteria are presented in Table 5.3. Protein concentration values are calculated on the basis of quantification using UV/vis spectrophotometry. Native BC3987 protein was purified from approximately 60 g of bacteria, resulting in two protein batches, while mutant proteins, as well as TrxR, were each purified from approximately 30 g of bacteria.

Table 5.3 Protein yield and final protein concentrations.

Protein	Final Yield		
	mg/ml	ml	mg
Native BC3987	52	1	52
D11W	6	0.5	3
T53A	45	0.75	34
TrxR	13	0.75	10

Protein purity was considered to be higher than 95% for all three kinds of BC3987 proteins, according to visual inspection of protein samples separated by SDS-PAGE. The final TrxR purity was considered quite low. Unfortunately, no further purification steps were performed.
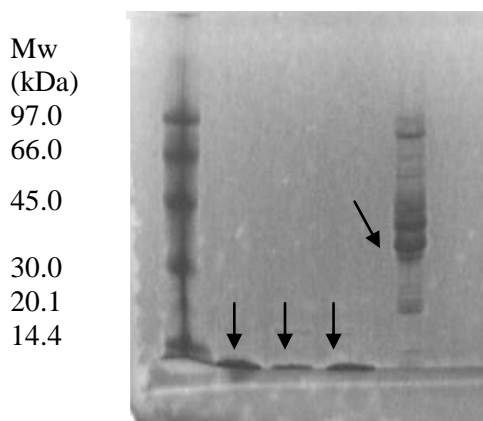

Figure 5.5 SDS-PAGE gel showing the purity of native BC3987, mutants D11W and T53A (~8.9 kDa) and TrxR (~37 kDa), respectively, starting from the second left column, indicated with arrows. The left lane shows a protein and peptide low-molecular weight marker from GE Health care, with the bottom band having a molecular weight of 14.4 kDa.

5.2 Characterization of the Nucleophilic Cysteine pK_a values and the Disulfide Redox Potential

Knowledge about the pK_a values of ionizable residues are important for understanding the pH-dependent characteristics of proteins and catalytic mechanisms of many enzymes. Ionizable groups with unusually low or high pK_a values tend to occur at protein active sites. Different subclasses of the Trx superfamily have nucleophilic cysteine pK_a values that correspond to their function, and thus, determination of these values is important for better understanding the biological role of different Trx enzymes. Studies indicate that the buried Cys residue of *E. coli* Trx has a higher pK_a value than the N-terminal nucleophilic Cys residue. An explanation for the proton abstraction of the C-terminal, buried Cys is believed to include a conserved Asp26 involved in acid/base catalysis, as described previously in this thesis. However, both active site cysteines appear to have lowered pK_a values in BC3987, and the stabilization of the two active site thiolates is the main topic of this thesis.

When determining the pK_a values of the active site cysteines of the native and mutant BC3987 proteins, DTT reduced samples were compared with diamide oxidized references. Only one experimental replicate of each protein was achieved, due to lack of time.

The pK_a value of the Cys residues of the native BC3987 was determined to be 7.3, corresponding to the value estimated by Røhr and Andersson (*63*). The pK_a value of the T53A mutant was estimated to be 7.7, and for the D11W mutant, a pK_a value of 6.5 was estimated. Hence, small shifts in the pK_a values of both mutants are observed, compared to the native BC3987. Graphs showing titration curves representing midpoint pK_a values of the active site cysteines in the native, D11W and T53A BC3987 proteins are presented in Figure 5.6.

(A)

(B)
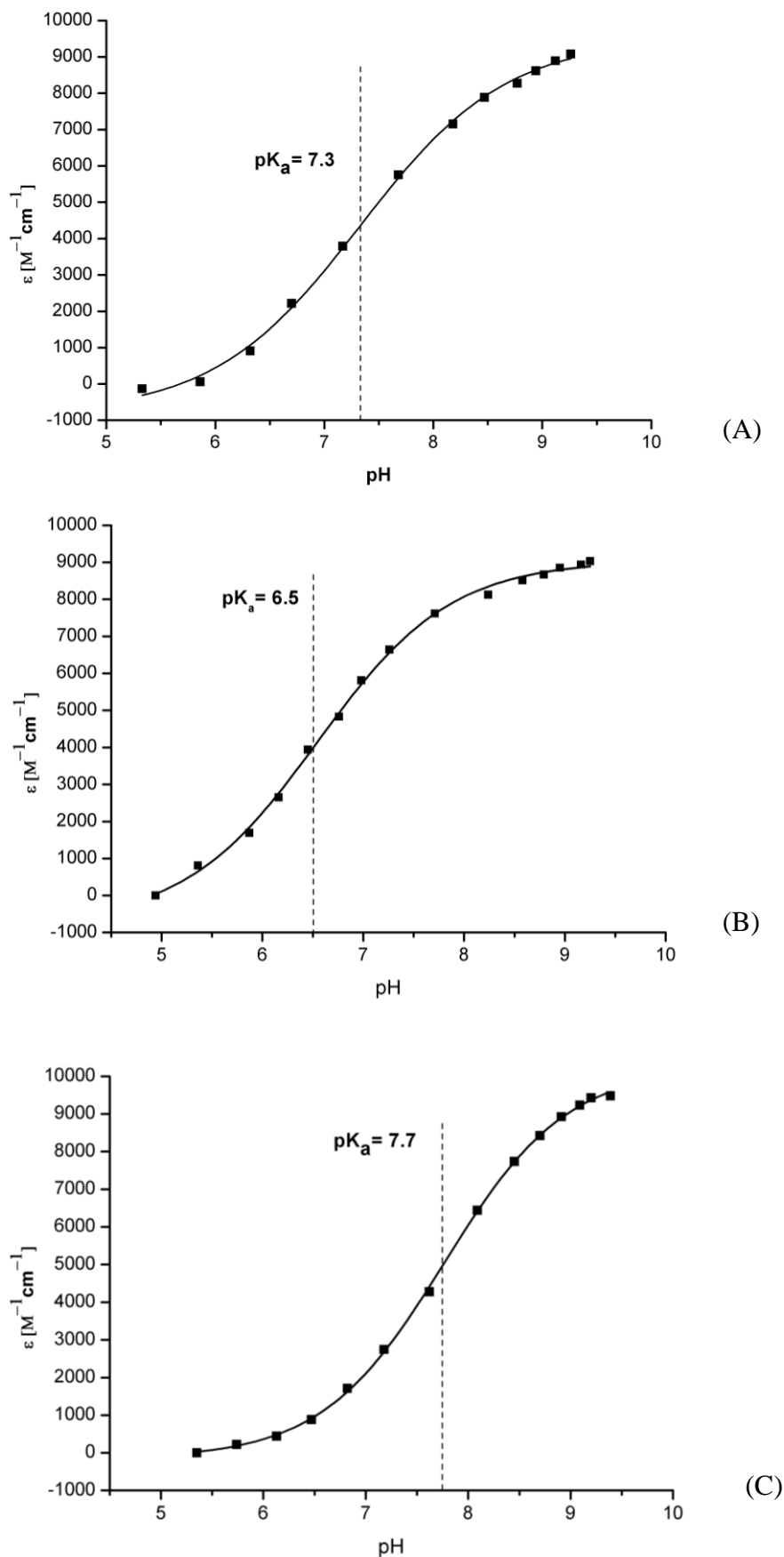
Figure 5.6 The pKa values of the active site cysteines in BC3987 were determined by pH titration. A cuvette containing 25 μM reduced protein in 1 mM polyBuffer pH 9.3 was added 2-4 uL aliquots of 25 mM HCl and the change in thiolate absorption at 240 nm were followed with a UV-vis spectrometer. For all proteins, the change in molar absorption at 240 nm during the titration indicates the occurrence of two thiols. The pKa -values estimated for the (A) native, (B) D11W and (C) T53A BC3987 were estimated to 7.3, 6.5 and 7.7, respectively.

(C)

The extinction coefficient difference at 240 nm ($\Delta\varepsilon_{240\ nm}$) due to the thiolate anion was observed to a value of approximately 9000 $M^{-1}cm^{-1}$ for the native protein and both mutants. The typical $\Delta\varepsilon_{240\ nm}$ value expected for a single thiolate is 3500-4000 $M^{-1}cm^{-1}$ (*119, 120*). The high values of extinction coefficient differences achieved in all experiments indicate the presence of two thiolates for the native, D11W mutant and T53A mutant BC3987. In all cases, based on the titration curves, both thiolates have similar pK_a values.

In order to calculate the redox potential of the native and mutant BC3987 disulfide bridges, the TrxR catalyzed equilibrium was monitored. From equilibrium constants determined at several NADPH, $NADP^+$ and BC3987 concentrations, redox potentials were calculated using a value of -315 mV for the $NADPH/NADP^+$ redox couple (*108*). Redox potentials were calculated according to Nernst Equation, which describes the electromotive force exerted between the half-reactions of a redox reaction. A titration curve showing one example of the the TrxR catalyzed reaction for the native BC3987 is presented in Figure 5.7.

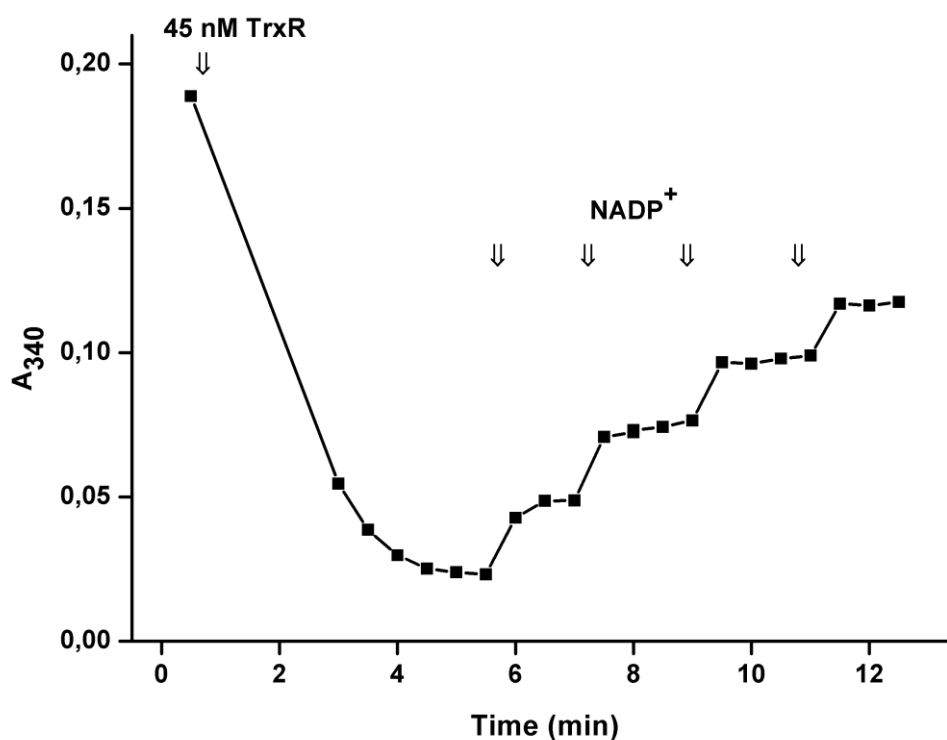**Figure 5.7** Determination of the redox potential of native BC3987. Reduction of disulfides in 40 μM BC3987 was started by addition of 30 μM NADPH, followed by addition of 45 nM TrxR. When the reaction had stopped, and A_{340} stabilized, four additions of $NADP^+$ were done, to final concentrations of 265, 520, 765 and 1000 μM, respectively.

The redox potential is estimated to values corresponding to a (S-S)/(-SH$_2$) ratio of 1, when the system is at equilibrium (See equations (9) to (14), section 4.13). For the native BC3987, the redox potential at pH 7.0 was determined to be -259 ± 3 mV using linear regression of 7 different (S-S)/(-SH$_2$) ratios ranging from 0.8 to 1.2 and the corresponding potentials calculated using the Nernst equation. Several experimental setups were explored when performing the redox potential determination of the native BC3987. (S-S)/(-SH$_2$) ratios in the range of approximately 0.5 to 1.5 were not achieved with a total protein concentration of 20 µM native BC3987, resulting in ratios in the range of 0.2 to 0.7. Experiments with elevated protein concentrations were therefore tried out. An increase in the amount of protein sample resulting in a total concentration of 40 µM gave satisfying (S-S)/(-SH$_2$) ratios suitable for calculations of redox potential. A graph representing the 7 (S-S)/(-SH$_2$) ratios plotted against the redox potential is given in Figure 5.8 A. A total concentration of 80 µM elevated the ratio to values above 2.0, not included in the calculations. Slight variations to the amount of NADP+ added to the solution were also performed in order to optimize the experiments. Experiments were performed on two different protein batches of the native BC3987.

Based on three experiments, linear regression of 9 different (S-S)/(-SH$_2$) ratios ranging from 0.5 to 1.5 was used in the estimation of the redox potential of the T53A mutant. The redox potential with a value of -256 ± 5 mV was determined. Contrary to the native BC3987, these (S-S)/(-SH$_2$) ratios were achieved using a total protein concentration of 20 µM. A graph representing the 9 (S-S)/(-SH$_2$) ratios plotted against the redox potential is given in Figure 5.8 B.
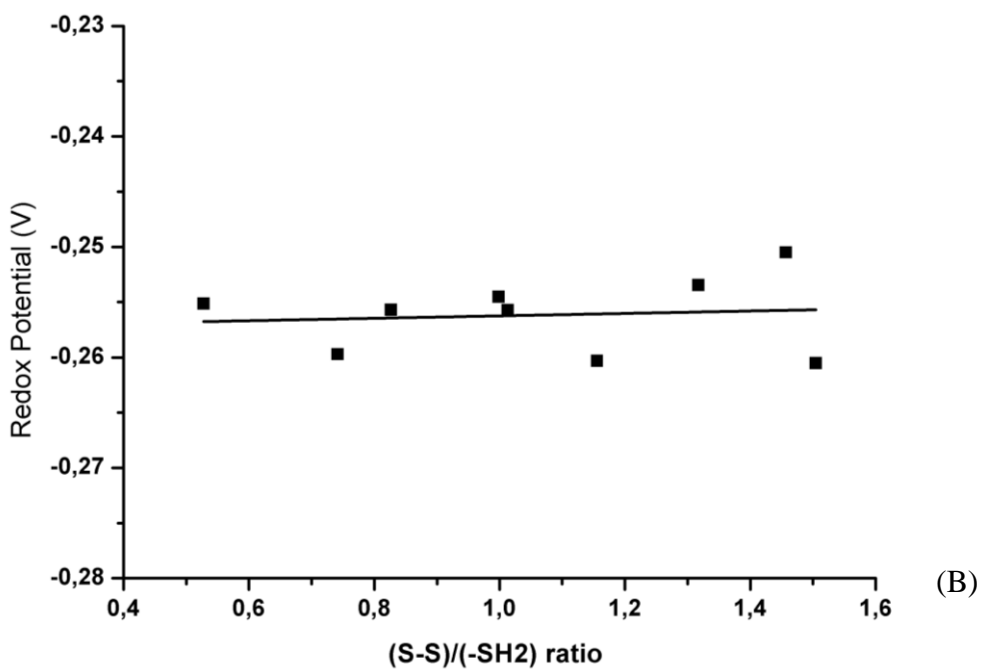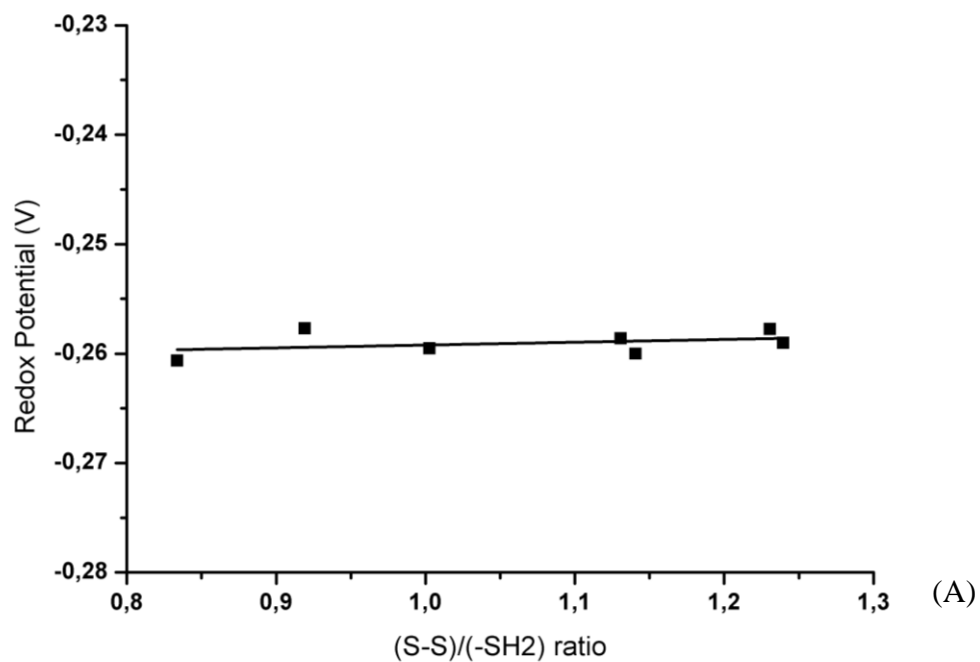
Figure 5.8 (S-S)/(-SH$_2$) ratios plotted against the redox potential for the (A) native BC3987 and (B) T53A BC3987. The redox potential calculations were based on TrxR catalyzed equilibrium. The redox potential is estimated to values corresponding to a (S-S)/(-SH$_2$) ratio of 1.

Unfortunately, successful redox potential determination of the D11W mutant was not achieved. Seven experiments were performed, resulting in (S-S)/(-SH$_2$) ratios of values between 0.02 and 0.4, non-functional in the redox potential calculations. The redox potential could not be calculated, and due to the low yield of the D11W mutant protein and limited time, no further experiments were performed.

A possible reason for the large experimental deviations in redox potential determinations of all proteins, may be due to the low purity of TrxR achieved. Also, other factors such as inadequate anaerobic experimental conditions and inaccurate measurements may have contributed to erroneous results.

Another reason for the poor results for redox potential determination of the D11W mutant could be due to structural hindrance caused by the bulky tryptophan residue. Restricting the interaction between BC3987 and TrxR would disrupt the catalytic mechanism involving these proteins. However, Trx from *E. coli* (PDBid:2TRX) encompasses a tryptophan residue in position 31, prior to the active site Cys32 and Cys35, analogous to the Trp11 insertion in the D11W mutant. The Trp residue in the BC3987 D11W mutant could, however, possibly influence the interaction between BC3987 and TrxR, in a different manner than observed for the classical interaction between *E. coli* Trx and TrxR. Nevertheless, such conclusions can not yet be drawn.

For proteins with Trx-like folds, like those discussed in this thesis, relatively high nucleophilic cysteines pK_a values are correlated with low redox potentials and vice versa. Experiments have indicated that the -X-X- residues in the active site motif contribute to changes in the pK_a values, and hence the tuning of redox potentials (*56*). There are reasons to believe that the pK_a values and redox potentials are also influenced by the nature of the amino acid residues in the vicinity of the active site. The elevated pK_a value estimated for the T53A mutant, compared to the native BC3987, is not correlated with a decrease in the redox potential. Since the pK_a variations vary with only small amounts, one can not reject the fact that changes may exist due to experimental errors. However, the increased pK_a value for this mutant may suggest that Thr53 in fact plays a role in lowering of the pK_a values of the active site cysteines of the native BC3987. Based on the lowered pK_a value estimated for the D11W mutant, this protein might exhibit a slightly higher redox potential than the native BC3987.

There are reasons to believe that both mutations performed may affect the Cys pK_a values and redox potential of BC3987. In order understand the effect of the mutations done in this thesis on protein redox potential and Cys pK_a values, additional experiments must be performed. The work done in this thesis was performed during a restricted period of time, and unfortunately, further studies are needed for a better understanding of the catalytic mechanism of BC3987.

5.3 Protein Crystallization and Structure Determination Using X-ray Diffraction

Trials to obtain crystal structures of the oxidized, as well as reduced forms of the native and two obtained mutant *B. cereus* BC3987 proteins were done in this thesis.

5.3.1 Crystal Growth

In order to obtain well diffracting crystals, various experimental setups were tried for all proteins under investigation. Each protein was crystallized using different protein concentrations, varying in the approximate range of 1.5 - 6 mg/ml, 11 – 45 mg/ml and 13 – 52 mg/ml, for the mutants D11W, T53A and native BC3987, respectively. All crystallization experiments involving native BC3987 and mutants T53A and D11W were based on Index screen conditions 55 and 65 (Hampton Research, CA, USA) (See section 7.2) as starting conditions, which was conditions previously used to crystallize the native BC3987 (*63*). The exact choice of PEG and buffer was not critical, showing that crystals could grow over a broader range of conditions. Replacing PEG MME 550 with PEG 600 in crystallization condition 55 still led to successful crystal growth. Crystal growth also appeared succeeding replacement of Bis-Tris with MES in crystallization condition 65. In addition to these exact conditions, experiments involving 95%, 90%, 85% and 70% crystallization solution diluted with mqH_2O were set up. For each protein, 15-well Nextal plates were used to screen simultaneously 15 individual conditions.

Crystals of the T53A mutant appeared after approximately 1 minute, indicating extremely fast crystal growth. The remaining crystals occurred after 1-5 days. In all cases, Index screen condition 55, with alterations as described above, resulted in plate-formed crystals of nice appearance. Crystals grown with Index screen condition 65 appeared as crystalline rosettes

each comprising a plurality of needle crystals (See Figure 5.5). Crystallization experiments involving crystallization solution not diluted with mqH$_2$O gave larger and nicer crystals compared to setups with diluted crystallization solutions.

The nicest crystals of all proteins resulted from conditions based on Index screen crystallization condition 55. This gave nice, plate-formed crystals in all cases. Crystal growth occurred from samples of varying protein concentrations, however, the largest crystals appeared from protein samples in the range of approximately 6 – 13 mg/ml. Pictures illustrating examples of crystal growth after 2 hours following set up of crystallization experiments are given in Figure 5.5.
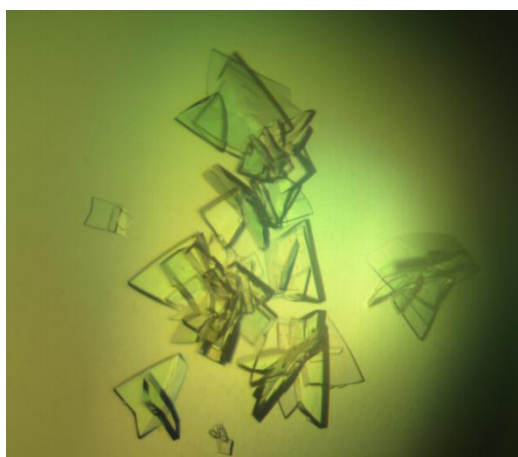
(A)
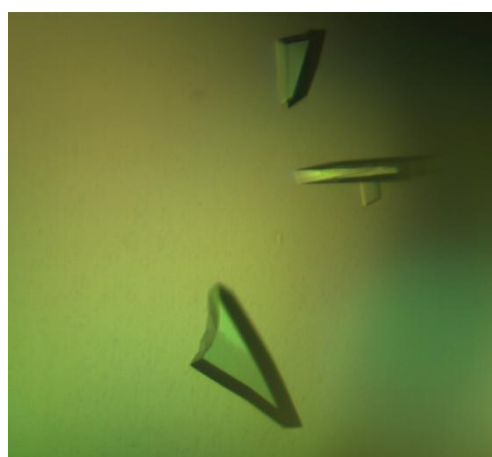
(B)
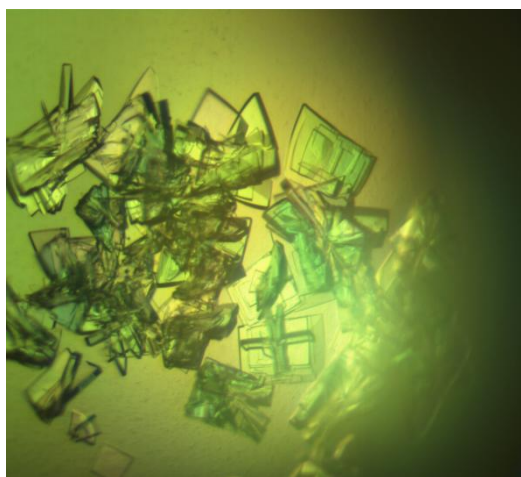
(C)
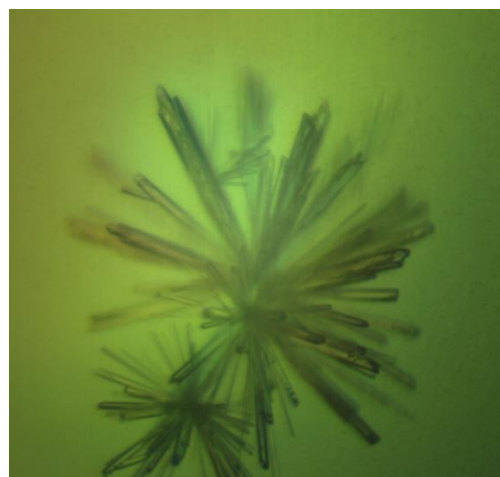
(D)

Figure 5.5 Crystals of the T53A-mutant BC3987 protein, 2 hours after crystallization setup. (A) Index screen condition 55, 11 mg/ml protein. (B) Nice, single crystals. Index screen condition 55, 11 mg/ml protein. (C) Index screen condition 55, 22 mg/ml protein. (D) Index screen condition 65, 11 mg/ml protein.

Prior to crystal freezing, single crystals were cryo-protected with mother liquor including 25 % PEG 400. Following the 30 second incubation in cryo-solution, crystals were flash frozen in a nylon loop in liquid nitrogen (Figure 5.6) and stored for later data collection.
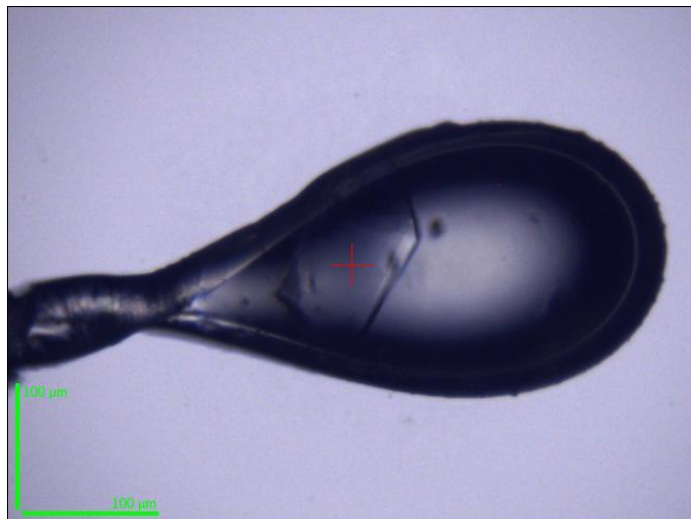
Figure 5.6 Crystal of the T53A mutant BC3987 in a fiber loop, suspended in a 100 K nitrogen stream.

For better understanding of the active site chemistry of the *B. cereus* BC3987 Trx, examination of crystal structures with a reduced active site motif of the native BC3987 as well as both mutants was attempted. To achieve crystals with a reduced active site C-P-P-C motif, crystals of all three protein forms were soaked in cryo-solution containing 100 mM DTT for 30 minutes, prior to crystal freezing.

5.3.2 Quality of the Crystal Structures

Prior to data collection, as well as after collection of X-ray data, UV-vis light absorption measurements were performed online on the protein crystal of the native BC3987 with a microspectrophotometer. The absorbance spectrum of X-ray irradiated crystal shows the appearing of a peak at approximately 400 nm. Disulphide-containing proteins are shown to form disulphide radicals at millimolar concentrations, with absorption maxima

around 400 nm(*121*). This suggests to some extent the formation of disulfide radicals upon X-ray irradiation of the BC3987 protein. The spectrum is displayed in Figure 5.7.
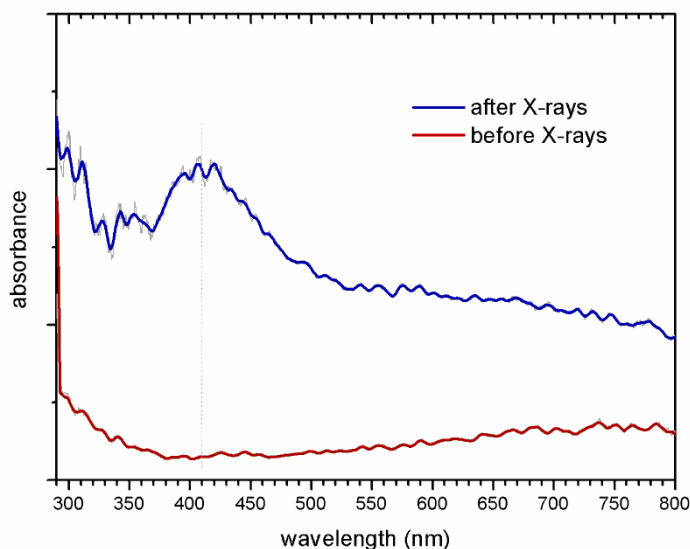
Figure 5.7 X-irradiated spectra of the native BC3987 protein crystal. An absorption peak at approximately 400 nm indicates the presence of disulfide radicals.

Data sets were collected for all 6 protein forms; native BC3987 and both mutant proteins exposed to oxidizing and reducing conditions. All structures were solved using molecular replacement. Examples of diffraction images from the collection of mutant T53A datasets are presented in Figure 5.8. All oxidized crystal structures were refined to resolutions better than 1.4 Å. Data sets of DTT-treated crystals were collected to resolutions better than 1.8 Å. However, none of the crystals treated with DTT included the chemically reduced active site motif. Instead, these crystals contained disulfides in their active sites, which were seen from the electron density maps, as well as from measurements of the disulfide bond distances. Complete refinement of only one DTT-treated crystal structure was completed, in order to illustrate that chemical reduction with DTT had failed. Therefore, the complete refinement and analysis of a total of 4 crystal structures; oxidized native BC3987, oxidized mutants T53A and D11W, as well as the DTT-treated structure of mutant T53A. Some of the disulfides in crystals of the T53A mutant protein were subjected to radiation damage.
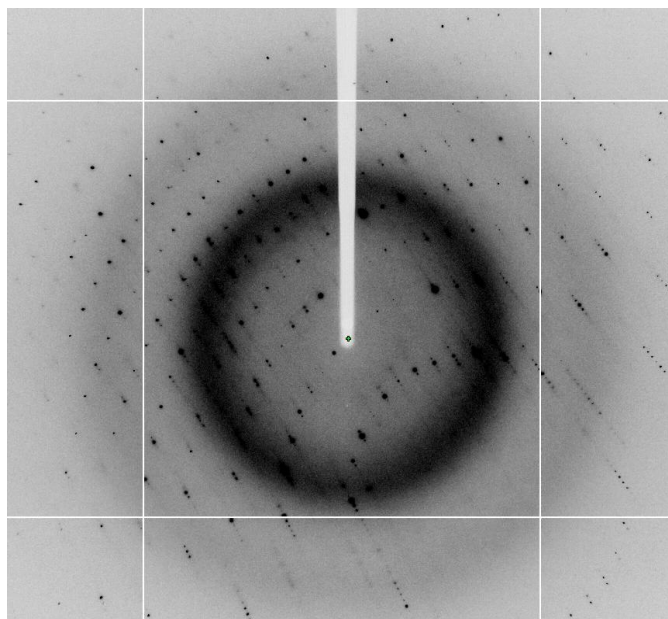
(A)
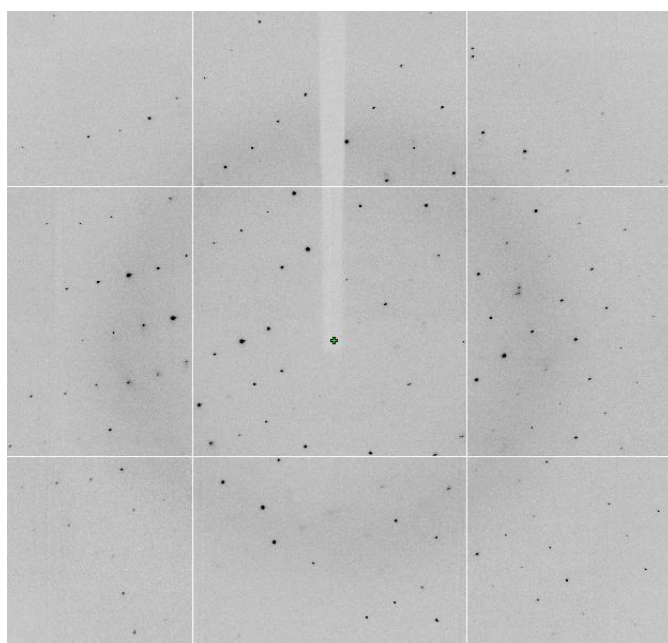
(B)

Figure 5.8 Diffraction images of the T53A mutant, showing gradual fading of intensity towards higher resolution. (A) Photograph from high resolution data collection, extending to 1.3 Å. (B) Photograph from data collection at lower resolution, extending to 2.0 Å.

Oxidized Native BC3987

The oxidized BC3987 structure was refined to 1.30 Å and contains two polypeptide chains in the asymmetric unit. Residues 2-76 and 1-78 are observed in chain A and B, respectively. Alternative conformations are observed at residues 11, 30, 31, 49 and 58 in chain A, and at residues 4, 31, 41, 49, 61 and 73 in chain B. None of the active site motifs seemed to be significant subject to radiation damage, based on inspection of the electron density difference maps and by comparing with standard distances of disulfide bonds in both chains. The total absorbed X-ray dose was calculated to a value of 0.24 MGy for the complete dataset, which is the lowest dose calculated among the crystals investigated in this thesis (see Table 5.6). This dose is far below the Henderson limit (global dose limit) of 20 MGy (*122*). However, specific radiation damage as disulfide bond rupture normally occurs at lower doses of X-ray irradiation (*123, 124*). Chain B shows the overall highest quality with all residues 1-78 clearly visible in the electron density map, even though residue 78 shows some negative density. A total of 155 water molecules was added to the structure. R_{work} and R_{free} values were determined to 14.4% and 20.1%, respectively. Refinement and validation statistics are presented in Table 5.4.

Oxidized D11W Mutant

The oxidized D11W mutant structure was refined to 1.35 Å and contains two polypeptide chains in the asymmetric unit. Residues 3-78 and 1-78 are observed in chain A and B, respectively. Alternative conformations are observed at residue 61 in chain A, and at residues 31 and 49 in chain B. None of the active site motifs were, by visible inspection of the electron density difference maps, significantly influenced by radiation damage. Total absorbed X-ray dose was calculated to a value of 0.80 MGy, somewhat higher than for the native BC3987 crystal. Both chains show good quality with all residues near the C-terminal, including Glu78, clearly visible in the electron density map. However, residues Met1 and Lys2 in chain A show poor density, and are not included in the structure. A total of 139 water molecules were added to the structure. R_{work} and R_{free} values were determined to 12.9% and 18.2%, respectively. Refinement and validation statistics are presented in Table 5.4. Substitution of Asp with Trp in position 11 was considered successful. Electron density surrounding the deleted Asp11 clearly indicated the presence of a large, aromatic residue (Figure 5.9)

(A)
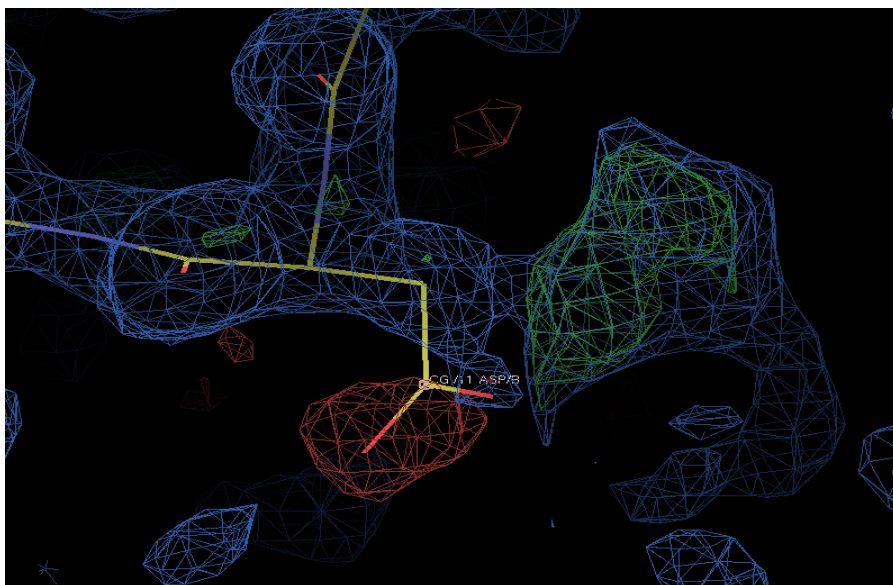
Figure 5.9 Electron density surrounding the Asp11Trp mutation, contoured at 1 σ, before and after the mutation was modeled into the new structure. (A) Model showing the presence of the substituted aspartate residue, with surrounding electron density corresponding to the D11W mutant. (B) The mutated tryptophane residue, with corresponding electron density showing good agreement to the model.

(B)

Oxidized T53A Mutant

The oxidized T53A mutant structure was refined to 1.15 Å and contains two polypeptide chains in the asymmetric unit. Residues 2-77 and 1-77 are obse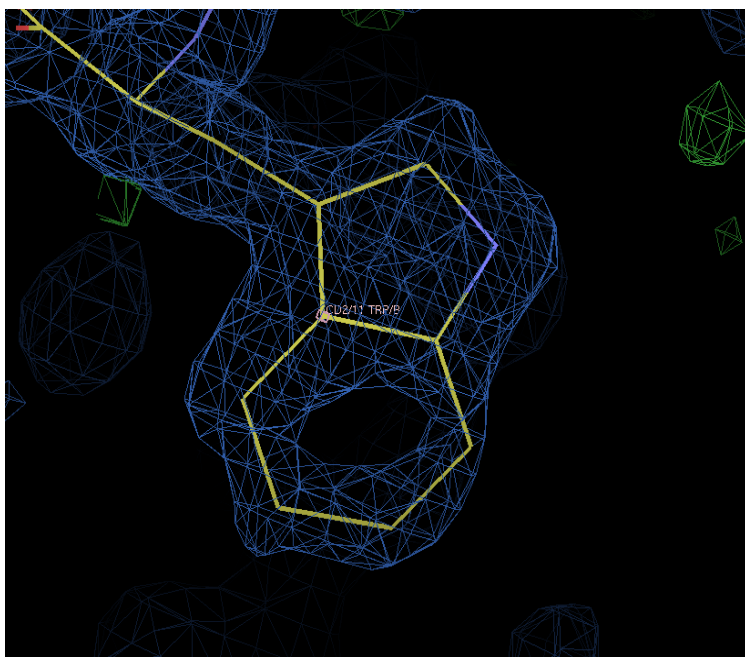rved in chain A and B, respectively. Alternative conformations are observed at residues 41, 47 and 73 in chain B. In contrast to the two structures described above, both active site motifs were clearly seen to be subject to radiation damage in the oxidized structure of T53A (See Figure 5.16). Residues Met1, Lys2 and Ile77 in chain A lack electron density at some side chain atoms, while chain B, with the exception of the non-detectable Gly78, show overall good electron density. Radiation damage is seen at cysteine bridges in both chains. The absorbed radiation dose calculated for this crystal was 1.00 MGy. A total of 118 water molecules were added to the structure. R_{work} and R_{free} values were determined to 15.0% and 19.5%, respectively. Refinement and validation statistics are presented in Table 5.4. Substitution of Thr with Ala in position 53 was considered successful. Electron density surrounding the deleted Thr53 clearly indicated the presence of a smaller residue lacking the hydroxyl side chain (Figure 5.10).
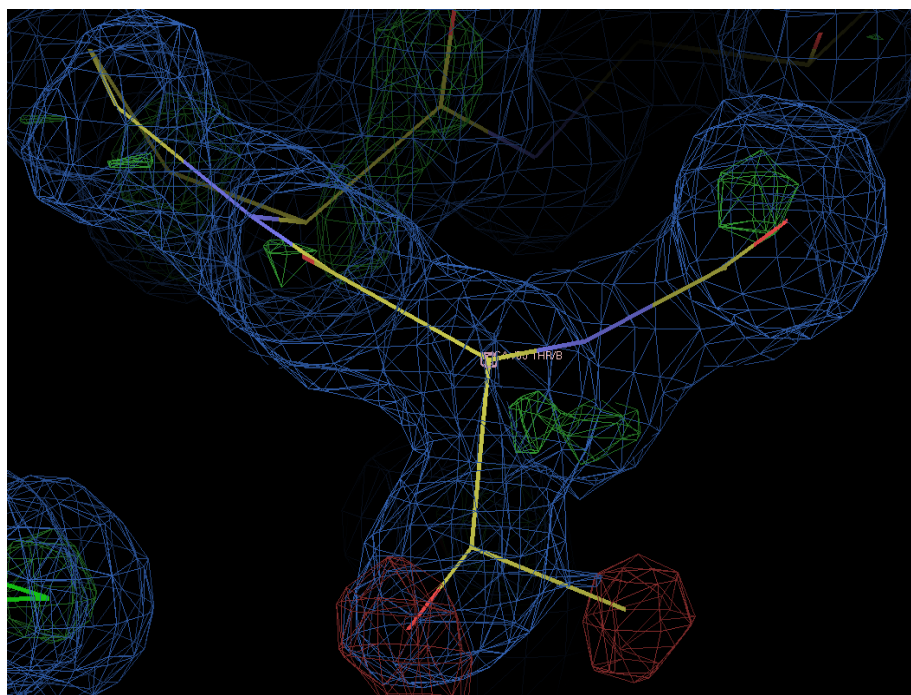
(A)
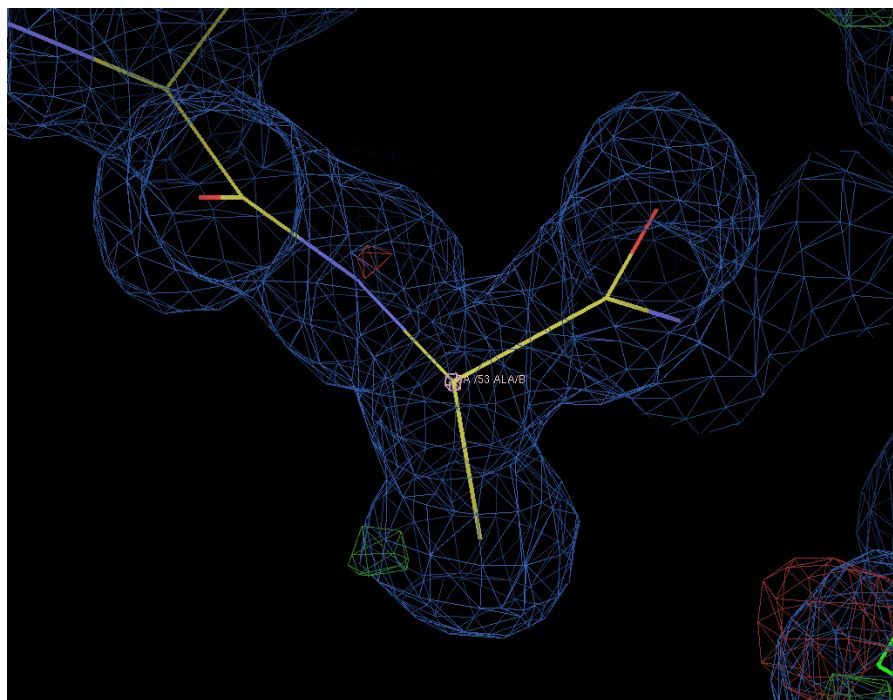
Figure 5.10 Electron density surrounding the Thr53Ala mutation, contoured at 1 σ, before and after the mutation was modeled into the new structure. (A) Model showing the presence of the substituted threonine residue. The surrounding electron density indicated the presence of a smaller residue. (B) The mutated alanine residue, with corresponding electron density showing good agreement to the model.

(B)

DTT-treated T53A Mutant

The structure of the T53A mutant treated with DTT was refined to 1.40 Å and contains two polypeptide chains in the asymmetric unit. Residues 3-75 and 1-77 are observed in chain A and B, respectively. Alternative conformations are observed at residues 31, 42 and 61 in chain A, and at residue 73 in chain B. The active site disulfide of chain A was subject to radiation damage. Residues Gln73, Leu74 and Leu75 in chain A lack electron density at some side chain atoms, while residues 1, 2, 76, 77 and 78 are not detectable. Chain B, with the exception of the non-detectable Gly78, shows overall good electron density. A reduced active site motif due to radiation damage is observed in chain A. However, the electron density surrounding the active site in chain B shows no indications of radiation damage to the disulfide bond. The absorbed radiation dose calculated for this crystal was 0.75 MGy. A total of 131 water molecules was added to the structure. R_{work} and R_{free} values were determined to 17.7% and 24.1%, respectively. Refinement and validation statistics are presented in Table 5.4.

Table 5.4 Crystal data, data collection and refinement statistics.

	Oxidized Native BC3987	Oxidized D11W Mutant	Oxidized T53A Mutant	DTT-treated T53A Mutant
Crystal data				
Space group	$P2_1$	$P2_1$	$P2_1$	$P2_1$
a, b, c (Å)	24.54/98.90/25.06	24.69/98.82/25.05	24.42/99.03/25.10	24.72/99.28/25.6
	90.00/92.16/90.00	90.00/92.06/90.00	90.00/91.79/90.00	90.00/91.41/90.00
Data collection				
X-ray source	ESRF-ID14-2	ESRF-ID14-1	ESRF-ID23-1	ESRF-ID14-1
Wavelength (Å)	0.9330	0.9334	0.9790	0.9334
Resolution range (Å)	33.0-1.30	33.0-1.35	50.0-1.15	33.2-1.40
Temeperature (K)	100	100	100	100
Completeness (%)[a]	99.1/99.1	99.8/100.0	99.7/99.0	99.4/99.4
Redundancy (%)[a]	3.7/3.2	4.8/3.6	4.7/3.7	3.7/3.2
$I/\sigma(I)$[a]	14.2/3.0	18.6/4.9	11.6/3.4	10.3/3.4
R_{Sym}[ab]	4.4/38.2	5.0/23.0	6.7/36.4	7.2/29.1
Refinement statistics				
R_{Work} (%)[c]	14.4	12.9	15.0	17.7
R_{Free} (%)[d]	20.1	18.2	19.5	24.1
Mean overall isotropic B-factor ($Å^2$)	19.1	19.0	20.2	17.7
Ramachandran plot: ration in most favoured/other allowed regions (%)	92.7/7.3	90.6/9.4	93.4/6.6	91.8/8.2
Estimated overall co-ordinate error based on R work/ maximum likelihood (Å)	0.061/0.040	0.060/0.039	0.042/0.027	0.085/0.061
Added waters	155	139	118	131
Volume not occupied by model (%)	12.6	12.7	13.1	15.2
PDB code	xxxx	xxxx	xxxx	xxxx

[a] The value before the backslash is for all data, and the value after the backslash is for the data in the highest resolution shell

[b] $R_{Sym} = \Sigma |I - \langle I \rangle| / \Sigma I$

[c] $R_{Work} = \Sigma (|F_{obs}| - |F_{calc}|) / \Sigma |F_{obs}|$

[d] R_{Free} is the R_{Work} calculated on the 5% reflections excluded for refinement

5.3.3 Overall Fold and Structure of the BC3987 Thioredoxin

The *B. cereus* BC3987 Trx includes the common architecture consisting of a four-stranded β-sheet and three flanking α-helices, shared by all Trx-like proteins, including *E. coli* NrdH. BC3987 Trx encompasses a $P12_11$ space group symmetry, with a primitive lattice and a 2-fold screw axis and crystallizes as two molecules in the asymmetric unit; chain A and chain B, thereby placing four molecules in one unit cell. The alignment of the two protein chains in the asymmetric unit, indicating the different secondary structure elements, is presented in Figure 5. 11.
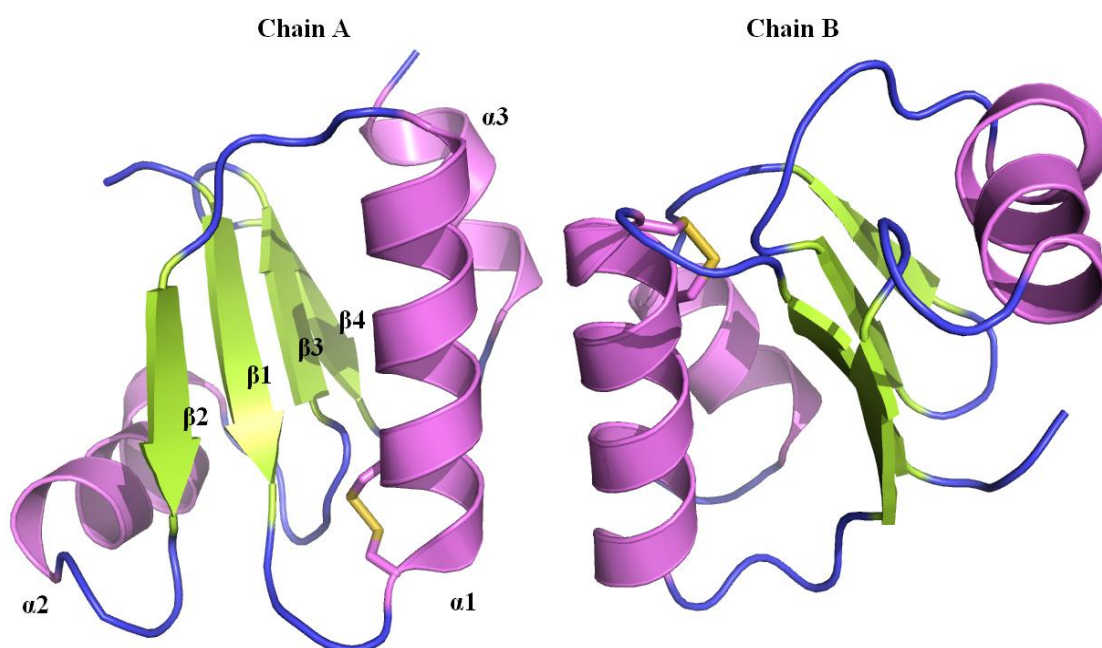
Figure 5.11 Crystal packing of BC3987 Trx in the asymmetric unit, showing chains A and B. Secondary structure elements are indicated in chain A.

As in all BC3987 crystal structures solved in this thesis, Met1 in chain A is not detectable in the electron density, and hence, not included in the models. However, this residue is clearly observed in the electron density of chain B in all structures, indicating a better ordered N-terminal of chain B contrary to chain A.

5.3.4 The Redox-active Disulfide and Environment

The oxidized crystal structures of the native and mutant BC3987 proteins show a redox-active disulfide formed between residues Cys12 and Cys15. The active site cysteine residues are located at the N-terminus of α-helix 1, proceeding a surface loop following β-sheet 1. The disulfide environment is constructed from the C-terminal residues of β-sheet 1, the turn that links β-sheet 1 and α-helix 1 and a loop connecting α-helix 2 and β-sheet 3. The N-terminal cysteine is solvent accessible, while the C-terminal cysteine is buried in the active site environment.

The crystal structures of the BC3987 proteins solved in this thesis confirmed the difference in threonine rotamers near the active site of the homologous proteins, BC3987 and NrdH, as previously described (*63*). The residue Thr8 in the vicinity of the disulphide bridge contributes to a hydrophilic environment for the buried cysteine. Contrary to what is seen in the crystal packing of NrdH-redoxins from *E. coli* and *C. ammoniagenes*, the Thr8 residue in BC3987 has a rotamer where the hydroxyl group is pointing away from the buried Cys15 Sγ-atom. This orientation of Thr8 is stabilized by a hydrogen bond to a water molecule in the case of the native BC3987 protein, as well as both mutants. Figures 5.12 A and B illustrate the overall fold of BC3987 (mutant protein D11W) compared to *E. coli* NrdH. In addition, Figures showing the active site cysteines with the neighbouring Thr8 and Thr7 rotamers, in BC3987 and NrdH, respectively, are given in Figures 5.12 C and D.

(A)   (B)

(C)   (D)
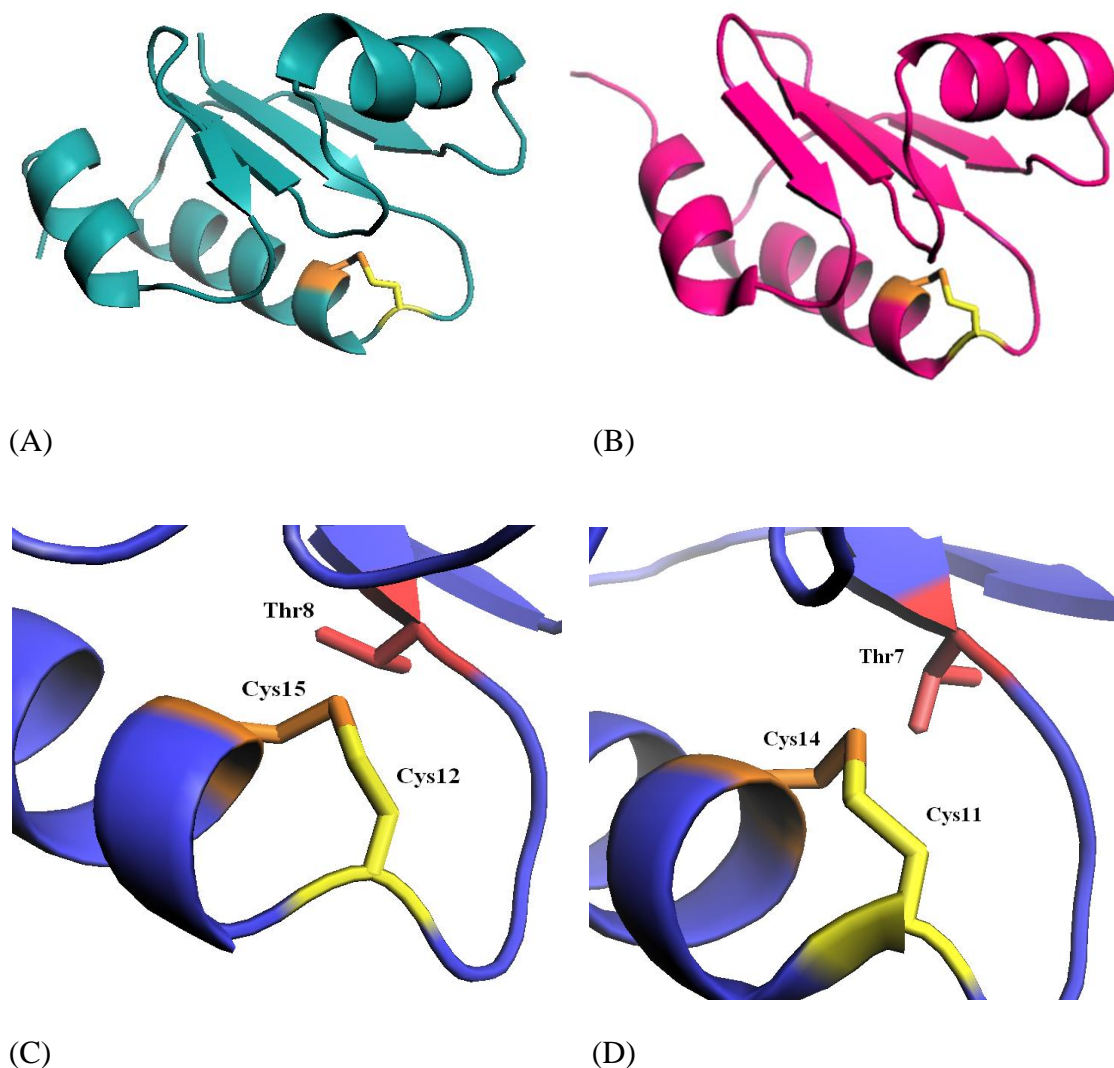
Figure 5.12 Overall structures of the two homolog's *B. cereus* BC3987 and *E. coli* NrdH, indicating the active site disulfide highlighted in yellow/orange. (A) BC3987 Trx (Asp11Trp-mutant, chain A). (B) NrdH-redoxin (PDBid:1H75). (C) Active site of BC3987 Trx. (D) Active site of NrdH. The different threonine rotamers in the vicinity of the disulfide bridge are highlighted in red.

Unfortunately, further investigation of the active site chemistry of BC3987, by examining the possible stabilization of the C-terminal buried cysteine through hydrogen bonding to an adjacent conserved Thr8 residue, failed due to unsuccessful substitution of Thr8. However, the successful generation of the two additional mutant versions of BC3987, and their solved crystal structures, has led to other findings around the possible catalytic mechanism of this Trx.

The D11W Mutant

Among all crystal structures solved in this thesis, the 1.35 Å crystal structure of the D11W mutant version of BC3987 was refined to the best R factor. Chain A, as in all structures, lacks density at the N-terminal methionine residue, which unable us to predict its orientation. Also, Lys2 of chain A show lacking electron density in this structure. Beside these inadequacies, electron density surrounding both chains shows overall good quality, and most side chain atoms are clearly visible. Contrary to the remaining structures solved, the C-terminal Glu78 residue is visible in both chains in the electron density of the D11W mutant. This clearly indicates that the presence of a tryptophan residue, instead of an aspartate, in position 11 plays a significant structural role in the stabilization of the N-terminal Glu78 during crystal packing. The residue in position 11 is positioned in close vicinity to the residue in position 78 in a neighbouring molecule in the crystal. Besides this possible effect on crystal packing and structural stabilization, the mutation in position 11 has not led to any significant environmental changes in the vicinity surrounding the active site. A ribbon diagram showing the BC3987 Trx with the D11W mutation, as well as a Figure showing the electron density map surrounding the active site motif and tryptophan mutation, is presented in Figure 5.13.

(A)   (B)
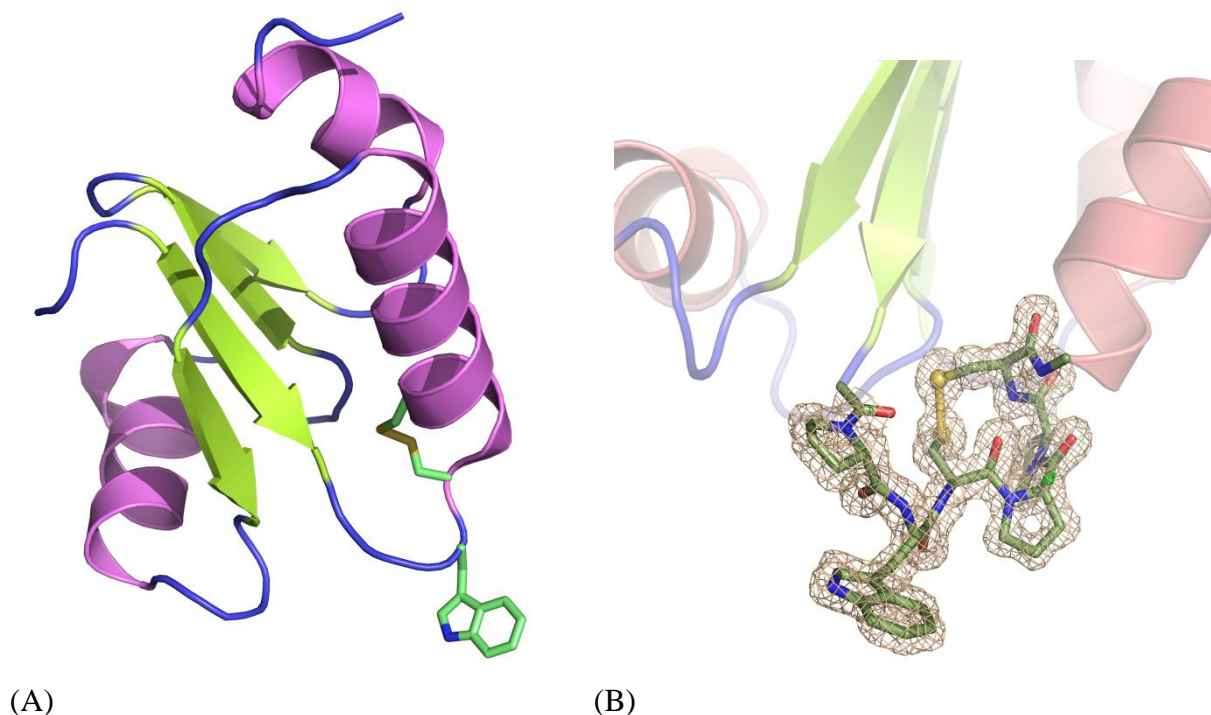
Figure 5.13 The D11W mutant. (A) Ribbon diagram showing the D11W mutant protein, with the active site disulfide and Trp11 illustrated with sticks. (B) Electron density map surrounding the mutant active site, showing the presence of the tryptophan residue in position 11.

The T53A Mutant

Residues 2-77 and 3-75 in chain A were visible in the electron density of the oxidized and DTT-treated T53A mutants, respectively. Residues 1-77 in chain B were detectable in both structures, with overall better quality compared to chain A. The mutation has not caused any significant structural changes to the environment surrounding the active site. A superimposition representing the active site of the native and T53A mutant structures is presented in Figure 5.14.
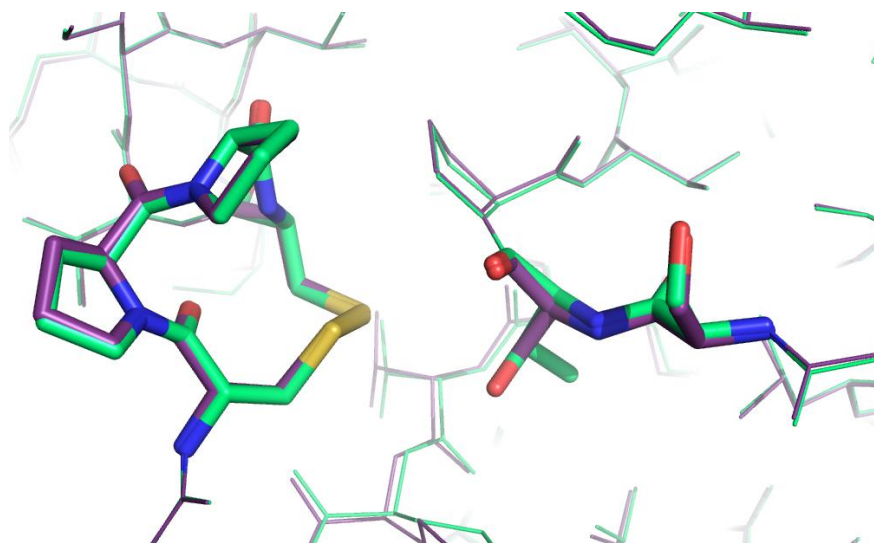
Figure 5.14 Superimposition of the active site vicinity of native (green) and T53A mutant (violet) structures. Native threonine and mutant alanine residues are seen on the right, while the active site motif is on the left, all presented as sticks.

Figure 5.15 shows a ribbon diagram of the BC3987 Trx with the T53A mutation. A Figure showing the electron density map surrounding the alanine mutation in the vicinity of the active site is also displayed.

(A) (B)
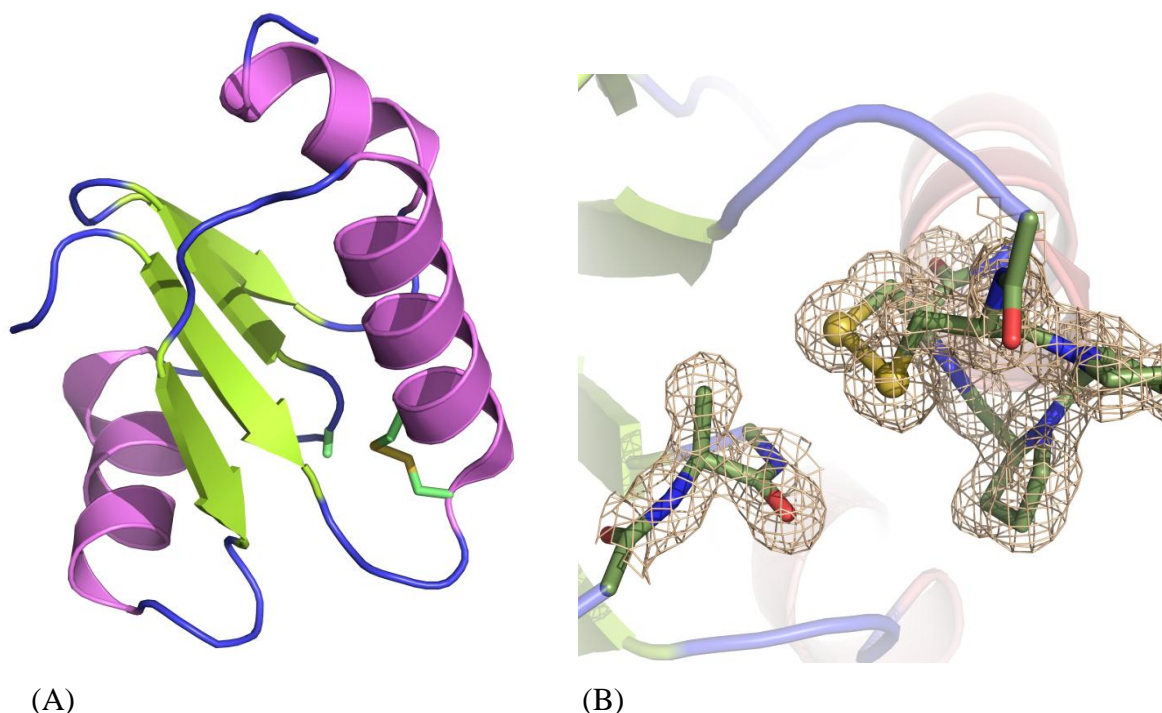
Figure 5.15 The T53A mutant. (A) Ribbon diagram showing the T53A mutant protein, with the active site disulfide and Ala53 illustrated with sticks. (B) Electron density map surrounding the mutant active site, showing the presence of the alanine residue in position 53, adjacent to the active site.

Reduction of the active site disulfide by DTT (as in all attempts of reduction regarding all structures) was not successful. Distances between the Sγ-atoms of Cys residues of disulfide bridges in all crystal structures were in the range between 2.11 and 2.23 Å, with a maximum deviation of approximately 0.1 Å. These values are close to ideal disulfide bonding distances (*125*). Also, the observed distances differ from distances between the Sγ-atoms of chemically reduced Cys residues in a structure of another member of the Trx superfamily, indicating that the active site S-atoms formed covalent bonds in all structures prior to data collection (*125*). To determine as accurately as possibly the disulfide distances, the restraints involving the S-S bond was releases, allowing the atoms to move more freely. Values indicating the distance between the Sγ-atoms of Cys residues are presented in Table 5.5. A few rounds of refinement of the structures refined in Refmac was performed using the program SHELX (*126*), to see if this could improve the models. No significant improvement was observed, and the values of disulfide bond lengths remained almost identical.

Table 5.5 Distances between sulfur atoms in disulfide bridges.

Protein	S-S Distance (Å), Chain A	S-S Distance (Å), Chain B
Native BC3987	2.12	2.11
D11W Mutant	2.18	2.17
T53A Mutant	2.19	2.23
T53A Mutant, DTT-Treated	2.22	2.19

However, active site cysteines in both chains of the oxidized T53A mutant structure were reduced to some extend, exhibiting negative density where the molecular model contained a disulfide bridge. This feature was also observed in chain A of the DTT-treated structure of T53A. Sulfur atoms have a significantly higher absorption cross section than do carbons, oxygens and nitrogens, and might be more affected by primary radiation damage. Disulfide bonds are sensitive to radicals, and therefore also secondary damage. Although the sulfur atoms in this structure do not seem to be affected by radiation damage, and complete radiation damage of the disulfides is not the case, disulfide bonds might be in an early stage of rupture. Studies have shown a disulfide elongation of ~0.7 Å upon X-ray irradiation if a disulfide radical, $H_2S_2\bullet^-$, is formed (*124, 127*). However, since no significant bond elongation has occurred in the crystals, radicals are most likely not generated to a high extend in crystals investigated in this thesis. The crystal of the oxidized T53A mutant, most subject to radiation damage, was exposed to the highest dose amount (Table 5.6). However, other crystals experiencing similar doses did not show a similar pattern of radiation damage, as in the case of the D11W mutant and DTT-treated T53A mutant, the latter encompassing negative electron density at the active site of one monomer. The other monomer, not showing this feature, has possibly remained unaffected by specific radiation damage due to the protective impact of DTT as a scavenger of solvated electrons (*128*). A factor possibly influencing the higher extend of radiation damage caused to the oxidized T53A mutant structure, is the dose rate (k_{dose}) (*128*). The X-ray flux has a strong effect on k_{dose}, and the ID23 beam line used for data collection of this mutant generates radiation of somewhat higher energy than the ID14 beam lines used in data collection of the remaining crystals. Since only one of the active site motifs in the dimeric DTT-treated T53A crystal, both monomers of the oxidized T53A mutants and none of the two remaining crystals showed visible signs of radiation damage, one can not reject the fact that the dose range exerted on all crystal covers opposite borders of an

area which will or will not potentially lead to radiation damage of disulfides. If this is the case, radiation damage observed in some active site motifs can have been caused by coincidence.

Table 5.6 Total absorbed dose per protein crystal.

	X-ray dose (MGy)
Native BC3987	0.24
D11W Mutant	0.80
T53A Mutant	1.00
T53A Mutant, DTT-Treated	0.75

Models showing the oxidized active site disulfide in chain B and the negative electron density surrounding the active site disulfide of chain A of the DTT-treated T53A crystal are presented in Figure 5.16.

(A)   (B)
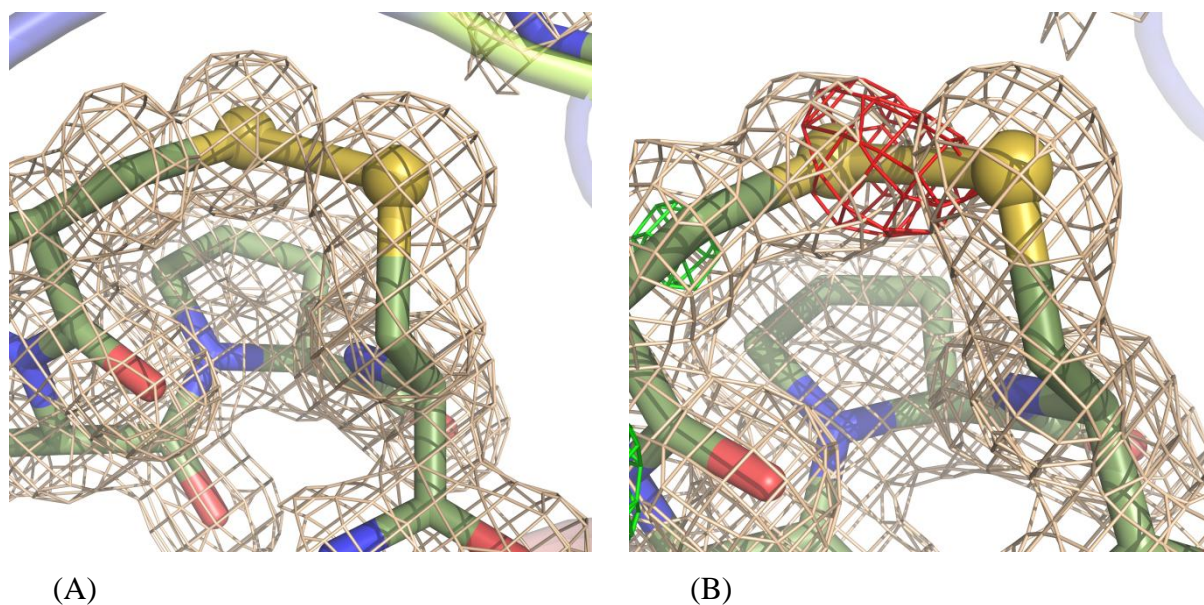
Figure 5.16 The T53A mutant. (A) Electron density surrounding the active site in chain B of the DTT-treated T53A crystal (B) Electron density surrounding the active site of chain A of the DTT-treated T53A crystal. Same feature observed in both chains of the oxidized T53A crystal.

6 Concluding Discussion

Site directed mutagenic studies combined with structural and functional studies are believed to give useful information regarding the catalytic mechanism of *B. cereus* BC3987 Trx, a possible electron donor for class Ib RNR.

Construction of the Mutants

The residues chosen for substitution in the vicinity of the active site were Val6, Thr8, Asp11, Pro13, Pro14, Arg41 and Thr53. The foundation for the mutations is summarized in Table 5.1, and some of them are discussed further in this section. The main goal of this thesis was to investigate the catalytic mechanism of BC3987 as a thiol-disulfide reductase. As described previously, BC3987 has been suggested to stabilize both active site cysteines in their deprotonated thiolate form, differing from the conventional active site chemistry exemplified by *E. Coli* Trx (*63, 74*). Contrary to *E. Coli* Trx, BC3987 does not contain a conserved Asp residue six amino acids prior to the N-terminal cysteine, believed to stabilize the buried C-terminal cysteine in Trx. Instead, conserved serine and threonine residues with polar side chains, prior to the active site motif, have been localized in Cp9, NrdH and BC3987 (See Table 2.2). It has been suggested that Thr8, positioned in the vicinity of the active site C-X-X-C motif of BC3987, functions a potential hydrogen bond donor to the buried C-terminal Cys15, and contributes to the lowering of the cysteine pK_a value in this protein. This Thr8 residue has therefore been of particular interest in mutational studies of the BC3987 active site environment. A mutation of this hydroxylic amino acid side chain position would most likely create an active site environment differing from what is seen in most NrdH-redoxins and other Trx-like proteins including a C-P-P-C active site motif (See Table 2.2). Replacing Thr8 with an Ala residue, would eliminate the potential stabilizing hydrogen-bonding thought to exist between Thr8 and Cys15. Also, a Thr in position 53 of BC3987 might participate in the deprotonation of the buried cysteines. The substitution of Thr53 with the aliphatic residue Ala, would potentially eliminate an additional hydrogen bond to the buried Cys15, and provide us with more knowledge regarding the active site chemistry of BC3987. NrdH-redoxins, however, encompass a conserved proline residue in position 52, analogous to position 53 in BC3987 (*18*). An Asp residue in the amino acid position prior to the N-terminal active site cysteine, as in *B. cereus* BC3987, is also found in *E. coli* NrdH-redoxin. A model of this NrdH bound to *E. coli* TrxR, based on the structure of the complex of Trx with TrxR (*129*), shows that this Asp residue is positioned close to the NrdH hydrophobic surface pocket

creating the NrdH-TrxR interaction site (*28*). This aspartate residue is however not conserved among all NrdH-redoxins in various organisms, showing that equivalent positions may also contain i.e. Asn (*S. typhimurium* NrdH) and Ala (*M. tuberculosis* NrdH) (*28*). It is not clear if this Asp residue plays an analogous role in the BC3987-TrxR interaction site, and a crystal structure of the *B. cereus* BC3987-TrxR complex has not yet been solved. *E. coli* Trx, on the other hand, contains a conserved bulky tryptophan residue in the position prior to the N-terminal active site cysteines, as in the case of the D11W mutant BC3987 (*33*). The D11W mutant was believed to mimic this Trx active site environment, leading to findings that could contribute to a better understanding of the BC3987 catalytic mechanism. Substituting Asp11 in BC3987 with a residue containing a large, aromatic side chain such as tryptophan, would create an active site environment more similar to the classical environment observed in *E. Coli* Trx. Shifts towards e.g. lower nucleophilic cysteines pK_a values, resembling Trx, would potentially prove this residue's role in tuning of pK_a values, and hence, the redox potential of BC3987.

Although the production of most BC3987 mutants failed, two successfully mutated proteins of full length were obtained (See section 5.1.1). The D11W mutant, containing a bulky tryptophan residue protruding from the loop connecting α-helix 1 and β-sheet 1, as well as the T53A mutant, with the removal of a potential hydrogen bonding residue in close vicinity to the active site motif, were subject for further investigation.

Functional and Structural Studies

The structural studies performed in this thesis have provided information about the three-dimensional structure of BC3987, which seems largely unaffected by the mutations introduced in the protein. The presence of a different rotamer of Thr8 compared to the analogous Thr7 in NrdH has been confirmed, as seen from a previously solved BC3987 crystal structure (*63*). Radiation-induced damage of several disulfide bridges in crystals of the T53A mutant proteins was observed in the corresponding electron density difference maps. Crystals exposed to reducing conditions with DTT, as well as untreated crystals, showed these features. This suggests that the substitution of a Thr residue bearing a polar, hydroxylic side chain with the small, aliphatic hydrocarbon side chain of Ala may have made the active site motif more exposed to radiation-induced reduction. However, due to the low X-ray dose

absorbed by all crystals, the radiation damage observed in these crystals may have been caused by incident. The elevated pK_a value of 7.7 estimated for the T53A mutant, compared to a pK_a value of 7.3, proposed for the native protein, may indicate that Thr53 contributes to some degree in the lowering of the active site Cys pK_a values in the native BC3987 Trx. This suggests that Thr53, not unexpectedly, can contribute to the stabilization of buried C-terminal cysteines. The experimental data resulting from the redox potential determination of this mutant included high standard deviations, and the participation of Thr53 as a hydrogen donor to the Cys15 Sγ-atom is still unclear. Regarding the D11W mutant protein, insertion of the nonpolar residue Trp, with its bulky, aromatic side chain, has suggested to play a significant stabilizing role in crystal packing in the BC3987 protein. Due to the presence of a Trp residue in position 11, the C-terminal glutamate residues in position 78 are clearly visible in the electron density maps surrounding both chains of this mutant structure, not detected in previous studies (*63*). No redox potential was estimated for this mutant, even though several attempts were made. The shift towards a lower pK_a value, compared to the native protein suggests that Asp11 could possibly contribute to the maintenance of a low redox potential.

Future Perspectives

Findings resulting from the functional studies in this thesis are relative estimations, and additional experiments are needed for reinforcement of the possible explanations discussed. Lacking the crucial Thr8 mutant necessary to test the deprotonation mechanism hypothesis, further investigation of the catalytic function and biological role of the BC3987 Trx is required. Investigation of additional mutant versions of BC3987 could provide us with more useful knowledge about this enzyme. Hence, more work is needed to pursue the goal of determining the biological function of BC3987 Trx in *B. cereus*, and investigating its ability to serve as an electron donor for various substrates, bringing us closer to a complete understanding of this enzymes unusual catalytic mechanism.

Through QM/MM calculations, previous observations have shown that the reduced form of BC3987 seems to possess two cysteines residues in the active site with lowered pK_a values, explained through intra-protein hydrogen bonding (*63*). Additional attempts to generate BC3987 crystals with a reduced active site motif would give further insights into this theory. Improvement of the crystallization procedure and the use of different reducing agents of

various concentrations, such as methyl viologen, could promote the generation of crystals with a reduced active site motif. Also, chemical reduction of proteins can be done prior to, or succeeding crystallization.

Crystallization of native and mutant versions of BC3987 in complex with its electron donor TrxR is also an interesting aspect, which would provide us with knowledge concerning the interaction between these enzymes. Studies of these protein complexes and conformational changes upon binding, compared to the crystal structure of the *E. coli* Trx-TrxR complex (*129*), could give us better understanding of their redox chemistry in *B. cereus*.

The biological function of BC3987 can hopefully be elucidated through biological assays, in order to investigate BC3987's potential role as an electron donor. Studies of the potential interaction between BC3987 and class Ia and Ib RNR is of interest. The sequence homology between BC3987 and Cp9-redoxins has suggested a functional relationship for these enzymes. The use of biological assays in the investigation of BC3987's role as a potential reductant of peroxiredoxins in *B. cereus* is of interest in addressing the biological role of BC3987.

Other spectroscopic studies of the native and mutant versions of BC3987, as well as BC3987 involved in different protein complexes are potential future goals.

7 Appendices

7.1 Appendix 1 - Materials

Table 1 – Chemicals

Chemical	Manufacturer
1 kb DNA ladder	Fermentas
6x Loading Dye Solution	Fermentas
Acetic Acid (100 %, p.a.)	Merck
Agar	Merck
Agarose	Merck
Ampicillin	CALBIOCHEM
Ammonia (25 %, p.a.)	Merck
Ammonium Acetate	Merck
Ammonium Sulfate (p.a.)	Merck
Antifoam	Sigma
Argon ((g), 99.9997 %)	AGA
Bacto Agar	Difco
Bacto Tryptone	Difco
Bacto Yeast Extract	Difco
Bis-Tris	Merck
Bromphenol Blue	Sigma
$CaCl_2$	Merck
Coomassie Blue	Amersham Biosciences
Di-Potassium Hydrogen Phosphate	Merck
Dithiothreitol	Sigma
dNTPs (dATP, dCTP, dGTP, dTTP)	Fermentas
Dpn I restriction enzyme	New England Biolabs
EDTA (> 99 %)	Sigma
Ethanol (Absolutt Prima)	Arcus
Ethidium Bromide	Amersham Biosciences

Glucose	Sigma
Glycerol (87 %, p.a.)	Merck
HEPES (>99.5 %, Free Acid)	Sigma
Hydrochloric Acid (36 % p.a.)	Prolabo
Isopropyl β-D-Thiogalactopyranoside	Sigma
Low Molecular Weight Standard	GE Healthcare
Magnesium Chloride Hexahydrate	Merck
Methanol (>99.5 %, p.a.)	Merck
Nitrogen (lq)	AGA
Oxygen (g)	AGA
PhastGel Blue R (Tablets)	GE Healthcare
Polyethylene Glycol 400	Sigma
Polyethylene Glycol 600	Sigma
Polyethylene Glycol 10 000	Sigma
Polyethylene Glycol Monomethyl Ether 550	Sigma
Potassium Chloride (p.a.)	Merck
Di-Potassium Hydrogen Phosphate (p.a)	Merck
Potassium Di-Hydrogen Phosphate (p.a.)	Merck
Potassium Hydroxide (p.a.)	Merck
Sodium Borate (p.a)	Hopkin & Williams
Sodium Chloride (p.a.)	Merck
Sodium Citrate (p.a)	Merck
Sodium Dithionite (~80 %)	Sigma
Sodium Dodecyl Sulfate (> 99 %)	Sigma
Sodium Hydroxide (p.a.)	Merck
Di-Sodium Hydrogen Phosphate (p.a)	Merck
Sodium Di-Hydrogen Phosphate (p.a)	Merck
Streptomycin Sulfate	Sigma
Taq DNA Polymerase buffer	Fermentas
Taq DNA Polymerase	Fermentas
Tris(hydroxymethyl)aminomethane (> 99.9 %)	Sigma

Table 2 - Chromatographic Column Materials

Material	Manufacturer
HiTrap Desalting Column	GE Healthcare
HiTrap Q HP Column	GE Healthcare
Superdex 200 Column	GE Healthcare

Table 3 – Hardware

Hardware	Manufacturer
Äkta purifier system	GE Healthcare
PCR Cycler (PTC-200)	MJ Research
HP8452A Spectrophotometer	Hewlett Packard
JA-10 Rotor	Beckman
JA-14 Rotor	Beckman
JA-20 Rotor	Beckman
NanoDrop (ND-1000)	NanoDrop Technologies
pH meter (PHM 240)	Radiometer Analytical
PhastSystem	GE Healthcare

Table 4 - Equipment

Equipment	Manufacturer
Centricon (YM-10)	Millipore
Amicon ultra 15	Millipore
Cryo Loops	Hampton Research
Crystal Caps & Vials	Hampton Research
Crystallization Plates (Nextal)	QIAGEN
Cuvettes (quarts)	Helmma
Precision Syringes	Hamilton
Millex-GP 0.22 μm filter	Millipore
NAP-5 Columns	GE Healthcare
Nitrocellulose Filters (0.45 μm)	Millipore
PD-10 Columns	GE Healthcare

PhastGel (10-15 Gradient)	GE Healthcare
PhastGel SDS buffer Strips	GE Healthcare

Table 5 – Kits

Kit	Manufacturer
NucleoSpin Plasmid	Machery Nagel
QuickChange® XL Site-Directed Mutagenesis Kit	Stratagene

7.2 Appendix 2 – Media and Solutions

H_2O used in all solutions and mediums was MilliQ filtered and ion-exchanged (mqH_2O). Buffer solutions were degassed for 20 minutes before application.

Culture Mediums

LB Culture Medium, 1 L

Bacto Tryptone	10 g
Bacto Yeast Extract	5 g
Sodium Chloride	10 g

Autoclave the contents solved in 1 L of mqH_2O, at 121ºC for 20 min. When preparing Petri dishes, add 15 g of Bacto Agar per litre LB medium, prior to autoclavation.

TB Culture Medium, 12 L

Bacto Tryptone	150 g
Bacto Yeast Extract	300 g
Glycerol	50 ml

Autoclave the contents solved in 11 L of mqH_2O, at 121ºC for 20 min. Add buffer A just before use, to avoid precipitation of phosphate salts, and adjust pH to 7.2.

SOC Medium, 0.1 L

Bacto Tryptone	2 g
Bacto Yeast Extract	0.5 g
Sodium Chloride	0.05 g
25 mM Potassium Chloride	1 ml
mqH$_2$O	95 ml
2 M Glucose	1 ml

Autoclave the all contents, except glucose, solved in 95 ml of mqH$_2$O, at 121ºC for 20 min.
Add 1 ml 2M glucose.

Buffers

Buffer A

KH$_2$PO$_4$	29 g
K$_2$HPO$_4$ x 3H$_2$O	156 g
mqH$_2$O	1.2 L

Buffer B

50 mM Tris

pH = 7.5

Adjust pH to 7.5 by adding concentrated HCl to the basic Tris-solution

Buffer C

50 mM Tris

1 M KCl

pH = 7.5

Adjust pH to 7.5 by adding concentrated HCl to the basic Tris-solution

Buffer D

50 mM Tris

100 mM KCl

pH = 7.5

Adjust pH to 7.5 by adding concentrated HCl to the basic Tris-solution

Polybuffer

1 mM Sodium Phosphate

1 mM Sodium Citrate

1 mM Sodium Borate

0.1 mM EDTA

Adjust pH to 9.3 by adding conncentrated NaOH.

Phosphate buffer

100 mM $NaH_2PO_4.H_2O$

100 mM $Na_2HPO_4.H_2O$

1 mM EDTA

Adjust pH to 7.0 by adding the 100 mM Na_2HPO_4 x H_2O solution to the 100 mM NaH_2PO_4 x H_2O solution. Add 1 mM EDTA, and correct for pH variations.

Agarose Gel

---

50 x TAE-buffer, 1 L

Tris	254 g
Glacial Acetic Acid	57.1 ml
500 mM EDTA, pH 8.0	100 ml
mqH2O	1 L

Autoclaved at 121 ºC for 20 min.

Agarose Gel, 1 %

Agarose	0.4 g
1 x TAE	50 ml

Heat in a microwave until the agarose is completely dissolved. After cooled down to ~60 ºC, add 3 µl ethidiumbromide.

PhastSystem Solutions

Phast Loadmix

10% SDS solution	500µl
2-Mercaptoethanol	100 µl
0.1% Bromphenol Blue solution	200 µl

Phast Staining Solution

Coomassie Blue solution	100 ml
20% Acetic acid	100 ml

Phast Destaining Solution

Methanol	90 ml
Acetic acid	30 ml
mqH$_2$O	180 ml

Phast Preservation Solution

Glycerol	8 ml
Acetic acid	8 ml
mqH$_2$O	64 ml

Crystallization Solutions

Crystallization Index Screen 55 (Hampton Research, CA, USA)

50 mM Magnesium Chloride Hexahydrate

100 mM HEPES, pH 7.5

30 % (w/v) Polyethylene Glycol Monomethyl Ether 550

Crystallization Index Screen 65 (Hampton Research, CA, USA)

100 mM Ammonium Acetate

100 mM BIS-TRIS, pH 5.5

17 % (w/v) Polyethylene Glycol 10,000

7.3 Appendix 3 – Sequences

Mutagenic Primers

Primer *	Sequence **
D11W F:	5' –GTTTATACACAACCCTGGTGTCCGCCATGTG- 3'
D11W R:	5' –CACATGGCGGACACCAGGGTTGTGTATAAAC- 3'
P13G F:	5' –CACAACCCGATTGTGGCCCATGTGTTATTG- 3'
P13G R:	5' –CAATAACACATGGGCCACAATCGGGTTGTG- 3'
P14H F:	5' –CAACCCGATTGTCCGCATTGTGTTATTG- 3'
P14H R:	5' –CAATAACACAATGCGGACAATCGGGTTG- 3'
P14W F:	5' –CAACCCGATTGTCCGTGGTGTGTTATTG- 3'
P14W R:	5' –CAATAACACACCACGGACAATCGGGTTG- 3'
P14Y F:	5' –CAACCCGATTGTCCGTATTGTGTTATTG- 3'
P14Y R:	5' –CAATAACACAATACGGACAATCGGGTTG- 3'
P13G + P14H F:	5' –GGTTTATACACAACCCGATTGTGGGCATTGTGTTATTGTAAAAG- 3'
P13G + P14H R:	5' –CTTTTACAATAACACAATGCCCACAATCGGGTTGTGTATAAACC- 3'
R41G F:	5' –GACGCTGCTGCTGGCAATCGTCTTTTATAC- 3'
R41G R:	5' –GTATAAAAGACGATTGCCAGCAGCAGCGTC- 3'
T53A F:	5' –CTATGATTCTTATTCAGCTCCAACAGTCGTAATTG- 3'
T53A R:	5' –CAATTACGACTGTTGGAGCTGAATAAGAATCATAG- 3'
T53S F:	5' –CTATGATTCTTATTCATCTCCAACAGTCGTAATTG- 3'
T53S R:	5' –CAATTACGACTGTTGGAGATGAATAAGAATCATAG- 3'
T8A F:	5' –GAAAAAAATTGAGGTTTATGCACAACCCGATTGTCCGCC- 3'
T8A R:	5' –GGCGGACAATCGGGTTGTGCATAAACCTCAATTTTTTTC- 3'
T8A F:	5' –AAAAAATTGAGGTTTATGCACAACCCGATTGTCCG- 3'
T8A R:	5' –CGGACAATCGGGTTGTGCATAAACCTCAATTTTTT- 3'
T8A F:	5' –TGAAAAAAATTGAGGTTTATGCACAACCCGATTGTCCGCCA- 3'
T8A R:	5' –TGGCGGACAATCGGGTTGTGCATAAACCTCAATTTTTTTCA- 3'
T8A F:	5' –GAGGTTTATGCACAACCCGATTGTCCG- 3'
T8A R:	5' –CGGACAATCGGGTTGTGCATAAACCTC- 3'
T8D F:	5' –GAAAAAAATTGAGGTTTATGATCAACCCGATTGTCCGCC- 3'

```
T8D R:              5' –GGCGGACAATCGGGTTGATCATAAACCTCAATTTTTTTC– 3'

T8S F:              5' –GAAAAAAATTGAGGTTTATTCACAACCCGATTGTCCGC– 3'
T8S R:              5' –GGCGGACAATCGGGTTGTGAATAAACCTCAATTTTTTTC– 3'

V6D F:              5' –CATATGAAAAAAATTGAGGATTATACACAACCCG– 3'
V6D R:              5' –CGGGTTGTGTATAATCCTCAATTTTTTTCATATG– 3'
```

*F=Forward primer, R=Reverse primer
**Mutagenic codons are highlighted in grey

7.4 Appendix 4 – Terms and Abbreviations

A	Absorption
A. aceti	*Acetobacter aceti*
Amp	Ampicillin
B. cereus	*Bacillus cereus*
C. pasteurianum	*Clostridium pasteurianum*
Da	Dalton
dNTP/dNDP	Deoxyribonucleotide Triphosphate / Deoxyribonucleoside Diphosphate
DTT	Dithiothreitol
E	Molar Extinction Coefficient
E. coli	*Escherichia coli*
EDTA	Ethylenediaminetetraacetic Acid
FAD	Flavin Adeninde Dinucleotide
ESRF	European Synchrotron Radiation Facility
GSH	Glutathione
Gor	Glutathione Reductase
Grx	Glutaredoxin
ID	Insertion Device
IPTG	Isopropyl β-D-1-Thiogalactopyranoside
λ	Wavelength of Electromagnetic Radiation
mqH_2O	Milli-Q Filtered and Ion-Exchanged Water
M	Molar
M. tuberculosis	*Mycobacterium tuberculosis*
MW	Molecular Weight
MWCO	Molecular Weight Cutoff
$NADP^+$	Nicotinamide Adenine Dinucleotide Phosphate, Oxidized Form
NADPH	Nicotinamide Adenine Dinucleotide Phosphate, Reduced Form
NTP/NDP	Nucleoside Triphosphate / Nucleoside Diphosphate
OD	Optical Density
Ox	Oxidized
PCR	Polymerase Chain Reaction
PDB	Protein data bank
PDI	Protein Disulfide Isomerase
PEG	Polyethylene Glycol
pK_a	Acid Dissociation Constant
QM/MM	Quantum Mechanical/ Molecular Mechanical

Red	Reduced
R_{Free}	R Factor, 'Unbiased' R Factor
RNR	Ribonucleotide Reductase
rpm	Revolutions per Minute
R_{Sym}	R Factor, measurement of differences between symmetry-related measurements
R_{Work}	R Factor, Reliability Factor
S. aureus	*Staphylococcus aureus*
S. typhimurium	*Salmonella typhimurium*
S_2	Oxidized Disulfide
SEC	Size Exclusion Chromatography
SH_2	Reduced Disulfide
SDS-PAGE	Sodium Dodecyl Sulfate Polyacrylamide Gel Electrophoresis
T	Temperature
T. brucei	*Trypanosoma brucei*
Trx	Thioredoxin
TrxR	Thioredoxin Reductase
UV	Ultra Violet
UV/ vis	Ultraviolet/ Visible Light Absorption Spectrophotometry
(w/v)	(weight /volume)
x g	times gravity

Amino Acid Abbreviations

Amino Acid	Three-Letter	One-Letter
Alanine	Ala	A
Arginine	Arg	R
Asparagine	Asn	N
Aspartic acid	Asp	D
Cysteine	Cys	C
Glutamic acid	Glu	E
Glutamine	Gln	Q
Glycine	Gly	G
Histidine	His	H
Isoleucine	Ile	I
Leucine	Leu	L
Lysine	Lys	K
Methionine	Met	M
Phenylalanine	Phe	F
Proline	Pro	P
Serine	Ser	S
Threonine	Thr	T
Tryptophan	Trp	W
Tyrosine	Tyr	Y
Valine	Val	V

Single Letter Abbreviations for the Bases

A   Adenine
C   Cytosine
G   Guanine
T   Thymine
U   Uracil

8 Reference list

1.   Reichard, P., Baldeste, A., and Rutberg, L. (1961) Formation of deoxycytidine phosphates from cytidine phosphates in extracts from *Escherichia coli*, *J. Biol. Chem. 236*, 1150-1157.

2.   Reichard, P. (1962) Enzymatic synthesis of deoxyribonucleotides. 1. formation of deoxycytidine diphosphate from cytidine diphosphate with enzymes from *Escherichia coli*, *J. Biol. Chem. 237*, 3513-3519.

3.   Andersson, K. K., (Ed.) (2008) *Ribonucleotide Reductase*, Nova Science Publishers, Inc., New York.

4.   Andersson, K. K., and Gräslund, A. (1995) Diiron-oxygen proteins, In *Advances in Inorganic Chemistry* (Sykes, A. G., Ed.), pp 359-408, Academic Press, Inc.; Academic Press Ltd.

5.   Reichard, P. (1993) From RNA to DNA, why so many ribonucleotide reductases?, *Science, 260*, 1773-1777.

6.   Sjöberg, B. M. (1997) Ribonucleotide reductases - A group of enzymes with different metallosites and a similar reaction mechanism, *Struct. Bonding, 88*, 139-173.

7.   Cotruvo, J. A., and Stubbe, J. (2010) An Active Dimanganese(III)-Tyrosyl Radical Cofactor in *Escherichia coli* Class Ib Ribonucleotide Reductase, *Biochemistry 49*, 1297-1309.

8.   Sjöberg, B. M., Reichard, P., Gräslund, A., and Ehrenberg, A. (1978) Tyrosine free-radical in ribonucleotide reductase from *Escherichia coli*, *J. Biol. Chem. 253*, 6863-6865.

9.   Nordlund, N., and Reichard, P. (2006) Ribonucleotide reductases, *Annu. Rev. Biochem. 75*, 681-706.

10.   Kolberg, M., Strand, K. R., Graff, P., and Andersson, K. K. (2004) Structure, function, and mechanism of ribonucleotide reductases, *Biochim. Biophys. Acta. - Proteins Proteomics 1699*, 1-34.

11.   Sintchak, M. D., Arjara, G., Kellogg, B. A., Stubbe, J., and Drennan, C. L. (2002) The crystal structure of class II ribonucleotide reductase reveals how an allosterically regulated monomer mimics a dimer, *Nat. Struct. Biol. 9*, 293-300.

12.   Jordan, A., and Reichard, P. (1998) Ribonucleotide reductases, *Annu. Rev. Biochem. 67*, 71-98.

13.   Högbom, M., Stenmark, P., Voevodskaya, N., McClarty, G., Gräslund, A., and Nordlund, P. (2004) The radical site in chlamydial ribonucleotide reductase defines a new R2 subclass, *Science*, 305, 245-248.

14. Mowa, M. B., Warner, D. F., Kaplan, G., Kana, B. D., and Mizrahi, V. (2009) Function and Regulation of Class I Ribonucleotide Reductase-Encoding Genes in *Mycobacteria*, *J. Bacteriol. 191*, 985-995.

15. Jiang, W., Yun, D., Saleh, L., Barr, E. W., Xing, G., Hoffart, L. M., Maslak, M. A., Krebs, C., and Bollinger, J. M. (2007) A manganese(IV)/iron(III) cofactor in Chlamydia trachomatis ribonucleotide reductase, *Science, 316*, 1188-1191.

16. Voevodskaya, N., Lendzian, F., Ehrenberg, A., and Gräslund, A. (2007) High catalytic activity achieved with a mixed manganese-iron site in protein R2 of Chlamydia ribonucleotide reductase, *FEBS Lett. 581*, 3351-3355.

17. Cotruvo, J. A., and Stubbe, J. (2008) NrdI, a flavodoxin involved in maintenance of the diferric-tyrosyl radical cofactor in *Escherichia coli* class Ib ribonucleotide reductase, *Proc. Natl. Acad. Sci. U. S. A. 105*, 14383-14388.

18. Jordan, A., Aslund, F., Pontis, E., Reichard, P., and Holmgren, A. (1997) Characterization of *Escherichia coli* NrdH - A glutaredoxin-like protein with a thioredoxin-like activity profile, *J. Biol. Chem. 272*, 18044-18050.

19. Gon, S., Faulkner, M. J., and Beckwith, J. (2006) In vivo requirement for glutaredoxins and thioredoxins in the reduction of the ribonucleotide reductases of *Escherichia coli*, *Antioxid. Redox Signal. 8*, 735-742.

20. Berndt, C., Lillig, C. H., and Holmgren, A. (2008) Thioredoxins and glutaredoxins as facilitators of protein folding, *Biochim. Biophys. Acta-Mol. Cell Res. 1783*, 641-650.

21. Laurent, T. C., Moore, E. C., and Reichard, P. (1964) Enzymatic synthesis of deoxyribonucleotides. IV. Isolation + characterixation of thioredoxin hydrogen donor from *Escherichia coli* B, *J. Biol. Chem. 239*, 3436-3444.

22. Fourquet, S., Huang, M. E., D'Autreaux, B., and Toledano, M. B. (2008) The dual functions of thiol-based peroxidases in H2O2 scavenging and signaling, *Antioxid. Redox Signal. 10*, 1565-1575.

23. Sevier, C. S., and Kaiser, C. A. (2002) Formation and transfer of disulphide bonds in living cells, *Nat. Rev. Mol. Cell Biol. 3*, 836-847.

24. Ritz, D., and Beckwith, J. (2001) Roles of thiol-redox pathways in bacteria, *Annu. Rev. Microbiol. 55*, 21-48.

25. Lambert, N., and Freedman, R. B. (1985) The latency of rat-liver microsomal protein disulfide-isomerase, *Biochem. J. 228*, 635-645.

26. Hillson, D. A., Lambert, N., and Freedman, R. B. (1984) Formation and isomerization of disulfide bonds in proteins - protein disulfide-isomerase, *Meth. Enzymol. 107*, 281-294.

27. Carvalho, A. P., Fernandes, P. A., and Ramos, M. J. (2006) Similarities and differences in the thioredoxin superfamily, *Prog. Biophys. Mol. Biol. 91*, 229-248.

28. Stehr, M., Schneider, G., Aslund, F., Holmgren, A., and Lindqvist, Y. (2001) Structural basis for the thioredoxin-like activity profile of the glutaredoxin-like NrdH-redoxin from *Escherichia coli*, *J. Biol. Chem. 276*, 35836-35841.

29. Pan, J. L., and Bardwell, J. C. (2006) The origami of thioredoxin-like folds, *Protein Sci. 15*, 2217-2227.

30. Martin, J. L. (1995) Thioredoxin - a fold for all reasons, *Structure 3*, 245-250.

31. Reinemer, P., Dirr, H. W., Ladenstein, R., Schaffer, J., Gallay, O., and Huber, R. (1991) The 3-dimensional structure of class-PI glutathione-S-transferase in complex with glutathione sulfonate at 2.3 Å resolution, *EMBO J. 10*, 1997-2005.

32. Epp, O., Ladenstein, R., and Wendel, A. (1983) The refined structure of selenoenzyme glutathione-peroxidase at 0.2-nm resolution, *Eur. J. Biochem. 133*, 51-69.

33. Holmgren, A., Soderberg, B. O., Eklund, H., and Branden, C. I. (1975) 3-dimensional structure of *Escherichia coli* thioredoxin-S2 to 2.8 Å resolution, *Proc. Natl. Acad. Sci. U. S. A. 72*, 2305-2309.

34. Eklund, H., Cambillau, C., Sjöberg, B. M., Holmgren, A., Jornvall, H., Hoog, J. O., and Branden, C. I. (1984) Conformational and functional similarities between glutaredoxin and thioredoxins, *EMBO J. 3*, 1443-1449.

35. Holmgren, A. (1976) Hydrogen donor system for *Escherichia coli* ribonucleoside-diphosphate reductase dependent upon glutathione, *Proc. Natl. Acad. Sci. U. S. A. 73*, 2275-2279.

36. Eklund, H., Ingelman, M., Soderberg, B. O., Uhlin, T., Nordlund, P., Nikkola, M., Sonnerstam, U., Joelson, T., and Petratos, K. (1992) Structure of oxidized bacteriophage-T4 glutaredoxin (thioredoxin) - refinement of native and mutant proteins, *J. Mol. Biol. 228*, 596-618.

37. Leiting, W. U., and Jianping, X. I. E. (2010) Comparative genomics analysis of *Mycobacterium* NrdH-redoxins, *Microb. Pathog. 48*, 97-102.

38. Katti, S. K., Lemaster, D. M., and Eklund, H. (1990) Crystal-structure of thioredoxin from *Escherichia coli* at 1.68 Å resolution, *J. Mol. Biol. 212*, 167-184.

39. Guddat, L. W., Bardwell, J. C. A., Glockshuber, R., HuberWunderlich, M., Zander, T., and Martin, J. L. (1997) Structural analysis of three His32 mutants of DsbA: Support for an electrostatic role of His32 in DsbA stability, *Protein Sci. 6*, 1893-1900.

40. Nordstrand, K., Sandström, A., Aslund, F., Holmgren, A., Otting, G., and Berndt, K. D. (2000) NMR structure of oxidized glutaredoxin 3 from *Escherichia coli*, *J. Mol. Biol. 303*, 423-432.

41. Chivers, P. T., and Raines, R. T. (1997) General acid/base catalysis in the active site of *Escherichia coli* thioredoxin, *Biochemistry 36*, 15810-15816.

42. **Foloppe, N., and Nilsson, L. (2004) The glutaredoxin -C-P-Y-C- motif: Influence of peripheral residues,** *Structure 12*, **289-300.**

43. **Shi, J., Vlamis-Gardikas, V., Aslund, F., Holmgren, A., and Rosen, B. P. (1999) Reactivity of glutaredoxins 1, 2, and 3 from** *Escherichia coli* **shows that glutaredoxin 2 is the primary hydrogen donor to ArsC-catalyzed arsenate reduction,** *J. Biol. Chem. 274*, **36039-36042.**

44. **Fernandes, A. P., Fladvad, M., Berndt, C., Andresen, C., Lillig, C. H., Neubauer, P., Sunnerhagen, M., Holmgren, A., and Vlamis-Gardikas, A. (2005) A novel monothiol glutaredoxin (Grx4) from** *Escherichia coli* **can serve as a substrate for thioredoxin reductase,** *J. Biol. Chem. 280*, **24544-24552.**

45. **Martin, J. L., Bardwell, J. C. A., and Kuriyan, J. (1993) Crystal-structure of the DsbA protein required for disulfide bond formation** *in-vivo*, *Nature 365*, **464-468.**

46. **Edman, J. C., Ellis, L., Blacher, R. W., Roth, R. A., and Rutter, W. J. (1985) Sequence of protein disulfide isomerase and implications of its relationnship to thioredoxin,** *Nature 317*, **267-270.**

47. **Fernandes, A. P., and Holmgren, A. (2004) Glutaredoxins: Glutathione-dependent redox enzymes with functions far beyond a simple thioredoxin backup system,** *Antioxid. Redox Signal. 6*, **63-74.**

48. **Vlamis-Gardikas, A. (2008) The multiple functions of the thiol-based electron flow pathways of** *Escherichia coli*: **Eternal concepts revisited,** *Biochim. Biophys. Acta. 1780*, **1170-1200.**

49. **Mustacich, D., and Powis, G. (2000) Thioredoxin reductase,** *Biochem J 346* **1-8.**

50. **Miranda-Vizuete, A., Damdimopoulos, A. E., Gustafsson, J. A., and Spyrou, G. (1997) Cloning, expression, and characterization of a novel** *Escherichia coli* **thioredoxin,** *J. Biol. Chem. 272*, **30841-30847.**

51. **Holmgren, A. (1979) Glutathione-dependent synthesis of deoxyribonucleotides - characterization of the enzymatic mechanism of** *Escherichia coli* **glutaredoxin,** *J. Biol. Chem. 254*, **3672-3678.**

52. **Holmgren, A. (1979) Glutathione-dependent synthesis of deoxyribonucleotides - characterization of the enzymatic mechanism of** *Escherichia coli J. Biol. Chem. 254*, **3664-3671.**

53. **Zeller, T., and Klug, G. (2006) Thioredoxins in bacteria: functions in oxidative stress response and regulation of thioredoxin genes,** *Naturwissenschaften 93*, **259-266.**

54. **Meyer, Y., Buchanan, B. B., Vignols, F., and Reichheld, J. P. (2009) Thioredoxins and glutaredoxins: unifying elements in redox biology,** *Annu.rev. genet. 43*, **335-367.**

55. **Carmel-Harel, O., and Storz, G. (2000) Roles of the glutathione- and thioredoxin-dependent reduction systems in the** *Escherichia coli* **and Saccharomyces cerevisiae responses to oxidative stress,** *Annu. Rev. Microbiol. 54*, **439-461.**

56.   Krause, G., Lundström, J., Barea, J. L., Delacuesta, C. P., and Holmgren, A. (1991) Mimmicking the active-site of protein disulfide-isomerase by substitution of proline 34 in *Eschirichia-coli* thioredoxin, *J. Biol. Chem. 266*, 9494-9500.

57.   Huber-Wunderlich, M., and Glockshuber, R. (1998) A single dipeptide sequence modulates the redox properties of a whole enzyme family, *Fold. Des. 3*, 161-171.

58.   Quan, S., Schneider, I., Pan, J., Von Hacht, A., and Bardwell, J. C. A. (2007) The CXXC motif is more than a redox rheostat, *J. Biol. Chem. 282*, 28823-28833.

59.   Messens, J., Van Molle, I., Vanhaesebrouck, P., Limbourg, M., Van Belle, K., Wahni, K., Martins, J. C., Loris, R., and Wyns, L. (2004) How thioredoxin can reduce a buried disulphide bond, *J. Mol. Biol. 339*, 527-537.

60.   Mossner, E., Huber-Wunderlich, M., and Glockshuber, R. (1998) Characterization of *Escherichia coli* thioredoxin variants mimicking the active-sites of other thiol/disulfide oxidoreductases, *Protein Sci. 7*, 1233-1244.

61.   Aslund, F., Berndt, K. D., and Holmgren, A. (1997) Redox potentials of glutaredoxins and other thiol-disulfide oxidoreductases of the thioredoxin superfamily determined by direct protein-protein redox equilibria, *J. Biol. Chem. 272*, 30780-30786.

62.   Reckenfelderbaumer, N., and Krauth-Siegel, R. L. (2002) Catalytic properties, thiol pK value, and redox potential of *Trypanosoma brucei* tryparedoxin, *J. Biol. Chem. 277*, 17548-17555.

63.   Røhr, Å. K., and Andersson, K. K. (2010) Stabilization of two nucleophilic cysteine thiolates in the active site of the BC3987 thioredoxin, *J. Biol. Chem. (Submitted)*.

64.   Nelson, J. W., and Creighton, T. E. (1994) Reactivity and ionization of the active site cysteine residues of DsbA, a protein required for disulfide bond formation in vivo, *Biochemistry 33*, 5974-5983.

65.   Hol, W. G. J. (1985) The role of the alpha-helix dipole in protein function and structure, *Prog. Biophys. Mol. Biol. 45*, 149-195.

66.   Tanford, C., and Kirkwood, J. G. (1957) Theory of protein titration curves. 1. General equations for impenettrable spheres, *J. Am. Chem. Soc. 79*, 5333-5339.

67.   Jensen, J. H., Li, H., Robertson, A. D., and Molina, P. A. (2005) Prediction and rationalization of protein pK(a) values using QM and QM/MM methods, *J. Phys. Chem. A 109*, 6634-6643.

68.   Li, H., Robertson, A. D., and Jensen, J. H. (2005) Very fast empirical prediction and rationalization of protein pKa values, *Proteins 61*, 704-721.

69.   Roos, G., Loverix, S., and Geerlings, P. (2006) Origin of the pK(a) perturbation of N-terminal cysteine in alpha- and 3(10)-helices: A computational DFT study, *J. Phys. Chem. B 110*, 557-562.

70. Chivers, P. T., Prehoda, K. E., Volkman, B. F., Kim, B. M., Markley, J. L., and Raines, R. T. (1997) Microscopic pK(a) values of *Escherichia coli* thioredoxin, *Biochemistry 36*, 14985-14991.

71. Eklund, H., Gleason, F. K., and Holmgren, A. (1991) Structural and functional relations among thioredoxins of different species, *Prot.-Struct. Funct. and Genet. 11*, 13-28.

72. Starks, C. M., Francois, J. A., MacArthur, K. M., Heard, B. Z., and Kappock, T. J. (2007) Atomic-resolution crystal structure of thioredoxin from the acidophilic bacterium *Acetobacter aceti*, *Protein Sci. 16*, 92-98.

73. Dyson, H. J., Jeng, M. F., Tennant, L. L., Slaby, I., Lindell, M., Cui, D. S., Kuprin, S., and Holmgren, A. (1997) Effects of buried charged groups on cysteine thiol ionization and reactivity in *Escherichia coli* thioredoxin: Structural and functional characterization of mutants of Asp 26 and Lys 57, *Biochemistry 36*, 2622-2636.

74. Kallis, G. B., and Holmgren, A. (1980) Differential reactivity of the functional sulfhydryl-groups of cysteine-32 and cysteine-35 present in the reduced form of thioredoxin from *Escherichia coli*, *J. Biol. Chem. 255*, 261-265.

75. Reynolds, C. M., Meyer, J., and Poole, L. B. (2002) An NADH-dependent bacterial thioredoxin reductase-like protein in conjunction with a glutaredoxin homologue form a unique peroxiredoxin (AhpC) reducing system in *Clostridium pasteurianum*, *Biochemistry 41*, 1990-2001.

76. Stehr, M., and Lindqvist, Y. (2004) NrdH-redoxin of *Corynebacterium ammoniagenes* forms a domain-swapped dimer, *Prot.-Struct. Funct. and Bioinf. 55*, 613-619.

77. Hofmann, B., Budde, H., Bruns, K., Guerrero, S. A., Kalisz, H. M., Menge, U., Montemartini, M., Nogoceke, E., Steinert, P., Wissing, J. B., Flohe, L., and Hecht, H. J. (2001) Structures of tryparedoxins revealing interaction with trypanothione, *Biol. Chem. 382*, 459-471.

78. Glusker, J. P., Lewis, M., Rossi, M. (1994) *Crystal Structure Analysis for Chemists and Biologists*, Wiley-VCH, Inc., New York.

79. Blow, D. (2002) *Outline of Crystallography for Biologists,* Oxford University Press, Oxford.

80. McPherson, A. (2003) *Introduction to Macromolecular Crystallography*, Wiley-Liss, Inc., New Jersey.

81. Sheehan, D. (2000) *Physical Biochemistry: Principles and Applications*, John Wiley & Sons Ltd., Chichester

82. Drenth, J. (1999) *Principles of Protein X-Ray Crystallography*, Vol. Second Edition, Springer-Verlag New York, Inc., New York.

83. Attwood, D. (1999) *Soft X-Rays and Extreme Ultraviolet Radiation: Principles and Applications*, Cambridge University Press, Cambridge.

84. **Geigé, R., and Ducruix, A. (1992)** *Crystallization of nucleic acids and proteins: a practical approach*, Oxford University Press, Oxford.

85. **Weber, P. C. (1997)** *Overview of Protein Crystallization Methods*, Vol. 276.

86. **Bergfors, T. M. (1999)** *Protein crystallization: techniques, strategies, and tips : a laboratory manual*, International University Line, La Jolla, Calif.

87. **Stura, E. A., and Wilson, I. A. (1990) Analytical and Production Seeding Techniques,** *Methods (Orlando) 1*, 38-49.

88. **Read, R. J., and Sussman, J. L. (2007)** *Evolving Methods for Macromolecular Crystallography: The Structural Path to the Understanding of the Mechanismof Action of CBRN Agents*, Vol. 245, Springer Science+Business Media B.V., Dordrecht.

89. **Parkin, S., and Hope, H. (1998) Macromolecular cryocrystallography: Cooling, mounting, storage and transportation of crystals,** *J. Appl. Crystallogr. 31*, 945-953.

90. **Teng, T.-Y. (1990) Mounting of crystals for macromolecular crystallography in a free-standing thin film,** *J. Appl. Crystallogr. 23*, 387-391.

91. **Lattman, E., and Loll, P. J. (2008)** *Protein Crystallography - A Concise Guide*, The John Hopkins University Press, Baltimore.

92. **Saiki, R. K., Gelfand, D. H., Stoffel, S., Scharf, S. J., Higuchi, R., Horn, G. T., Mullis, K. B., and Erlich, H. A. (1988) Primer-directed enzymatic amplification of DNA with a thermostable DNA polymerase,** *Science, 239*, 487-491.

93. **Sambrook J, R. D. (2001)** *Molecular Cloning: A Laboratory Manual* Vol. 3, 3rd ed., Cold Spring Harbor Laboratory Press. Cold Spring Harbor, NY.

94. **Chen, I., and Dubnau, D. (2004) DNA uptake during bacterial transformation,** *Nature rev. 2*, 241-249.

95. **Kang, Y., Son, M. S., and Hoang, T. T. (2007) One step engineering of T7-expression strains for protein production: increasing the host-range of the T7-expression system,** *Protein Expr. Purif. 55*, 325-333.

96. **Baneyx, F. (1999) Recombinant protein expression in** *Escherichia coli*, *Curr. Opin. Biotechnol. 10*, 411-421.

97. **Ulrika Rova, K. G., Rolf Ingemarson, Gity Behravan, Astrid Graeslund, Lars Thelander. (1995) Evidence by Site-Directed Mutagenesis Supports Long-Range Electron Transfer in Mouse Ribonucleotide Reductase,** *Biochemistry 34*, 4267–4275.

98. **Mann, G. J., Gräslund, A., Ochiai, E. I., Ingemarson, R., and Thelander, L. (1991) Purification and characterization of recombinant mouse and herpes-simplex virus ribonucleotide reductase R2 subunit,** *Biochemistry 30*, 1939-1947.

99. **Magnusson, K. E., and Edebo, L. (1976) Influence of cell concentration, temperature, and press performance on flow characterics and disintefration in freeze-pressing of *Saccharomyces-cerevisiae* with X-press, *Biotechnol. Bioeng. 18*, 865-883.**

100. **Voet, D., and Voet, J. G. (2004) *Biochemistry*, Vol. 3rd edn., Wiley, New York.**

101. **Greibrokk, T., Lundanes, E. & Rasmussen K. E. (1994) *Kromatografi*, Universitetsforlaget, Oslo.**

102. **Laemmli, U. K. (1970) Cleavage of structural proteins during the assembly of the head of bacteriophage T4, *Nature 227*, 680-685.**

103. **Pace, C. N., Vajdos, F., Fee, L., Grimsley, G., and Gray, T. (1995) How to measure and predict the molar absorption coefficient of a protein, *Protein Sci. 4*, 2411-2423.**

104. **Leach, S. L. (1969) *Physical principles and techniques of protein chemistry*, Academic Press, New York.**

105. **Cleland, W. W. (1964) Dithiothreitol New Protective Reagent for Sh Groups, *Biochemistry 3*, 480-482.**

106. **Bisswanger, H. (2002) *Enzyme kinetics: principles and methods*, Wiley, Weinheim.**

107. **Colleen, E., Reichard, P., and Thelander, L. (1964) Enzymatic synthesis of deoxyribonucleotides .V. Purification + properties of thioredoxin reductase from *Escherichia coli B*, *J. Biol. Chem. 239*, 3445-3452.**

108. **Clark, W. M. (1960) *Oxidation-reduction potentials of organic systems*, Williams & Wilkins, Baltimore, Md.**

109. **Powell, H. R. (1999) The Rossmann Fourier autoindexing algorithm in MOSFLM, *Acta Crystallogr. Sect. D-Biol. Crystallogr. 55*, 1690-1695.**

110. **Collaborative Computational Project, N. (1994) The CCP4 Suite: Programs for protein crystallography, *Acta Crystallogr. Sect. D-Biol. Crystallogr. 50*, 760-763.**

111. **McCoy, A. J., Grosse-Kunstleve, R. W., Adams, P. D., Winn, M. D., Storoni, L. C., and Read, R. J. (2007) Phaser crystallographic software, *J. Appl. Crystallogr. 40*, 658-674.**

112. **Murshudov, G. N., Vagin, A. A., and Dodson, E. J. (1997) Refinement of macromolecular structures by the maximum-likelihood method, *Acta Crystallogr. Sect. D-Biol. Crystallogr. 53*, 240-255.**

113. **Emsley, P., and Cowtan, K. (2004) Coot: model-building tools for molecular graphics, *Acta Crystallogr. Sect. D-Biol. Crystallogr. 60*, 2126-2132.**

114. **Lamzin, V. S., and Wilson, K. S. (1993) Automated refinement of protein models, *Acta Crystallogr. Sect. D-Biol. Crystallogr. 49*, 129-147.**

115. **Murshudov, G. N., Vagin, A. A., Lebedev, A., Wilson, K. S., and Dodson, E. J. (1999) Efficient anisotropic refinement of macromolecular structures using FFT,** *Acta Crystallogr. Sect. D-Biol. Crystallogr. 55*, 247-255.

116. **Merritt, E. A. (1999) Expanding the model: anisotropic displacement parameters in protein structure refinement,** *Acta Crystallogr. Sect. D-Biol. Crystallogr. 55*, 1109-1117.

117. **Paithankar, K. S., and Garman, E. F. (2010) Know your dose: RADDOSE,** *Acta Crystallogr. Sect. D-Biol. Crystallogr. 66*, 381-388.

118. **Murray, J. W., Garman, E. F., and Ravelli, R. B. G. (2004) X-ray absorption by macromolecular crystals: the effects of wavelength and crystal composition on absorbed dose,** *J. Appl. Crystallogr. 37*, 513-522.

119. **Polgar, L. (1974) Spectrophotometric determination of mercaptidine ion, an activated form of SH-group in thiol enzymes,** *FEBS Lett. 38*, 187-190.

120. **Witt, A. C., Lakshminarasimhan, M., Remington, B. C., Hasim, S., Pozharski, E., and Wilson, M. A. (2008) Cysteine pK(a) depression by a protonated glutamic acid in human DJ-1,** *Biochemistry 47*, 7430-7440.

121. **McGeehan, J., Ravelli, R. B. G., Murray, J. W., Owen, R. L., Cipriani, F., McSweeney, S., Weik, M., and Garman, E. F. (2009) Colouring cryo-cooled crystals: online microspectrophotometry,** *J. Synchrot. Radiat. 16*, 163-172.

122. **Henderson, R. (1990) Cryoprotection of protein crystals against radiation-damage in electron and x-ray-diffraction,** *Proc. R. Soc. Lond. Ser. B-Biol. Sci. 241*, 6-8.

123. **Carugo, O., and Carugo, K. D. (2005) When X-rays modify the protein structure: radiation damage at work,** *Trends Biochem. Sci. 30*, 213-219.

124. **Weik, M., Berges, J., Raves, M. L., Gros, P., McSweeney, S., Silman, I., Sussman, J. L., Houee-Levin, C., and Ravelli, R. B. G. (2002) Evidence for the formation of disulfide radicals in protein crystals upon X-ray irradiation,** *J. Synchrot. Radiat. 9*, 342-346.

125. **Banaszak, K., Mechin, I., Frost, G., and Rypniewski, W. (2004) Structure of the reduced disulfide-bond isomerase DsbC from** *Escherichia coli*, *Acta Crystallogr. Sect. D-Biol. Crystallogr. 60*, 1747-1752.

126. **Sheldrick, G. M. (2008) A short history of SHELX,** *Acta Crystallogr. Sect. A 64*, 112-122.

127. **Weik, M., Ravelli, R. B. G., Kryger, G., McSweeney, S., Raves, M. L., Harel, M., Gros, P., Silman, I., Kroon, J., and Sussman, J. L. (2000) Specific chemical and structural damage to proteins produced by synchrotron radiation,** *Proc. Natl. Acad. Sci. U. S. A. 97*, 623-628.

128. **Holton, J. M. (2009) A beginner's guide to radiation damage,** *J. Synchrot. Radiat. 16*, 133-142.

129. **Lennon, B. W., Williams, C. H., and Ludwig, M. L. (2000) Twists in catalysis: Alternating conformations of *Escherichia coli* thioredoxin reductase, *Science, 289*, 1190-1194.**